X-520-66-3

NASA TM X-55504

FINAL REPORT ON THE ASEE—UNIVERSITY OF MARYLAND—CATHOLIC UNIVERSITY NASA SUMMER FELLOWSHIP PROGRAM

GPO PRICE $ _____

CFSTI PRICE(S) $ _____

Hard copy (HC) 4.00

Microfiche (MF) .75

ff 653 July 65

FACILITY FORM 602

N66 31154 (ACCESSION NUMBER)	N66 31161 (THRU)
107 (PAGES)	1 (CODE)
TMX-55504 (NASA CR OR TMX OR AD NUMBER)	07 (CATEGORY)

JANUARY 1966

NASA — GODDARD SPACE FLIGHT CENTER — GREENBELT, MARYLAND

INTRODUCTION

This subject program was instituted in FY 1965. It is a cooperative endeavor of the American Society for Engineering Education, the University of Maryland, the Catholic University of America, and Goddard. This program is intended to operate on a two-year cycle. Professors agree to participate during two consecutive summers.

The objectives of this program are many; some of them are listed below:

1. Stimulation of schools to become interested in the research problems now confronting Goddard.

2. Creation of interest on the part of professors to continue their research after completing the formal program.

3. Stimulation of our people professionally through associations with the professors and through their participation in the program's seminars.

4. Establishment of closer ties with the Universities. We have been able, through this program, to develop working relationships with the University of Maryland and Catholic University which are outstanding. This is important for we have more than 150 employees attending these schools.

5. An advertising tool for Goddard which is most acceptable professionally. Every major educational organization has been exposed to the fact of our participation. ASEE is an influential professional organization.

Now that we have completed the first summer of this program we are happy to report that the progress made on the above objectives was beyond our expectations considering that this was the first summer.

One of the goals that has been implied is the solution or approach to the solution of Goddard problems that might be of interest to the Summer Fellowship participants: The problems that they selected are listed in the table of contents and the results are compiled in this report. It should be borne in mind that the time allotted for the solution of the problem was very short (an equivalent of seven weeks) and consequently some of the problems need more time for complete solution. Most of the 1965 Summer Fellows are expected to return for the summer of 1966 in addition to the 15 new Fellows that we hope to have this summer.

JTMengel

John T. Mengel
Assistant Director, Tracking & Data Systems

CONTENTS

	Page
DIGITAL FILTER DESIGN W. D. Stanley	1
DESIGN PROBLEMS IN A CONTROL SYSTEM USED FOR PRECISE OPTICAL TRACKING OF SATELLITES AND STARS R. V. Monopoli	27
TRACKING ACCURACY ANALYSIS OF THE 85-FOOT PARABOLIC ANTENNA AT ROSMAN, NORTH CAROLINA C. Ghaznavi and T. Mercado-Jimenez	43
NOTES ON THE SPIN-HAMILTONIAN H. A. Sabbagh	63
A PRELIMINARY STUDY OF HOLOGRAPHY L. G. McCracken	77
CORRELATION BETWEEN JITTER AND INFORMATION RECOVERY IN PCM TELEMETERED DATA P. Goodman	89
DEVELOPMENT OF THE 10.6-MICRON LASER Z. D. Jastrzebski	95

PRECEDING PAGE BLANK NOT FILMED.

SUMMER FELLOWSHIP PARTICIPANTS

Administration

Dr. C. C. Chang	Policy Committee	Professor and Head, Space Sciences Dept., CU
Dr. B. Fang	Co-director	Professor, Spaces Dept., CU
Mr. C. Looney	Policy Committee and Co-director	Assoc. Div. Chief, Advanced Development Div., GSFC
Dr. A. Marcovitz	Co-director	Professor, EE Dept., Univ. of Md.
Mr. J. Morakis	Co-director	Sr. Eng., Advanced Development Div., GSFC
Mr. J. Reese	Co-director	Head, Employee Development Branch, GSFC
Dr. H. E. Tompkins	Chairman, Policy Committee	Professor and Head, EE Dept., Univ. of Md.
Messrs. C. Veri and C. Zuzak	General Administrators	Conference and Institutes Division, Univ. of Md.

Goddard Working Colleagues

Mr. R. Fitzgerald, Head, Network Engineering Branch
Mr. C. Johnson, RF Systems Branch
Mr. N. McAvoy, Optical Systems Branch
Mr. B. Narrow, Data Processing Branch
Mr. W. Poland, Head, Processor Development Branch
Mr. M. Shawe, Head, Space Data Control Branch
Mr. G. Winston, Antenna Systems Branch

Summer Fellows

Dr. H. M. Curran	Professor, St. Edward's University
Dr. C. Ghaznavi	Associate Professor, Pratt Institute
Dr. P. Goodman	Assistant Professor, Newark College of Engineering
Dr. Z. Jastrzebski	Professor and Head, Chemistry Eng. Dept., Lafayette College
Dr. L. G. McCracken	Associate Professor, Lehigh University
Dr. T. Mercado-Jimenez	Assistant Professor, University of Puerto Rico
Dr. R. V. Monopoli	Associate Professor, University of Massachusetts
Dr. H. A. Sabbagh	Assistant Professor, Rose Polytechnic Institute
Dr. W. D. Stanley	Assistant Professor, Clemson University

N66 31155

DIGITAL FILTER DESIGN

by

William D. Stanley
Assistant Professor, Clemson University
NASA-ASEE Fellow

I. INTRODUCTION

Large-scale processing of telemetry data frequently requires filtering processes to remove undesirable signals and noise that perturb the signal. In the case of analog signals, this process is normally accomplished by the use of RLC passive or RC active filters whose effect on the signal is usually described by the Fourier transform of the impulse response. This characteristic is called the frequency response and consists of an amplitude response and a phase response.

In processing sampled or digital data, it is often inconvenient or undesirable to employ analog filters for such filtering operations. Rather, it seems more feasible to program a numerical algorithm on a digital computer which accomplishes the same task on the digital data. The computer then becomes an integral part of the overall system, and furthermore, it has the extra advantages of flexibility and ease of adjustment and change that is usually not present in an analog filter.

The purpose of this paper is to present a study of the design of digital filters. Both the approximation and the realization problems will be considered, and techniques will be presented for designing both low-pass and bandpass filters. A survey of the literature dealing with the fundamental theory will be made, and this will be followed by step-by-step design procedures. The resulting "design" in each case will be a numerical algorithm whose effect on the data is the desired filtering operation.

II. BASIC THEORY

For the purposes of this paper, the term "digital filter" will be used to designate any numerical operation that can be performed on a set of data to alter the spectral representation of the data in some desirable manner. Theoretically, such a filtering operation could be done by pencil and paper or by a desk calculator if the proper sequence of operations is known. A more practical approach is to program the filter algorithm on a digital computer and allow the computer to perform the filtering operation. The filter operation can be performed on-line in real time or the data may be stored on tape and processed at a lower rate.

The underlying approach to any digital filter is the theory of sampled-data systems. There is an extensive amount of literature pertaining to the subject, and no exhaustive survey of this literature will be attempted. Among the texts pertaining to sampled-data systems are Ragazzini and Franklin (1), Jury (2), Tou (3), Monroe (4), and Kuo (5). All of these books contain extensive bibliographies of the research literature pertaining to sampled-data systems.

This paper will draw basic theorems and results freely from the above-named references. The proofs of these results will be repeated only when necessary for clarity or further development.

A sampled signal may be represented as the product of the continuous signal and a periodic pulse train. As far as a numerical process is concerned, the pulse train may be considered as an impulse train. Let $x(t)$ represent a continuous signal and $x^*(t)$ represent the sampled signal. The sampled signal may be represented as

$$x^*(t) = x(t)\delta_T(t) \tag{1}$$

where T is the time between samples and

$$\delta_T(t) = \sum_{0}^{\infty} \delta(t - nT) \tag{2}$$

as illustrated in Figure 1.

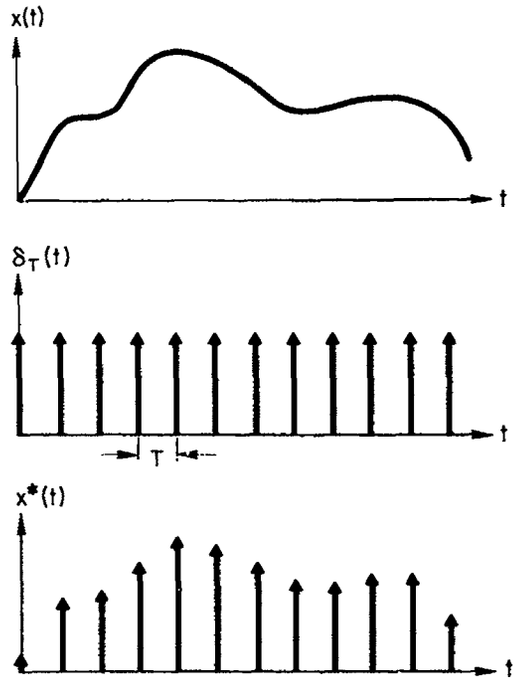

Figure 1

Equations (1) and (2) are equivalent to

$$x^*(t) = \sum^{\infty} x(nT)\,\delta(t - nT) \tag{3}$$

Let $\mathcal{L}$ represent the process of Laplace transformation. The following definitions are made:

$$\mathcal{L}[x(t)] = X(s) \tag{4}$$

$$\mathcal{L}[x^*(t)] = X^*(s) \tag{5}$$

Transformation of Eq. (3) yields

$$X^*(s) = \sum_{0}^{\infty} x(nT)\, e^{-nTs} \tag{6}$$

It can also be shown that (6) is equivalent to

$$X^*(s) = \frac{1}{T} \sum_{-\infty}^{\infty} X\left(s + j\,\frac{2\pi n}{T}\right) \tag{7}$$

According to Eq. (7) the spectral representation of $X^*(s)$ is periodic. This idea is illustrated in Figure 2 for $s = j\omega$ (Fourier transform). As long as the minimum Nyquist sampling rate is maintained, the original spectrum of $x(t)$ is preserved, although modified by a factor, and the same spectrum is repeated on both sides at multiples of $1/T$.

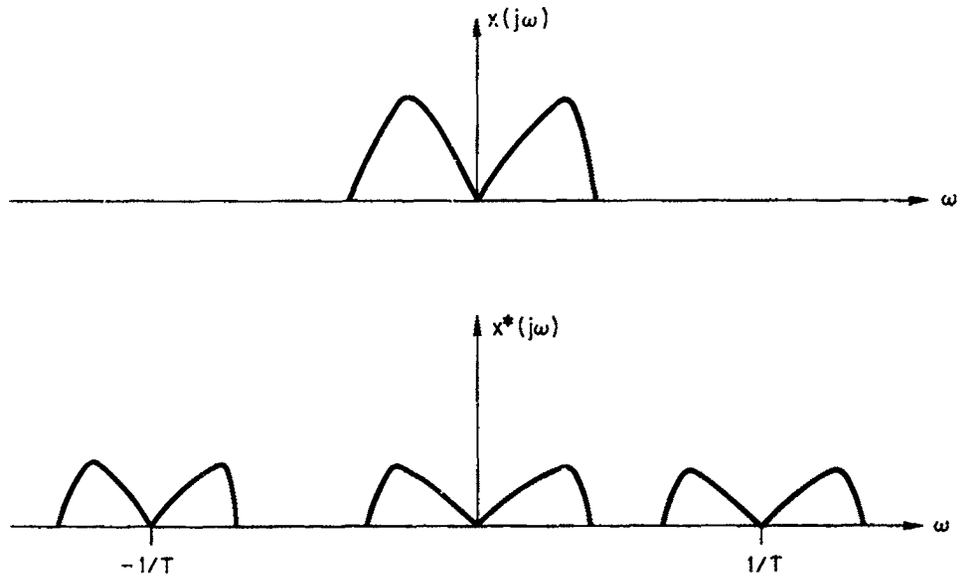

Figure 2

The z-transform is ordinarily introduced to simplify the operation of a numerical process. Let

$$z = e^{Ts} \tag{8}$$

and

$$X(z) = \mathcal{L}\,[x^*(t)] = X(s)\,]_{z=e^{Ts}} \tag{9}$$

thus

$$X(z) = \sum_{0}^{\infty} x(nT)\, z^{-n} \tag{10}$$

Now assume that $x^*(t)$ (or equivalently $X(z)$) is applied to the input of a linear numerical processor as shown in Figure 3. Let $y^*(t)$ represent the output and let

$$Y(z) = \mathcal{Z}[y^*(t)] \tag{11}$$

It can be shown that

$$Y(z) = G(z)\,X(z) \tag{12}$$

Where $G(z)$ represents a type of transfer function. In the case where the processor is a hardware item such as an electrical network, $G(z)$ is called the pulse-transfer function. In the case where the processor is a software item such as a computer program (the case of primary interest in this paper), $G(z)$ is simply an algorithm whose form will be discussed in a later section.

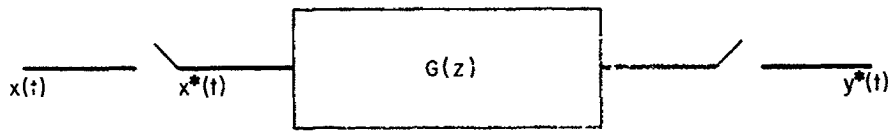

Figure 3

The transformation of Eq. (8) maps the left-hand half of the s-plane to the inside of the unit circle in the z-plane and the right-hand half of the s-plane to the outside of the unit circle in the z-plane. In the same manner as the spectrum of $X^*(s)$ as predicted by Eq. (7) is periodic, so is the spectrum of $Y^*(s)$ periodic. Thus

$$Y^*(s) = \frac{1}{T} \sum_{m=-\infty}^{\infty} Y\left(s + j\,\frac{2\pi m}{T}\right) \tag{13}$$

This periodic property is an inherent characteristic of the sampling process and must be clearly interpreted in any numerical process. Basically it is related to the familiar uncertainty principle. Since there is uncertainty in the time function between samples, there is a corresponding ambiguity in the frequency domain representation.

All this means that it is impossible in a sense to create any digital filter with an arbitrary form of characteristic at all frequencies. Instead, the approximation must be done in a "local" sense with the expectation that the given frequency function will repeat itself at other frequencies in its present sense. This does not mean that the digital filter is more limited in its utility than the analog filter. On the contrary, a sufficiently high sampling rate may be chosen along with accurate digital to analog conversion in such a manner as to essentially eliminate the unwanted portions of the spectrum. Furthermore, complex filters may be synthesized quite readily on a digital computer in cases where the corresponding analog filters would be very difficult to build.

III. FILTER REALIZATION FROM TRANSFER FUNCTIONS

It is normally advantageous to study the realization problem before considering the approximation problem, although an actual design usually proceeds in the referse order.

It can be shown that any physically realizable linear numerical transfer function can be written as the ratio of two polynomials in z^{-k} of the form

$$G(z) = \frac{Y(z)}{X(z)} = \frac{\sum_{k=0}^{N} a_k z^{-k}}{1 + \sum_{k=1}^{M} b_k z^{-k}} \tag{14}$$

For a stable system, the poles of $G(z)$ must lie within the unit circle in the z-plane.

A more intuitive form of Eq. (14) can be obtained by writing it in the form:

$$Y(z)\left[1 + \sum_{k=1}^{M} b_k z^{-k}\right] = X(z)\left[\sum_{k=0}^{N} a_k z^{-k}\right] \tag{15}$$

The quantity z^{-k} operating on any $F(z)$ corresponds to delaying $f(t)$ by kT sec. More generally

$$\mathcal{Z}^{-1}[z^{-k} F(z)] = f(nT - kT) \tag{16}$$

Performing the inverse z-transformation of Eq. (15) yields

$$y(nT) + \sum_{k=1}^{M} b_k y(nT - kT) = \sum_{k=0}^{N} a_k x(nT - kT) \tag{17}$$

or

$$y(nT) = \sum_{k=0}^{N} a_k x(nT - kT) - \sum_{k=1}^{M} b_k y(nT - kT) \tag{18}$$

Thus, the transfer function of Eq. (14) is equivalent to the numerical operation of Eq. (18). The reason for the unity term in Eq. (14) is now clear. A block diagram representing the sequence of operations expressed by Eq. (18) is shown in Figure 4.

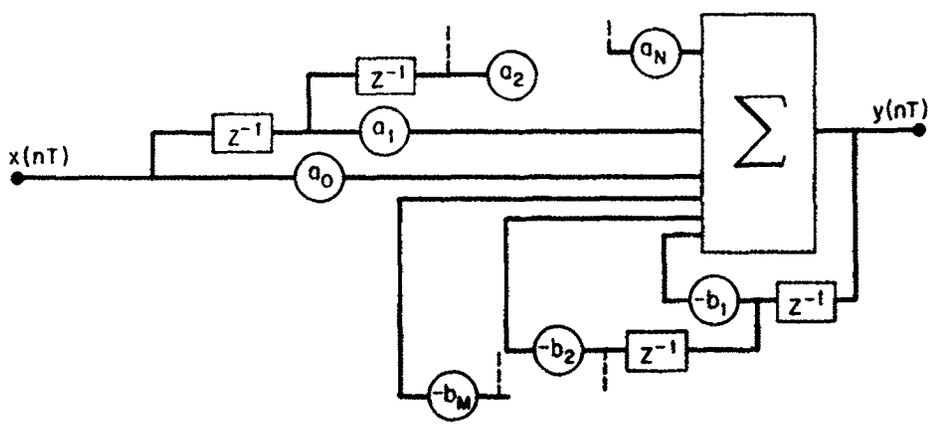

Figure 4

The form of synthesis (or programming) expressed by Eq. (18) is called a "direct programming" scheme. There are a number of other techniques which are discussed in the texts referenced earlier, along with the direct method, but they will not be discussed here. It is felt that the direct method is the easiest technique to implement directly on the computer, although some of the other techniques may yield fewer computer operations in some instances.

As an illustration of this method consider the transfer function given by

$$G(z) = \frac{3z^2 + 2z + 5}{8z^2 + 6z + 1} \tag{19}$$

The first step in realizing $G(z)$ is to put it in the form of Eq. (14). Dividing numerator and denominator by the value 8 and multiplying numerator and denominator by z^{-2} results in

$$G(z) = \frac{\frac{3}{8} + \frac{1}{4} z^{-1} + \frac{5}{8} - z^{-2}}{1 + \frac{3}{4} z^{-1} + \frac{1}{8} z^{-2}} \tag{20}$$

Thus from Eq. (18),

$$y(nT) = \frac{3}{8} x(nT) + \frac{1}{4} x(nT - T) + \frac{5}{8} (nT - 2T)$$

$$- \frac{3}{4} y(nT - T) - \frac{1}{8} y(nT - 2T) \tag{21}$$

If desired, the notation may be modified to read

$$y(n) = \frac{3}{8} x(n) + \frac{1}{4} x(n - 1) + \frac{5}{8} x(n - 2)$$

$$- \frac{3}{4} y(n - 1) - \frac{1}{8} y(n - 2) \tag{22}$$

In subsequent work, the notation of Eq. (22) will be employed with the sampling time T implied. A flow diagram for Eq. (22) is shown in Figure 5.

IV. ANALOG TO DIGITAL FILTER TRANSFORMATION

Now that the basic form of the numerical transfer function has been stated, the next question is: How does one relate the basic specifications of a desired filtering operation to the final transfer function to be realized? This problem, of course, is the familiar approximation problem, and the solution is evidently not unique. One possible approach would be to attempt to approximate the transfer function directly in terms of a ratio of

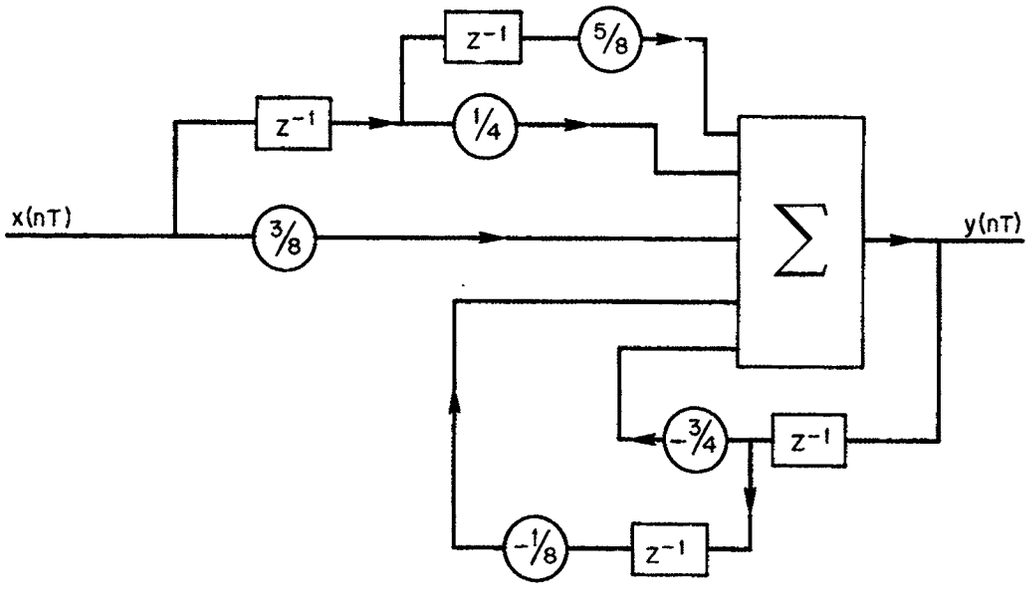

Figure 5

polynomials in z^{-1} (or equivalent e^{-sT}). However, this approach appears to have received very little attention due to the difficulty of working with exponential functions.

On the other hand, there is a wealth of literature available on the approximation problem of analog filters. If one can obtain some direct relationship between the analog domain and the digital domain, the approximation problem can be carried out in the analog domain, and then a suitable transformation may map the function into the digital domain, thus achieving the desired result.

The most intuitive approach to this problem is to find an analog transfer function representing the desired response and then compute the z-transform corresponding to this function. However, as pointed out by Steiglitz (6), (7) and Hauptschein (8), this method yields rather poor results due to poor correspondence between a sampled-input and a continuous input applied to the same structure. Consequently, this method will not be pursued any further.

It appears that the use of the bilinear transformation is the most fruitful approach to correlating the analog domain to the digital domain. The use of this transformation in studying digital filters and control systems has been investigated by Johnson, Lindorff, and Nording (9), Lewis (10), Carney (11), and all the references previously mentioned in this paper (1-8).

The basic form of the bilinear transformation is given by

$$p = K \frac{(z - 1)}{z + 1} \tag{23}$$

or the inverse transformation

$$z = \frac{K + p}{K - p} \tag{24}$$

where K is a normalizing constant.

It can be shown that the left-hand half of the p-plane is mapped into the interior of the unit circle in the z-plane; whereas, the right-hand half of the p-plane is mapped to the outside of the unit circle in the z-plane. In other words, there is a similar correspondence between the p-plane and z-plane as is true with the s-plane and z-plane. On the other hand the relationship between the p plane and z-plane is a simple ratio of first-degree polynomials and is not complicated by exponentials.

The basic procedure for using the p-plane approach is to carry out the basic approximation in the p-plane using the conventional analog approximation technique. Once the desired function of p has been obtained, one merely makes the substitution of Eq. (23) and manipulates the expression into the final desired form of a numerical transfer function.

Normally the approximation process is performed along the imaginary axis in the s-plane. It can be shown that the imaginary axis of the artificial p-plane maps to the imaginary axis of the s-plane, and thus the normal approximation will usually be performed along the imaginary axis of the p-plane. An interesting point of consideration is the relationship between the imaginary axes of the two planes. In this context, let

$$s = \alpha + jw = \text{ transform variable of final interest} \tag{25}$$

$$p = \sigma + j\lambda = \text{ transform variable in artificial p-plane} \tag{26}$$

since $z = e^{sT}$, from Eq. (23) we have

$$p = K \frac{\epsilon^{sT} - 1}{\epsilon^{sT} + 1} = K \tanh \frac{sT}{2} \tag{27}$$

and

$$s = \frac{2}{T} \tanh^{-1} \frac{p}{K} \tag{28}$$

For $s = jw$, p is imaginary and thus

$$\lambda = K \tan \frac{wT}{2} \tag{29}$$

and

$$w = \frac{2}{T} \tan^{-1} \frac{\lambda}{K} \tag{30}$$

The transformation between λ and w of Equations (29) and (30) is illustrated in Figure 6. The periodic nature of the resulting transfer function can be deduced from the multivalued nature of Eq. (30). Any form of response in λ will be repeated at certain multiples of the sampling rate along the axes.

In any particular approximation problem the constant K is determined from either Eq. (29) or (30) such as to map any particular λ to correspond to any particular w. For example, the given analog function of p might be normalized for a cutoff frequency of 1 rad/sec. Then for a desired cutoff in w, Eq. (29) is solved for K. Thus, if λ_r is to correspond to w_r, K is determined from

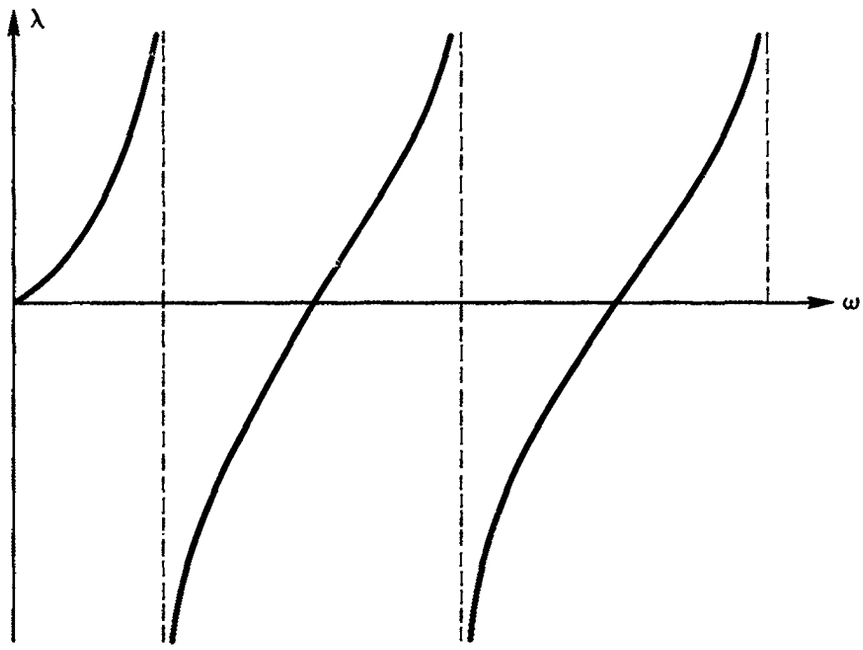

Figure 6

$$K = \frac{\lambda r}{\tan \frac{w_r T}{2}} \tag{31}$$

The bilinear transformation has been shown to possess another interesting feature that will be considered in the next section. It will be shown that if the trapezoidal integration rule is used to approximate an analog system, the resulting numerical operation will be identical with the bilinear transformation applied to the analog function. The reader interested only in practical filter design may omit the next section without loss of continuity.

V. RELATIONSHIP OF BILINEAR TRANSFORMATION TO NUMERICAL INTEGRATION

In this section, the following theorem will be developed and discussed:

Theorem

The bilinear transformation from the p-domain to the z-domain of the form

$$p = \frac{2}{T} \frac{z - 1}{z + 1} \tag{32}$$

is equivalent to applying the trapezoidal integration rule to the set of n-simultaneous differential equations that describe the corresponding analog system.

In order to prove this theorem a few techniques will first be discussed. The first is the well-known trapezoidal rule of integration. Consider a single first-order equation of the following form:

$$\frac{dy}{dt} + by = a_1 \frac{dx}{dt} + a_0 x \tag{33}$$

The best approximation in the first-order sense to Eq. (33) is achieved from the equation

$$\frac{y_n - y_{n-1}}{T} + \frac{b(y_n + y_{n-1})}{2} = a_1 \frac{(x_n - x_{n-1})}{T} + a_0 \frac{(x_n + x_{n-1})}{2} \tag{34}$$

where T is the sampling period. Eq. (34) is a general form of the trapezoidal rule for the first-order linear differential equation. The solution for y_n proceed

$$y_n \left(1 + \frac{bT}{2}\right) - y_{n-1} \left(1 - \frac{bT}{2}\right) = x_n \left(a_1 + \frac{a_0 T}{2}\right) - x_{n-1} \left(a_1 - \frac{a_0 T}{2}\right) \tag{35}$$

or

$$y_n = \frac{\left(1 - \frac{bT}{2}\right)}{\left(1 + \frac{bT}{2}\right)} y_{n-1} + \frac{\left(a_1 + \frac{a_0 T}{2}\right)}{\left(1 + \frac{bT}{2}\right)} x_n - \frac{\left(a_1 - \frac{a_0 T}{2}\right)}{\left(1 + \frac{bT}{2}\right)} x_{n-1} \tag{36}$$

now let

$$Y(p) = \mathcal{L}\,[y(t)] \tag{37}$$

$$X(p) = \mathcal{L}\,[x(t)] \tag{38}$$

$$Y(z) = \mathcal{Z}\,[y(n)] = \mathcal{Z}\,[y_n] \tag{39}$$

$$X(z) = \mathcal{Z}\,[x(n)] = \mathcal{Z}\,[x_n] \tag{40}$$

Assuming that the system is initially relaxed, application of the Laplace transformation to Eq. (33) yields

$$pY(p) + bY(p) = a_1\, p\, X(p) + a_0\, X(p)$$

The transfer function $G(p)$ is

$$G(p) = \frac{Y(p)}{X(p)} = \frac{a_1 p + a_0}{p + b} \tag{41}$$

With the same initial assumption, application of the z-transformation to (35) yields

$$Y(z)\left[\left(1 + \frac{bT}{2}\right) - \left(1 - \frac{bT}{2}\right)z^{-1}\right] = X(z)\left[\left(a_1 + \frac{a_0 T}{2}\right) - \left(a_1 - \frac{a_0 T}{2}\right)z^{-1}\right] \tag{42}$$

The transfer function $H(z)$ is

$$H(z) = \frac{Y(z)}{X(z)} = \frac{\left[\left(a_1 + \frac{a_0 T}{2}\right) z - \left(a_1 - \frac{a_0 T}{2}\right)\right]}{\left[\left(1 + \frac{bT}{2}\right) z - \left(1 - \frac{bT}{2}\right)\right]} \tag{43}$$

The transformation between p and z can be determined by equating the righthand sides of Equations (41) and (43). Thus

$$\frac{a_1 p + a_0}{p + b} = \frac{\left[\left(a_1 + \frac{a_0 T}{2}\right) z - \left(a_1 - \frac{a_0 T}{2}\right)\right]}{\left[\left(1 + \frac{bT}{2}\right) z - \left(1 - \frac{bT}{2}\right)\right]} \tag{44}$$

After some manipulation, the following result is obtained:

$$p = \frac{2}{T} \frac{z - 1}{z + 1} \tag{45}$$

which is clearly the bilinear transformation with $K = 2/T$. With this choice of K, the relationship between λ and w is

$$\lambda = \frac{2}{T} \tan \frac{wT}{2} \tag{46}$$

For very low frequencies,

$$\lambda \approx w \text{ for } w << \frac{\pi}{T} \tag{47}$$

Thus, the trapezoidal approximation is seen to yield an approximate one-to-one correspondence between the analog domain and the digital domain for very low frequencies.

The quantities $H(z)$ and $G(p)$ are related by

$$H(z) = G\left(\frac{2}{T} \frac{z - 1}{z + 1}\right) \tag{48}$$

as proposed.

The theorem originally stated has thus been proved for the first order case. The extension to the more general order can best be achieved by means of the state-variable approach. The state variable formulation represents a system of order n by n first order equations of the given form. It can be shown that one possible form for expressing such a system can be achieved by the techniques to follow.

It can be shown that a lumped, linear, time-invariant system can be described by a differential equation of the form.

$$\frac{d^n y}{dt^n} + b_{n-1} \frac{d^{n-1} y}{dt^{n-1}} + \cdot \cdot \cdot b_0 y = a_n \frac{d^n x}{dt^n} + a_{n-1} \frac{d^{n-1} x}{dt^{n-1}} + \cdot \cdot \cdot + a_0 x \tag{49}$$

which is equivalent to the transfer function

$$G(p) = \frac{a_n p^n + a_{n-1} p^{n-1} + \cdot \cdot \cdot \cdot \cdot + a_0}{p^n + b_{n-1} p^{n-1} + \cdot \cdot \cdot \cdot \cdot + b_0} \tag{50}$$

Let

$$\begin{aligned} y_1 &= \frac{d^{n-1} y}{dt^{n-1}} \\ y_2 &= \frac{d^{n-2} y}{dt^{n-2}} \\ &\vdots \\ y_n &= y \end{aligned} \tag{51}$$

The following constants are defined:

$$\begin{aligned} A_n &= a_n \\ A_{n-1} &= a_{n-1} - b_{n-1} A_n \\ A_{n-2} &= a_{n-2} - b_{n-1} A_{n-1} - b_{n-2} A_n \\ A_1 &= a_1 - b_{n-1} A_2 - b_{n-2} A_3 \cdot \cdot \cdot \cdot \cdot b_1 A_n \end{aligned} \tag{52}$$

The system can then be described by the equations

$$\frac{dy_1}{dt} + b_{n-1}\, y_1 + b_{n-2}\, y_2 + \cdots + b_0 = A_1 \frac{dx}{dt} + a_0\, x$$

$$\frac{dy_2}{dt} - y_1 = A_2 \frac{dx}{dt} \tag{53}$$

$$\frac{dy_n}{dt} - y_{n-1} = A_n \frac{dx}{dt}$$

Let

$$\bar{y} = \begin{bmatrix} y_1 \\ y_2 \\ \vdots \\ y_n \end{bmatrix} \tag{54}$$

$$[B] = \begin{bmatrix} b_{n-1} & b_{n-1} & \cdots & b_0 \\ -1 & 0 & \cdots & 0 \\ 0 & -1 & 0 \cdots & 0 \\ \vdots & & & \vdots \\ 0 & \cdots & 0 & -1 \quad 0 \end{bmatrix} \tag{55}$$

$$\bar{A} = \begin{bmatrix} A_1 \\ A_2 \\ A_n \end{bmatrix} \quad \bar{A}_0 = \begin{bmatrix} a_0 \\ 0 \\ 0 \end{bmatrix} \tag{56}$$

Then, the set of equations of (53) are equivalent to

$$\frac{d\bar{y}}{dt} + [B]\, \bar{y} = \bar{A} \frac{dx}{dt} + \bar{A}_0\, x \tag{57}$$

which places the entire system in matrix form in a manner analogous to that of the simple first-order equation. The extension of the theorem can be done on the individual equations as in (53) or on the matrix form in (57).

VI. PRACTICAL "LOW-PASS" DIGITAL FILTER DESIGN

The problem of the practical design of low-pass digital filters will be considered in this section. Strictly speaking, such a filter should actually be termed a pseudo-low-pass filter due to its periodic nature as previously discussed. The form of a typical characteristic is shown in Figure 7. Thus, if a true low-pass action is desired, the sampling rate must be considerably higher than the "cutoff" frequency, and accurate digital-to-analog conversion must be employed.

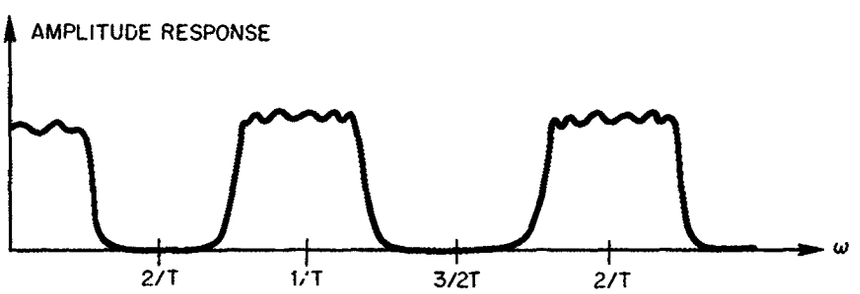

Figure 7

Using the bilinear transformation, the technique for synthesizing a filter from the transfer function can be summarized as follows:

1. Using the theory of the analog approximation problem, obtain a transfer function for the low-pass filter of the desired form in the analog domain. In this context, the ITT Handbook (12) contains response curves for the Butterworth, Chebyshev, and maximally flat-time delay filters, and the text by Weinberg (13) contains normalized element values. Any of the other texts on network synthesis can be employed in this task.

   Thus, by some standard approximation method, a function of p, say $G(p)$, is obtained as a ratio of polynomial representing the desired response in the analog domain. It is not necessary (or desirable) to denormalize $G(p)$ at this point such that the cutoff frequency in the analog domain has some unique correspondence to the cutoff frequency in the digital domain. Rather it is simpler to develop a normalized $G(p)$ such that $p = j\lambda = j1$ is the reference frequency in the analog domain. The total process of normalization results from step 2 to follow.

2. The second step is the determination of the normalization constant K. Assume that some particular reference analog frequency, λ_r, is to correspond to some final real reference frequency w_r. The quantity K is determined from the relationship

$$K = \lambda_r \cot \frac{w_r T}{2} \tag{58}$$

3. With K known, the final transfer function $H(z)$ is determined by substituting

$$p = K \frac{z-1}{z+1} \tag{59}$$

into $G(p)$. In other words

$$H(z) = G(p)\Big]_{p = \frac{k(z-1)}{(z+1)}} \tag{60}$$

4. The quantity $H(z)$ is arranged in descending powers of z and synthesized according to the technique of Sec. III.

5. If a plot of the frequency response of the digital filter is desired, the transformation curve of Figure 8 can be used as will be discussed in the next section. Notice that the abscissa of the curve is the normalized quantity f/f_T, where

$$f_T = \frac{1}{2T} = \text{half of sampling rate} \tag{61}$$

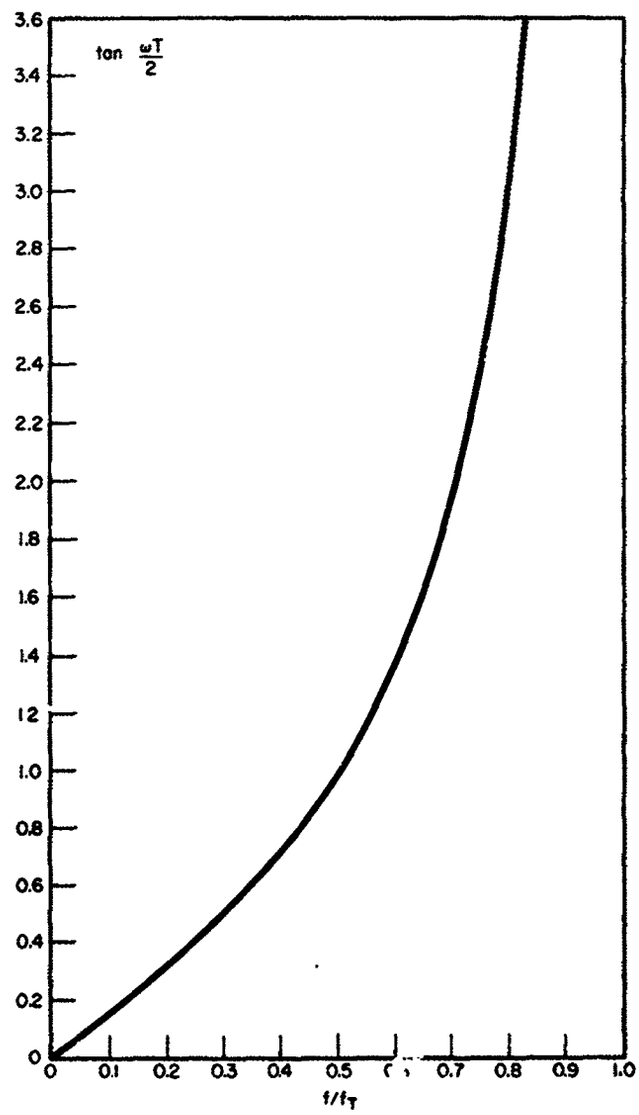

Figure 8

VII. LOW PASS DESIGN EXAMPLES

Example 1. A second-order filter of the Butterworth or maximally-flat class will be synthesized with the following specifications:

Sampling Frequency = $f_s = 1/T = 2$ kc

Cutoff Frequency = $f_c = 500$ cps = 0.5 kc

The analog response for such a filter with $\lambda_c = 1$ rad/sec is shown by Van Valkenburg (14) to be

$$G(p) = \frac{1}{p^2 + \sqrt{2}\, p + 1} \tag{62}$$

The constant K must now be determined such that $\lambda = 1$ maps into $w = 2\pi \times 500$ rad/sec. Thus, from Eq. (58)

$$K \quad \cot \frac{500\pi}{2000} = 1 \tag{63}$$

The desired transformation is

$$p = \frac{z - 1}{z + 1} \tag{64}$$

which substituted into Eq. (62) yields

$$H(z) = \frac{z^2 + 2z + 1}{(2 + \sqrt{2})\, z^2 + (2 - \sqrt{2})} \tag{65}$$

This can be put in the proper form for programming by dividing numerator and denominator by $(2 + \sqrt{2})\, z^2 = 3.4142$. Thus,

$$H(z) = \frac{0.29289\,(1 + 2z^{-1} + z^{-2})}{1 + 0.82841\, z^{-2}} \tag{66}$$

The appropriate algorithm is

$$y_n = 0.29289\,(x_n + 2x_{n-1} + x_{n-2}) - 0.82841\, y_{n-2} \tag{67}$$

A curve of the frequency response may be plotted by using the ITT Handbook curves and the transformation curve of Figure 8. A number of points are tabulated in the following table. The quantity G(db) represents the input-output attenuation in decibels obtained from the curves, and the quantity G represents the magnitude of output to input. A plot of several "cycles" of the response is shown in Figure 9. In this case the periodic nature of the response is quite apparent due to the low-ratio of sampling frequency to cutoff frequency.

λ	.3	.4	.5	.6	.7	.8	.9	1.0	1.5	2	2.5	∞
G(db)	.05	.11	.28	.54	.94	1.48	2.15	3	8	12	16	∞
G			.968	.94	.897	.84	.78	.707	.395	.25	.158	0
f/1kc			.3	.345	.39	.43	.47	.5	.623	.705	.76	1.0

Note: Table is accurate only to slide rule and curve accuracy.

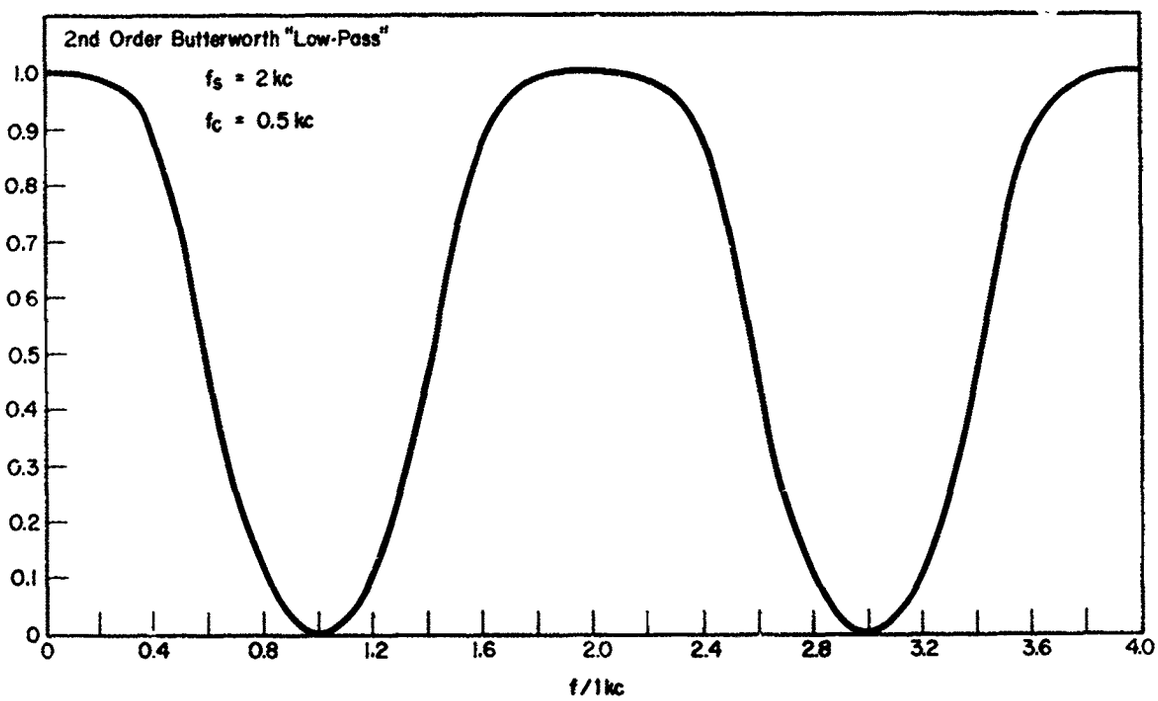

Figure 9

Example 2. As a more complex example, a fourth-order Chebyshev filter will be synthesized to meet the following specifications:

Pass-band Ripple = ϵ = 1 db

f_s = 2 kc

f_c = 200 cps = 0.2 kc

The "cutoff" frequency in this case is considered to be the last 1 db-down frequency. For w_c = 1, the analog transfer function is

$$G(p) = \frac{1}{1 + 2.6943\,p + 5.2748\,p^2 + 3.4568\,p^3 + 3.6280\,p^4} \tag{68}$$

The constant K is determined from Eq. 58 with $\lambda r = 1$ and $wr = 2\pi \times 200$

$$K = \cot \frac{\pi}{10} = \cot 18^\circ = 3.0777 \tag{69}$$

The transformation is

$$p = 3.0777 \frac{z - 1}{z + 1} \tag{70}$$

Substitution of Eq. (70) into Eq. (68) yields after a lengthy but straight-forward computation

$$H(z) = \frac{0.024717\,(1 + 4z^{-1} + 6z^{-2} + 4z^{-3} + z^{-4})}{1 - 3.0543z^{-1} + 3.8290z^{-2} - 2.2925z^{-3} + 0.550742^{-4}} \tag{71}$$

The associated algorithm is

$$y_n = 0.024717\,[x_n + 4x_{n-1} + 6x_{n-2} + 4x_{n-3} + x_{n-4}] + 3.0543\,y_{n-1}$$

$$- 3.8290\,y_{n-2} + 2.2925\,y_{n-3} - 0.55\text{v}74\,y_{n-4} \tag{72}$$

A table consisting of a few points of the frequency response is shown below, and a plot of this response is shown in Figure 10.

λ	0	.383	.707	.924	1	1.05	1.58	2.1	2.63	∞
$\frac{\lambda}{*3.0777}$	0	.124	.23	.3	.325	.341	.513	.683	.855	∞
f/1kc	0	.08	.14	.18	.2	.21	.305	.38	.455	.5
G(db)	1	0	1	0	1	3	24	36	45	∞
G	.891	1	.891	1	.891	.707	.063	.016	.006	0

Note: Table is accurate only to slide rule and curve accuracy.

*Since $p = 3.0777 \frac{z - 1}{z + 1} = 3.0777 \tanh \frac{sT}{2}$,

$$\lambda = 3.0777 \tan \frac{wT}{2} \text{ or } \frac{\lambda}{3.0777} = \tan \frac{wT}{2}$$

VIII. BAND-PASS FILTER TRANSFORMATION

The techniques under consideration may be used to design a pseudo-band-pass filter of which a typical frequency response curve is sketched in Figure 11. As in the low-pass case, the response is periodic along the w-axis. The point that characterizes the band-pass case is the fact that in the first "cycle," the pass-band occurs somewhere removed from the lowest frequencies.

One way to approach the design of a band-pass filter is to first obtain the transfer function of an analog band-pass filter and employ the method of the preceding two sections. However, this method may require a lengthy set of computations in the analog domain, and the transformation in maintaining correct bandwidth is more difficult to interpret. Rather a method will be developed that will yield directly a band-pass digital filter from a low-pass analog prototype by means of an extension of the basic bilinear transformation.

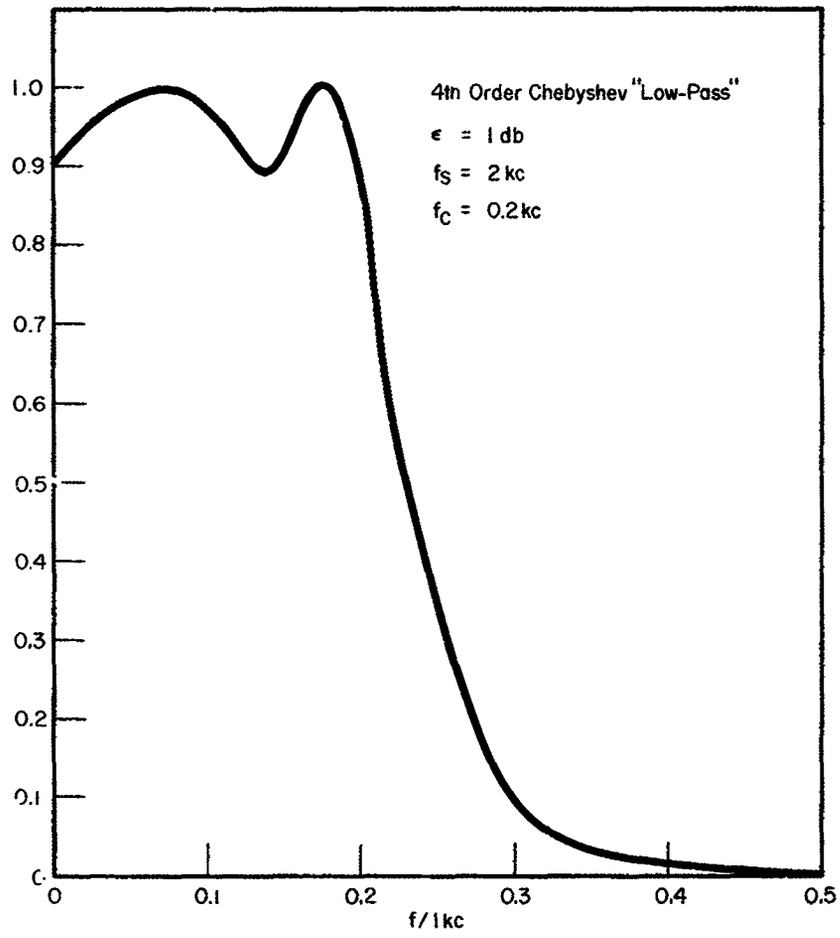

Figure 10

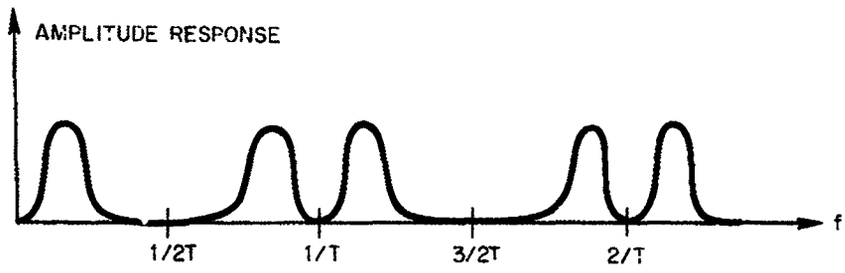

Figure 11

Assume then that a given low-pass prototype is known in the analog domain with transfer function $G(p)$. It will be shown that the following transformation will yield a pseudo-band-pass digital filter.

$$p = A\left[\frac{z-1}{z+1} + \frac{a^2(z+1)}{(z-1)}\right] \tag{73}$$

$$= A\left[\tanh\frac{ST}{2} + a^2\coth\frac{ST}{2}\right] \tag{74}$$

The relationship between the w-axis and the λ-axis is obtained by letting $s = jw$ and $p = j\lambda$. The result is

$$\lambda = A\left[\tan\frac{wT}{2} - a^2\cot\frac{wT}{2}\right] \tag{75}$$

Let

$$x = \frac{\tan wT/2}{a}, \tag{76}$$

Then Eq. 75 reduces to

$$\lambda = aA\left[x - \frac{1}{x}\right] \tag{77}$$

which is equivalent to the normalized low-pass to band-pass transformation of analog filter theory. Sketches of Equations (75) and (76) are shown in Figure 12.

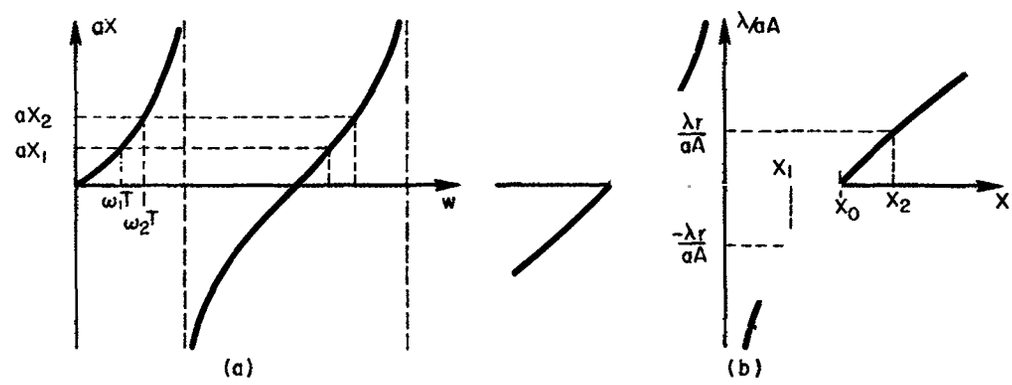

Figure 12

From Figure 12b, it can be observed that for a low-pass reference frequency λr and the corresponding negative frequency $-\lambda r$, there exists two values of x, x_1, and x_2 that lie on either side of some "band-center" x_0. Of course, x_0 corresponds to d-c on the λ-axis.

It can be readily shown that

$$x_0^2 = x_1 x_2 \tag{78}$$

From Figure 12a, it can be seen that the points x_0, x_1, and x_2 map to some band-pass region on the w-axis. In addition, there are other band-pass regions as expected.

From Equations (78) and (76) the following relationship is easily derived:

$$\tan^2 \frac{w_0 T}{2} = \tan \frac{w_1 T}{2} \tan \frac{w_2 T}{2} \tag{79}$$

Letting $\lambda = 0$, and $w = w_0$ in Eq. (75) results in

$$\tan^2 \frac{w_0 T}{2} = a^2 \tag{80}$$

Thus Eq. (79) reduces to

$$\tan \frac{w_1 T}{2} - \tan \frac{w_2 T}{2} = a^2 \tag{81}$$

IX. PRACTICAL "BAND-PASS" DIGITAL FILTER DESIGN

As a prelude to explaining the steps in a band-pass filter design, it will be assumed that the following parameters are specified:

lower "cutoff" frequency = w_1

upper "cutoff" frequency = w_2

bandwidth = $w_2 - w_1$

In some cases it may be desirable to specify the "center" frequency W_0, although it is more convenient to use the upper and lower frequency references, and this is the only case that will be considered. The design steps follow:

1. Obtain an analog low-pass transfer function of the type desired in the band-pass of the digital filter from an appropriate approximation technique. The most convenient choice of "cutoff" frequency in the low-pass prototype is $\lambda = 1$.

2. Determine the constants a^2 and A from the relationships:

$$a^2 = \tan \frac{w_1 T}{2} \tan \frac{w_2 T}{2} \tag{82}$$

$$A = \frac{\lambda r}{\tan \frac{w_2 T}{2} - \tan \frac{w_1 T}{2}} \tag{83}$$

where λr is usually the reference low-pass "cutoff" frequency.

3. The required transformation is

$$P = A\left[\frac{z-1}{z+1} + \frac{a^2(z+1)}{(z-1)}\right] \tag{84}$$

This expression is substituted into $G(p)$ thus yielding $H(z)$.

4. The quantity $H(z)$ is synthesized according to the techniques of Sec. III.

5. If desired, the frequency response of the filter may be plotted with the aid of Figure 13 and Figure 8 of Sec. VI.

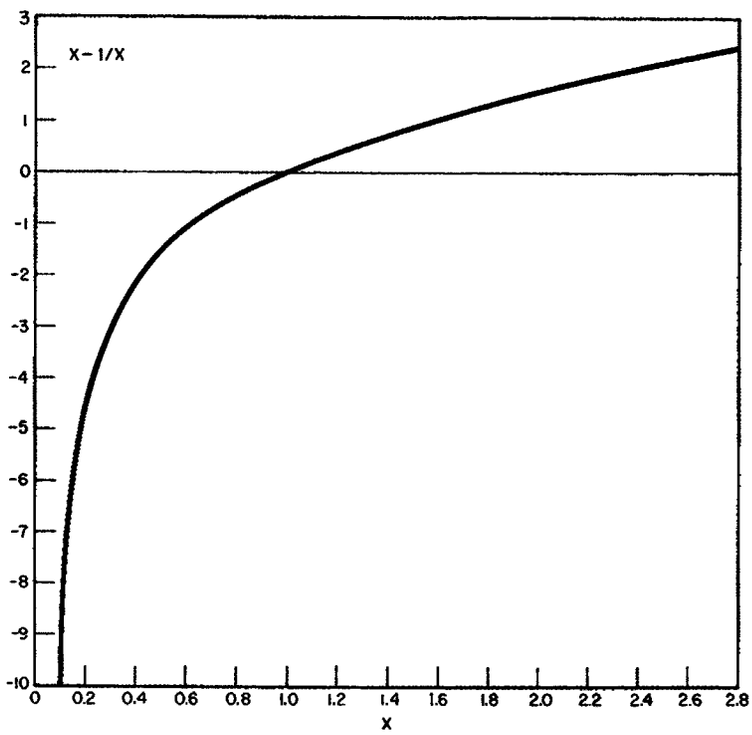

Figure 13

X. BAND PASS DESIGN EXAMPLE

As an illustration of the design procedure, a band-pass filter will be designed using the low-pass prototype of Example 2 in Section VII. The low-pass prototype was a Chebyshev filter with 1 db ripple in the pass band and a normalized cutoff frequency of $\lambda = 1$. Suppose the following band-pass specifications are given:

$f_s = 2$ kc

$f_1 = 300$ cps $= 0.3$ kc

$f_2 = 400$ cps $= 0.4$ kc

$BW = 400 - 300 = 100$ cps $= 0.1$ kc

The low-pass prototype is

$$G(p) = \frac{1}{1 + 2.6943p + 5.2748p^2 + 3.4568p^3 + 3.6280p^4} \tag{85}$$

The constants a^2 (along with a) and A are determined from Equations (82) and (83)

$$\begin{aligned} a^2 &= \tan .15\pi \tan .2\pi \\ &= \tan 27^\circ \tan 36^\circ \\ &= 0.50953 \times 0.72654 \\ &= 0.37019 \end{aligned} \tag{86}$$

$$a = 0.6084 \tag{87}$$

$$\begin{aligned} A &= \frac{1}{\tan 36^\circ - \tan 27^\circ} \frac{1}{0.72654 - 0.50953} \\ &= 4.6081 \end{aligned} \tag{88}$$

The required transformation is

$$p = 4.6081 \left[\frac{z-1}{z+1} + \frac{0.37019\,(z+1)}{(z-1)} \right] \tag{89}$$

which may be inserted into Eq. (85) to yield $H(z)$, the desired transfer function. The procedure is straightforward, but the computations are rather lengthy and messy for this case. Consequently, the actual synthesis will not be carried to completion for this case. As a final exercise for this example, the frequency response will be plotted. Figures 8 and 13 and the low-pass tabulated data may be used in this context. Consider the normalized forms of Equations (76) and (77) which are repeated

$$\lambda = aA \left(x - \frac{1}{x} \right) \tag{90}$$

where

$$x = \frac{\tan wT/2}{a} \tag{91}$$

These equations are further written as

$$\frac{\lambda}{aA} = x - \frac{1}{x} \tag{92}$$

and

$$ax = \tan wT/2 \tag{93}$$

Thus the vertical axis of Figure 13 is interpreted as λ/aA and the vertical scale of Figure 8 is interpreted as ax. The quantity aA is numerically equal to 2.804. Hence,

$$\frac{\lambda}{2.804} = x - \frac{1}{x} \tag{94}$$

and

$$0.6084\, x = \tan wT/2 \tag{95}$$

The results are tabulated below, and a plot is shown in Figure 14.

λ	0	.383	.707	.924	1	1.05	1.58	2.1	2.63		
G	.891	1	.891	1	.891	.707	.603	.016	.006	0	
$\lambda/2.8$	0	.137	.252	.33	.357	.375	.564	.75	.94		
X_a	1	.935	.88	.84	.835	.83	.755	.7	.64	0	
X_b		1.08	1.14	1.19	1.2	1.215	1.32	1.445	1.62	1.44	1
.608 X_a	.608	.568	.535	.511	.507	.504	.459	.425	.389	0	
.608 X_b		.657	.693	.723	.73	.739	.802	.876	.973		
f_a/1 kc	.35	.33	.313	.3	.299	.298	.275	.255	.233	0	
f_b/1 kc		.369	.387	.4	.401	.402	.431	.458	.492	1	

Note: Table is accurate only to slide-rule and curve accuracy.

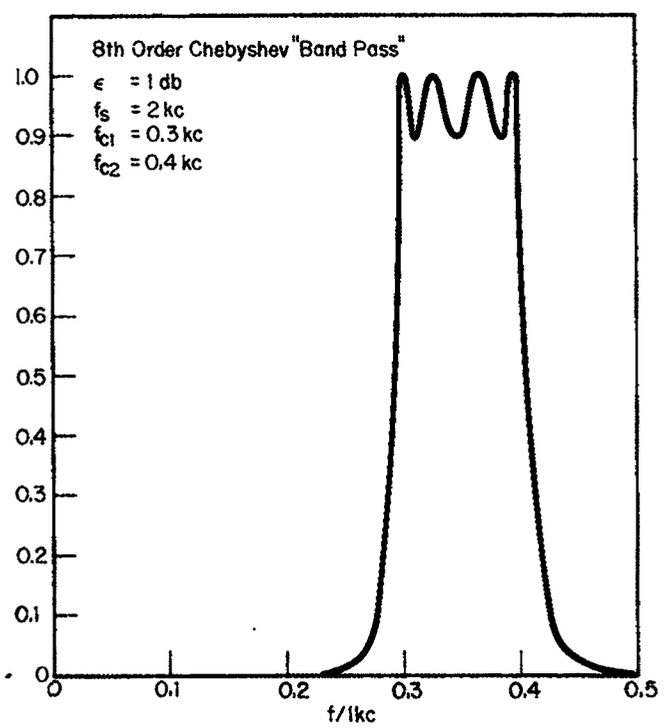

Figure 14

XI. SUMMARY

Digital Filters provide a means for altering the spectral representation of sampled data in the same manner as RLC filters do for continuous analog data. Furthermore, the versatility of the computer allows the filter characteristic to be quickly changed to conform to rapidly changing characteristics of telemetry data.

In a sense all digital filters have periodic frequency response characteristics. However, if the sampling rate is chosen sufficiently high and if accurate digital-to-analog conversion is employed, the periodic effect of the response may be removed.

The procedures presented in this paper depend on the bilinear transformation to map an analog domain response into the digital domain. The approximation problem is first performed in the analog domain using conventional network synthesis tables, and then this response is mapped into the digital domain. The use of the z-transform results in a numerical algorithm that can be easily programmed on a computer.

REFERENCES

1. J. R. Ragazzini and G. F. Franklin, "Sampled Data Control Systems," McGraw-Hill Book Co., Inc., New York, N. Y., 1958.

2. E. I. Jury, "Sampled Data Control Systems," John Wiley and Sons, Inc., New York, N. Y., 1958.

3. I. T. Tou, "Digital and Sampled-Data Control Systems," McGraw-Hill Book Co., Inc., New York, N. Y., 1959.

4. A. J. Monroe, "Digital Processes for Sampled Data Systems," John Wiley and Sons, Inc., New York, N. Y., 1962.

5. B. C. Kuo, "Analysis and Synthesis of Sampled-Data Control Systems," Prentice-Hall, Inc., Englewood Cliffs, N. J., 1963.

6. K. Steiglitz, "The Approximation Problem for Digital Filters," Technical Report 400-56, Department of Electrical Engineering, School of Engineering and Science, New York University, March 1962.

7. K. Steiglitz, "The General Theory of Digital Filters with Applications to Spectral Analysis," D. Sc. Thesis, Department of Electrical Engineering, School of Engineering and Science, New York University, May 1963.

8. A. Hauptschein, "Digital Filter Design," Technical Memorandum 35, Department of Electrical Engineering, School of Engineering and Science, New York University, January 20, 1964.

9. G. W. Johnson, D. P. Lindorff, and C. G. A. Nordling, "Extension of Continuous-Data System Design Techniques to Sampled-Data Control Systems," AIEE Transactions, vol. 74, pt II, 1955, pp. 252-263.

10. P. M. Lewis II, "Synthesis of Sampled-Signal Networks," IRE Trans. on Circuit Theory, Vol. CT-5, March 1958, pp. 74-77.

11. R. Carney, "Design of a Digital Notch Filter with Tracking Requirements," IEEE Trans. on Space Electronics and Telemetry, Vol. SET-9, December 1963, pp. 109-114.

12. International Telephone & Telegraph Co., "Reference Data for Radio Engineers," 1956.

13. L. Weinberg, "Network Analysis and Synthesis," McGraw-Hill Book Co., Inc., New York, N. Y., 1962.

14. M. E. Van Valkenburg, "Introduction to Modern Network Synthesis," John Wiley and Sons, Inc., New York, N. Y., 1960.

N66 31156

DESIGN PROBLEMS IN A CONTROL SYSTEM USED FOR PRECISE OPTICAL TRACKING OF SATELLITES AND STARS

by

Dr. Richard V. Monopoli,
Associate Professor, University of Massachusetts
Amherst, Massachusetts
ASEE-NASA Faculty Fellowship Program

I. INTRODUCTION

Tracking of satellites and stars with optical devices requires that these devices be precisely pointed in space. A system for obtaining a high degree of pointing accuracy is currently being developed at the Goddard Space Flight Center by the Automatic Control Group of the Antenna Systems Branch. Called the "multi-mode mount," it consists of a two gimbal structure capable of positioning optical equipment weighing 3,500 pounds and having maximum dimensions of 14 feet in length and three feet in diameter. The angles of the gimbals' axes correspond to X and Y position coordinates of the object being tracked. The specified position accuracy is 0.0001 degrees in both coordinates, and the system is required to move smoothly at rates from 0.001 degrees per second to 5 degrees per second in order to track stars as well as low altitude satellites.

The control system for the multi-mode mount is to be a hybrid (digital-analog) type consisting of a "tight" inner rate loop and a relatively "loose" outer position loop. This same scheme is applied independently to both the X and Y axes. A functional block diagram for the X axis control system is shown in Figure 1. Digital position and rate feedback signals are obtained from digital encoders located on the axes of the gimbals. These encoders provide position information accurate to within ±0.001 degree. Analog rate signals are also available from dc tachometer generators mounted on the axes.

Though both loops operate on digital signals, the equivalent sampling rate of the inner loop under most operating conditions is high enough to assume that the signals are analog.

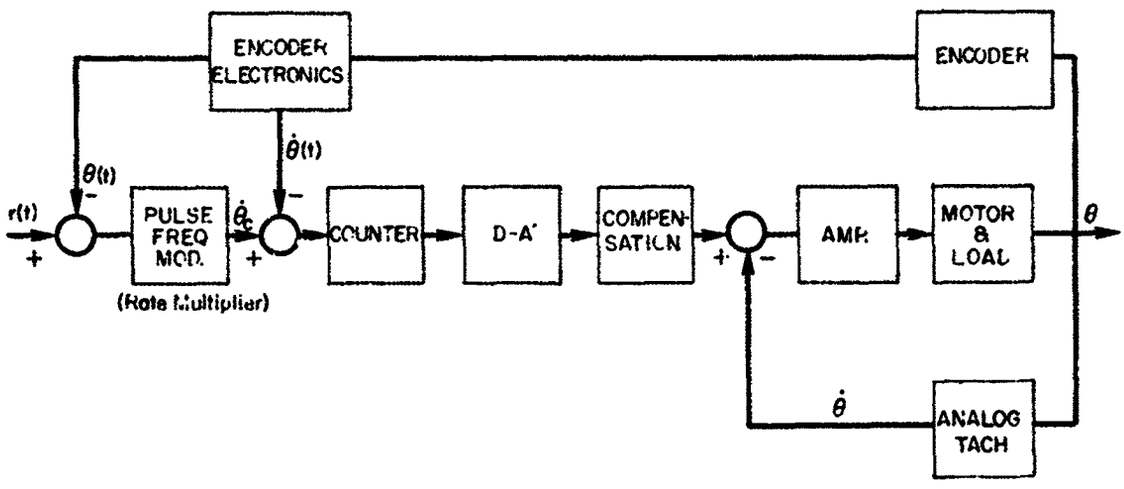

Figure 1–System Functional Block Diagram

This is not true, however, in the case of the outer loop. Thus, a continuous signal analysis is applicable to the design of the inner loop, but discrete signal analysis must be applied to the outer loop. Quantization effects were not included in the initial analysis. Errors due to quantization should be small since quantization is in steps of 0.0001 degree.

The study performed by this author relates to system input requirements in the program mode of operation, analysis of experimental results obtained in the rate mode of operation, and compensation requirements for the rate loop. In the program mode, the input is to the position loop and consists of a digital signal corresponding to the sampled and held value of the satellite's position T seconds in the future. Sampling is performed once every T seconds. The present mount position is subtracted from this signal, and the difference is sampled and held for T seconds. A rate signal generated on the basis of the sampled difference drives the rate loop at a rate required to reduce the difference to zero in T seconds. The rate signal is constant over the T second interval. In the rate mode, the position loop is open and a command rate signal is applied directly to the rate loop. Experimental results referred to for this mode of operation were limit cycles of unacceptably large amplitude which occurred when driving the system at low rates.

The analysis of the system input requirements in the program mode showed that in the case of a satellite with a 100-mile orbit on a worst case (horizon) pass, the sampling period, T, must be less than 0.282 second to obtain errors less than 0.001 degrees. An alternative solution is proposed in which the input to the position loop is derived from the satellite's present position, velocity, and acceleration. With this input a sampling period of one second would be sufficient to maintain 0.001 degree accuracy.

From an analysis of the experimental results, it was determined that the most likely cause of the undesired limit cycles is the stick-slip phenomena associated with bearing static friction. To eliminate this problem, the damping of the rate loop must be increased. This in turn requires a reduction of the rate loop bandwidth and a concomitant decrease in response time. A design was suggested in which a feedforward path in the rate loop is used to maintain required response time while allowing a reduction of loop bandwidth and an increase in loop damping.

This report is divided into four sections exclusive of Introduction and Conclusions. Section II deals with pulse models of the system to which z transform analysis may be applied. In Section III, requirements for the reference input are discussed. An analysis of experimental results is given in Section IV, and some design suggestions are included in Section V.

II. SIMPLIFIED MODEL FOR DISCRETE TIME ANALYSIS

In order to arrive at a mathematically tractable pulse model for the system, some simplifying assumptions must be made. First the quantizing effect due to the D/A converter in the digital tach loop is neglected. Since the quantization level is quite small, this should not lead to serious errors. Next, the digital tach loop transfer function is assumed to be simply 1/s. This assumption neglects dynamics which should have a short transient relative to the sampling period T. On this basis the pulse model in Figure 2 applies.

In the figure, H and G are the Laplace transforms of the hold and digital tach loop respectively, T is the sampling period, $\dot{\theta}_c$ is the command rate, i.e., the output of the rate multiplier, and R(s) is the reference input which is discussed in detail in Section III. The actual dynamics and design of the digital tach loop are considered in Section V.

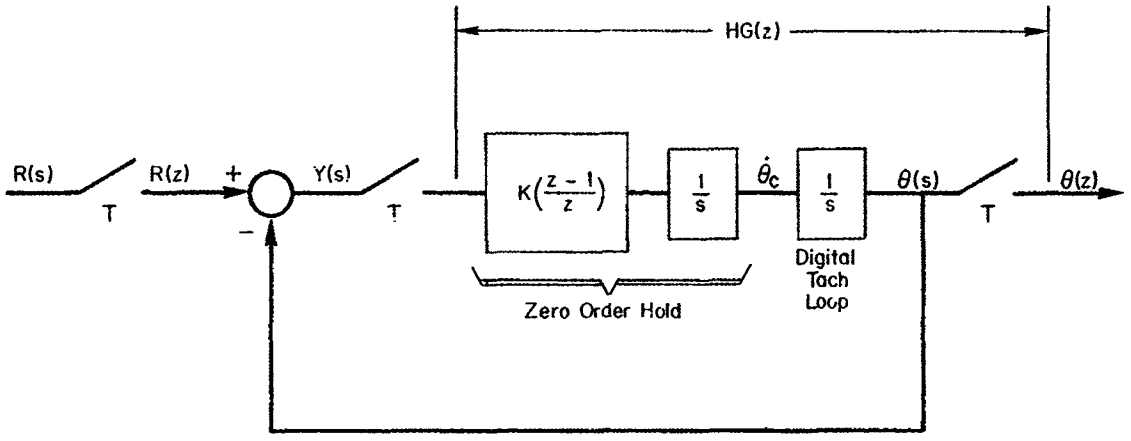

Figure 2–Pulse Model for Simplified System

The basis for the z transform analysis to be applied to the pulse model may be found in many texts. Several are listed as References 1 and 2. The analysis is as follows:

Let the integration of the zero order hold be combined with the integration representing the digital tach loop to form a single transfer function G_1 which is

$$G_1(s) = \frac{1}{s} G(s) = \frac{1}{s^2} \tag{1}$$

In this way, the problem of finding $HG(z)$ is reduced to finding the z transform of $G_1(s)$. This is

$$Z\left\{ G_1(s) \right\} = \frac{Tz}{(z-1)^2} \tag{2}$$

Use of (2) allows $HG(z)$ to be determined as

$$HG(z) = \frac{K(z-1)}{z} \cdot \frac{Tz}{(z-1)^2} = \frac{KT}{z-1} \tag{3}$$

The closed loop pulse transfer function relating $\theta(z)$ and $R(z)$ is found to be

$$\frac{\theta(z)}{R(z)} = \frac{HG(z)}{1 + HG(z)} = \frac{KT}{z - 1 + KT} \tag{4}$$

For $KT = 1$, (4) becomes

$$\frac{\theta(z)}{R(z)} = \frac{1}{z}; \quad (KT = 1) \tag{5}$$

It is necessary to consider the nature of the reference input, $r(t)$, to determine whether or not the closed loop pulse transfer function given by (5) is desirable. The reference input presently used is

$$r(t) = \theta_r(nT+T)\,;\; nT \leqq t \leqq nT+T \tag{6}$$

where $\theta_r(t)$ is the computed value of present satellite position.

Since the reference input used is the satellite position one sample period in advance of present time, the following z transform relationship holds

$$Z\left\{r(t)\right\} = zZ\left\{\theta_r(t)\right\} \tag{7}$$

If (7) is combined with (5) the result is

$$\frac{\theta(z)}{\theta_r(z)} = 1 \tag{8}$$

where $\theta_r(z)$ is the z transform of $\theta_f(t)$.

According to (8), (5) is a desirable transfer function since with the $r(t)$ used, it results in the output being identically equal to the computed satellite position at least at the sampling instants.

The above analysis is only approximate since the digital loop transfer function is not a pure integrator as assumed. It is well to investigate the situation when a better approximation to the digital tach loop transfer function is used. Toward this end, let $G(s)$ be given by

$$G(s) = \left[s\left(\frac{s}{a_1}+1\right)^2\right]^{-1} \tag{9}$$

Then $G_1(s)$ is

$$G_1(s) = \left[s^2\left(\frac{s}{a_1}+1\right)^2\right]^{-1} \tag{10}$$

and the z transform of $G_1(s)$ becomes,[1]

$$G_1(z) = \frac{g_1(T)\,z\,(z-\beta_1)(z-\beta_2)}{(z-1)^2(z-\alpha_1)^2} \tag{11}$$

where $\alpha_1 = e^{-a_1T}$, β_1 and β_2 are solutions of

$$\beta^2 - \frac{2(2\alpha_1 a_1 T + \alpha_1^2 - 1)}{2\alpha_1 + \alpha_1 a_1 T - 2 + a_1 T}\beta + \alpha_1 = 0$$

and

$$g_1(T) = \frac{T(1-\alpha_1)^2}{(1-\beta_1)(1-\beta_2)}$$

The values of β_1 and β_2 may be found from curves on page 79 of Reference 1.

The solution for $HG(z)$ in the case becomes

$$HG(z) = \frac{Kg_1(T)(z-\beta_1)(z-\beta_2)}{(z-1)(z-a_1)^2} \tag{12}$$

The closed loop pulse transfer function corresponding to (12) is

$$\frac{\theta}{R}(z) = \frac{Kg_1(T)(z-\beta_1)(z-\beta_2)}{(z-1)(z-a_1)^2 + Kg_1(T)(z-\beta_1)(z-\beta_2)} \tag{13}$$

Making use of (7) in (13) gives

$$\frac{\theta}{\theta_r}(z) = \frac{Kg_1(T)\,z(z-\beta_1)(z-\beta_2)}{(z-1)(z-a_1)^2 + Kg_1(T)(z-\beta_1)(z-\beta_2)} \tag{14}$$

The design parameters available in (14) are K, T, and a_1. If the desired response cannot be obtained through selection of these parameters, then digital compensation must be added. This may be done either within the position loop or before it in the form of a prefilter.

III. REQUIREMENTS FOR THE REFERENCE INPUT

In order for $\theta(t)$ to track $\theta_r(t)$ within a few seconds of arc, the reference input $r(t)$ must meet certain requirements. It is the purpose of this section to determine what these requirements are.

The system is represented in simplifed form in Figure 3.

The command rate $\dot{\theta}_c$ is generated from $y(t)$ and is constant over period T. For the purpose of determining requirements on the reference input, assume that the loop L_1 is such that $\dot{\theta}(t) \equiv \dot{\theta}_c$, i.e., it follows the command rate exactly.

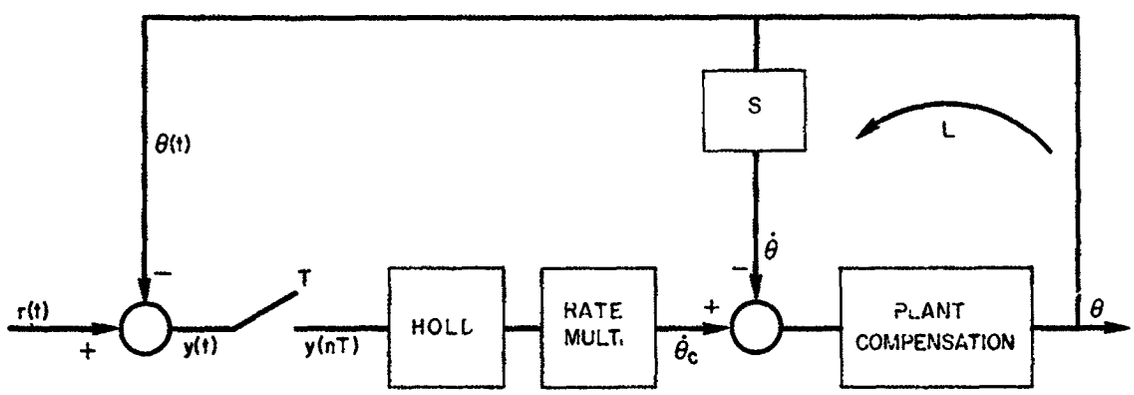

Figure 3–Simplif.ed Functional Diagram

The command rate, and thus $\dot{\theta}$, during the nth sampling period is given by

$$\dot{\theta}(t) = \dot{\theta}_c(t) = \frac{y(nT)}{T} - \frac{r(nT) - \theta(nT)}{T}; \quad nT \leq t \leq (n+1)T \tag{15}$$

If the reference input is given by

$$r(t) = \theta_r(nT + T); \quad nT \leq t \leq (n+1)T \tag{16}$$

then an equivalent representation for the system input is as shown in Figure 4.

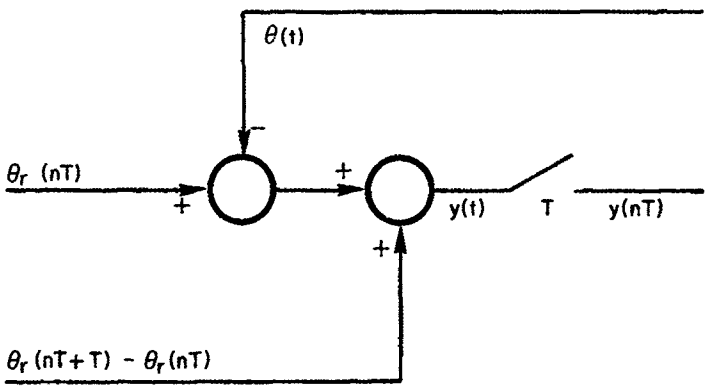

Figure 4—Equivalent Representation for System Input

This representation is derived through use of the relationship

$$y(t) = \theta_r(nT+T) - \theta(t) = \theta_r(nT+T) - \theta_r(nT) + \theta_r(nT) - \theta(t) \tag{17}$$

Substitution of (17) into (15) gives

$$\dot{\theta}(t) = \frac{\theta_r(nT+T) - \theta_r(nT)}{T} + \frac{\theta_r(nT) - \theta(nT)}{T} \tag{18}$$

The first term on the right side of (18) is an approximation to $\dot{\theta}_r(t)$, while the second is an additional component of velocity to correct for the error $e(nT)$ existing at the beginning of the nth interval. Since the first term is only an approximation to $\dot{\theta}_r(t)$, then the ultimate error will depend on the accuracy of this approximation. In order to demonstrate this, consider an interval for which

$$e(nT) = \theta_r(nT) - \theta(nT) = 0 \tag{19}$$

Then integration of (18) for the interval of interest gives

$$\theta(t) = \theta(nT) + \frac{\left[\theta_r(nT+T) - \theta(nT)\right]\tau}{T} \tag{20}$$

for $0 \leq \tau \leq T$ where $\tau = t - nT$

Thus, during this interval,

$$e(t) = \theta_r(t) - \theta(t)$$

$$= -\frac{\left[\theta_r(nT+T) - \theta_r(nT)\right]\tau}{T} + \theta_r(t) \tag{21}$$

where $\theta_r'(t) = \theta_r(t) - \theta_r(nT)$

It is clear from (21) that

$$e(nT+T) = 0 \tag{22}$$

since by definition

$$\theta_r'(nT+T) = \theta_r(nT+T) - \theta_r(nT)$$

The maximum error occurring during the interval is at $t = t_1$ for which

$$\frac{de}{dt}\Big/ t = t_1 = 0.$$

Time t_1 is found from the solution of the equation

$$\frac{d\theta_r'(t)}{dt} = \frac{\theta_r(nT+T) - \theta_r(nT)}{T} \tag{23}$$

In general

$$\theta_r'(t) = \int_{nT}^{t} \dot{\theta}_r\, dt;\ nT \leqq t \leqq (n+1)T \tag{24}$$

Let $\dot{\theta}_r$ be given by

$$\dot{\theta}_r(\tau) = a + b\tau \tag{25}$$

where a and b are the satellite velocity and acceleration evaluated at $t = nt$. Use of (23), (24), and (25) gives

$$\frac{d\theta_r'(t)}{dt} = a + b\tau = \frac{\Delta}{T} \tag{26}$$

where $\Delta = \theta_r(nT+T) - \theta_r(nT)$

Thus, the time at which the maximum error occurs is found from (26) to be

$$\tau_1 = \frac{1}{b}\left[\frac{\Delta}{T} - a\right] \tag{27}$$

and since $\Delta = aT + (bT^2)/2$, this is

$$\tau_1 = \frac{T}{2} \tag{28}$$

The maximum error is

$$e_{max} = e\left(\frac{T}{2}\right) = -\frac{bT^2}{8} \tag{29}$$

For a satellite in a 100-mile orbit, b may be as large as 0.1 degree per second^2. In this case then, $e_{max} = .0125°$ at $T/2 = 0.5$ if T is one second. Under the best circumstances, then, this is the ultimate attainable accuracy if $r(t)$ is chosen as in (16) and $T = 1$ second is used. Reducing T to 0.5 seconds decreases e_{max} to .003125°. In order to maintain $|e_{max}| < .001$ degree, T must be less than 0.282 seconds.

There is a problem in trying to reduce the error by simply decreasing T. This is that the approximation that $\dot{\theta} = \dot{\theta}_c$ will be less valid over an interval as T decreases. A possible way to decrease the error while maintaining $T = 1$ second is now considered.

Since the error results from the fact that the command velocity differs from true satellite velocity over an interval, a way must be found to bring the two into closer agreement. One possible way for doing this is to generate the command rate from a function of the satellite's present position, velocity and acceleration. The reference input required for accomplishing this is

$$r(\tau) = \dot{\theta}_r(nT) + \ddot{\theta}_r(nT) + \theta_r(nT) \tag{30}$$

for $0 \leqq \tau \leqq T$, where $\tau = t - nT$. The command velocity would then be generated according to the equation

$$\dot{\theta}_c(\tau) = \frac{\theta_r(nT) - \theta(nT)}{T} + \dot{\theta}_r(nT) + \ddot{\theta}_r(nT)\,\tau \tag{31}$$

An alternative method for obtaining the same result indicated above is possible even if velocity and acceleration signals are not available. This is to generate the command rate according to the equation

$$\dot{\theta}_c(\tau) = \frac{y(nT - T)}{T} + \frac{2\,[y(nT) - y(nT - T)]\,\tau}{T^2} \tag{32}$$

where y is defined as in Figure 3. In this case the reference input to be used is that given by (16).

Either of these two approaches should give errors less than .001 degrees without requiring sampling periods less than one second.

IV. ANALYSIS OF EXPERIMENTAL RESULTS

Experiments on the multi-mode mount revealed the existence of limit cycles while driving the system at low rates. The cause of this phenomena is most likely the bearing friction. A detailed exposition of limit cycles of this type may be found in Reference 3. A brief discussion is given below to explain their occurrence in this system.

The analogue tach loop is shown in Figure 5a. The nature of the bearing friction, $f_B(\dot{\theta})$, though not known exactly, is probably as shown in Figure 5b. This characteristic is simplified in that hysteresis effects are neglected. Though it would be necessary to include hysteresis effects to obtain an accurate quantitative description for different drive rates, the simplified representation of bearing friction is adequate to explain the presence of the limit cycles.

Consider the input to be a constant velocity, $\dot{\theta}_i$. A describing function can be derived for the bearing friction about f_{BO}, where

$$f_{BO} = f(\dot{\theta}_i) \tag{33}$$

This describing function defines an equivalent gain for f_B as a function of $\Delta\dot{\theta}$. It is developed by assuming a sinusoidal variation of velocity, $(\Delta\dot{\theta})$ sin ωt, and calculating the fundamental component in the output waveform which will vary between f_{B1} and f_{B2}. Note that it will be a function of $\dot{\theta}_i$ as well as $\Delta\dot{\theta}$. Let this describing function be

$$N(\dot{\theta}_i, \Delta\dot{\theta}) \tag{34}$$

With this definition, the effects of bearing friction can be introduced into the system block diagram as shown in Figure 6.

It is important to note that the effect of the feedback of $\dot{\theta}$ through N is destabilizing, i.e., an increase in $\dot{\theta}$ causes a decrease in retarding torque. This is in contrast to feedback through D and K_T, which is stabilizing.

The transfer function relating $\dot{\theta}$ to $\dot{\theta}_i$ is

$$\frac{\dot{\theta}(s)}{\dot{\theta}_i(s)} = \frac{\dfrac{k_1 K}{1 + k_1 KK_T}}{\dfrac{\tau_e \tau_m'}{1 + k_1 KK_T} s^2 + \dfrac{\tau_e + \tau_m'}{1 + k_1 KK_T} s + 1} \tag{35}$$

where $k_1 = 1/(D - N)$ and $\tau_m' = (\tau_m)\,[(D/D - N)]$.

Since k_1 and τ_m' are dependent on N, it is clear that this transfer function can change considerably with $\dot{\theta}_i$. For example, from (35) it is seen that

$$\omega_n^2 = \frac{D - N + KK_T}{\tau_e \tau_m D} \tag{36}$$

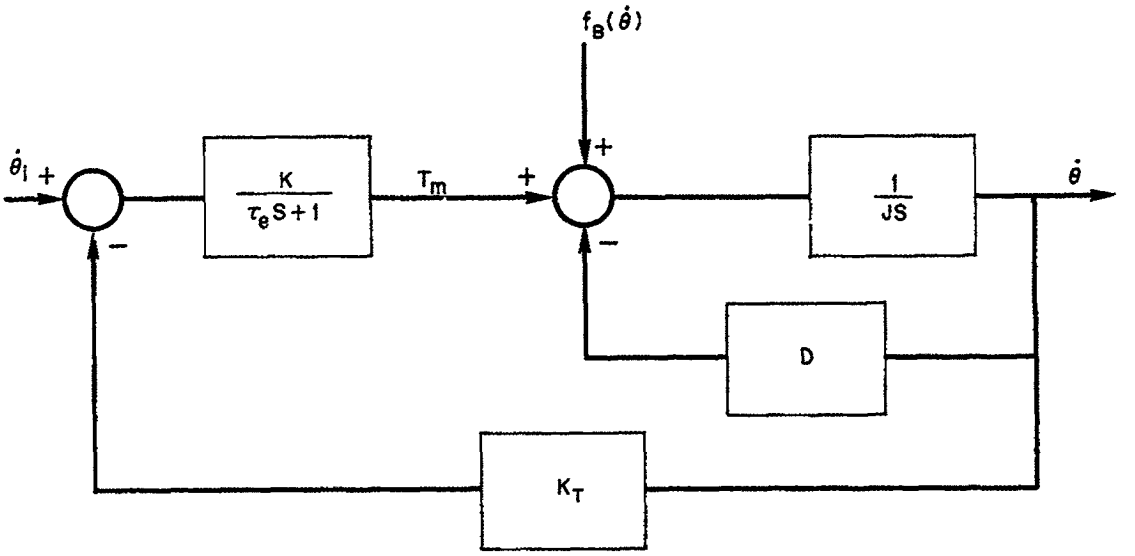

Figure 5a–Analog Tach Loop

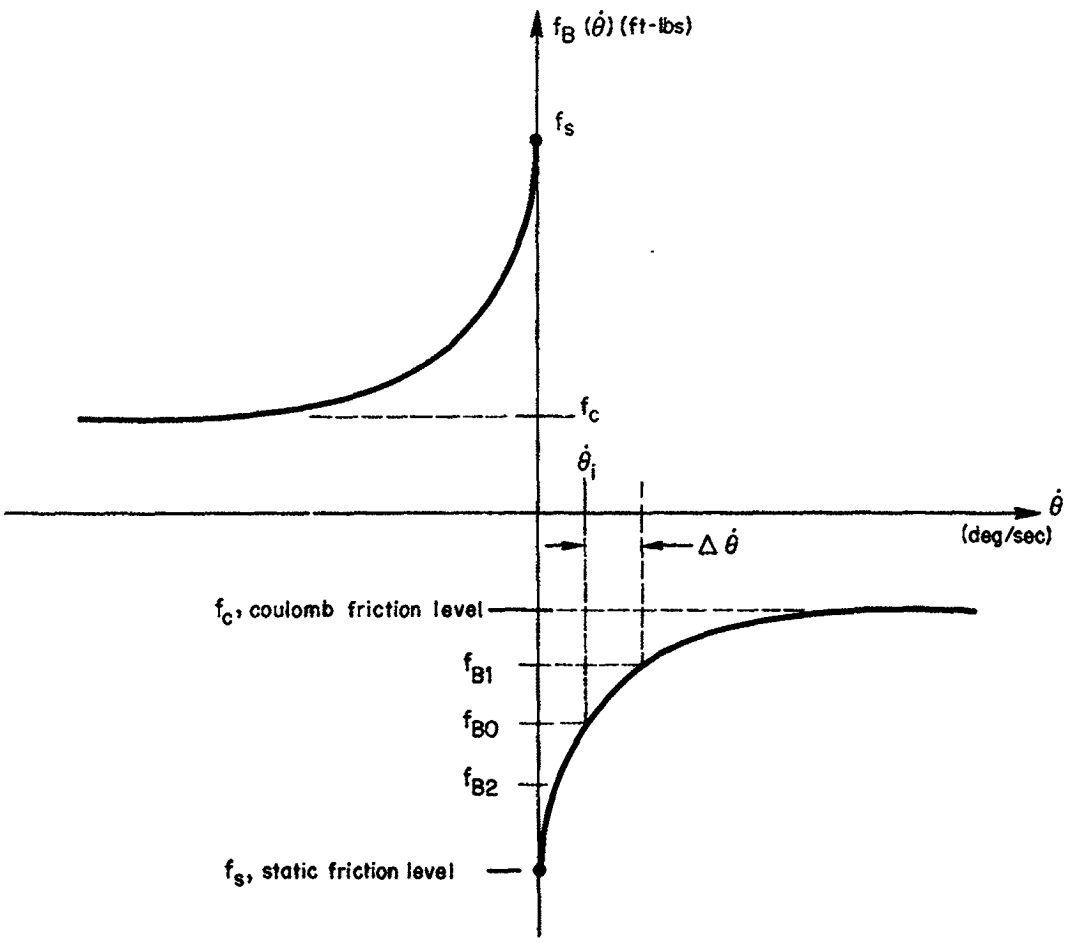

Figure 5b–Bearing Friction Characteristic

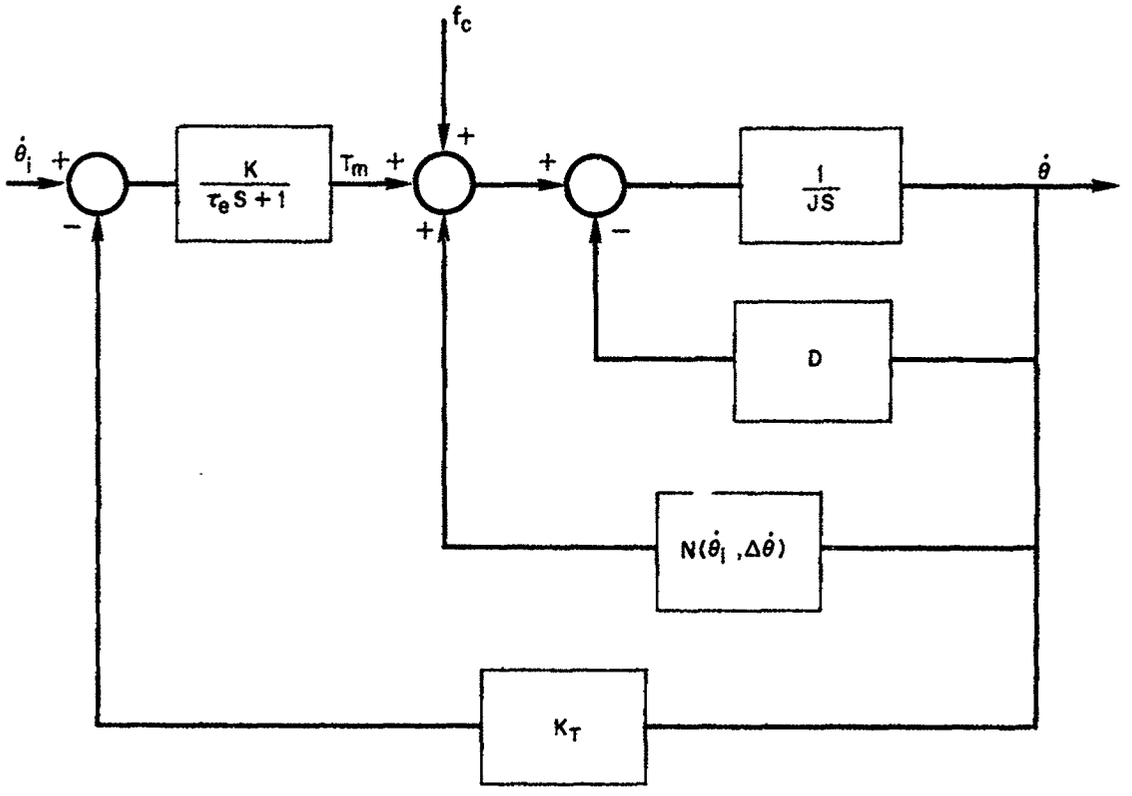

Figure 6–Alternative Representation of Bearing Friction in Analog Tach Loop

and

$$\xi = \frac{1}{2}\left[t_e(D - N) \quad D\tau_m\right] \sqrt{\frac{1}{(D - N + KK_T)(\tau_e \tau_m D)}} \tag{37}$$

Thus, the natural frequency, ω_n, decreases for increasing N. The damping ratio may increase or decrease depending on relative magnitudes of other system parameters compared to N.

The gain of the transfer function given by (35) is

$$\frac{k_1 K}{1 + k_1 K_T} = \frac{K}{D - N + KK_T} \tag{38}$$

This gain increases for increasing N. Thus, the combination of increasing gain and decreasing natural frequency can lead to conditions required to sustain a limit cycle in the closed digital tach loop which has the open loop transfer function

$$L_1(s) = \frac{112(.6S + 1)^2}{s^2(3s + 1)} \left[\frac{\dot{\theta}}{\dot{\theta}_i}(s)\right] \tag{39}$$

One limit cycle frequency which occurred in the experiments was 5 cps when driving at 0.1 degree per second. It can be seen from a Bode plot of $L_1(s)$ (Figure 7) that the complex conjugate poles of $\dot{\theta}/\dot{\theta}_i(s)$ could move to a position to give 180° phase shift and 0 db gain at 5 cps.

When driving at 0.04 degree per second, the resulting limit cycle was not sinusoidal. To quantitatively account for this case, hysteresis and the exact form of $f_B(\dot{\theta})$ would have to be taken into account.

V. DESIGN SUGGESTIONS

The limit cycles occurring at low drive rates may be substantially reduced or elimnated if the response of the tach loop is made overdamped. This fact is noted in References 3 and 4. Reference 4 deals with nonlinear compensation schemes intended to overcome this type of limit cycle. The design discussed herein does not use this approach since it would require extensive modification of existing equipment. Instead, the design suggested herein for the digital tach loop requires only linear compensating elements, and requires only a minimum of modification to existing equipment.

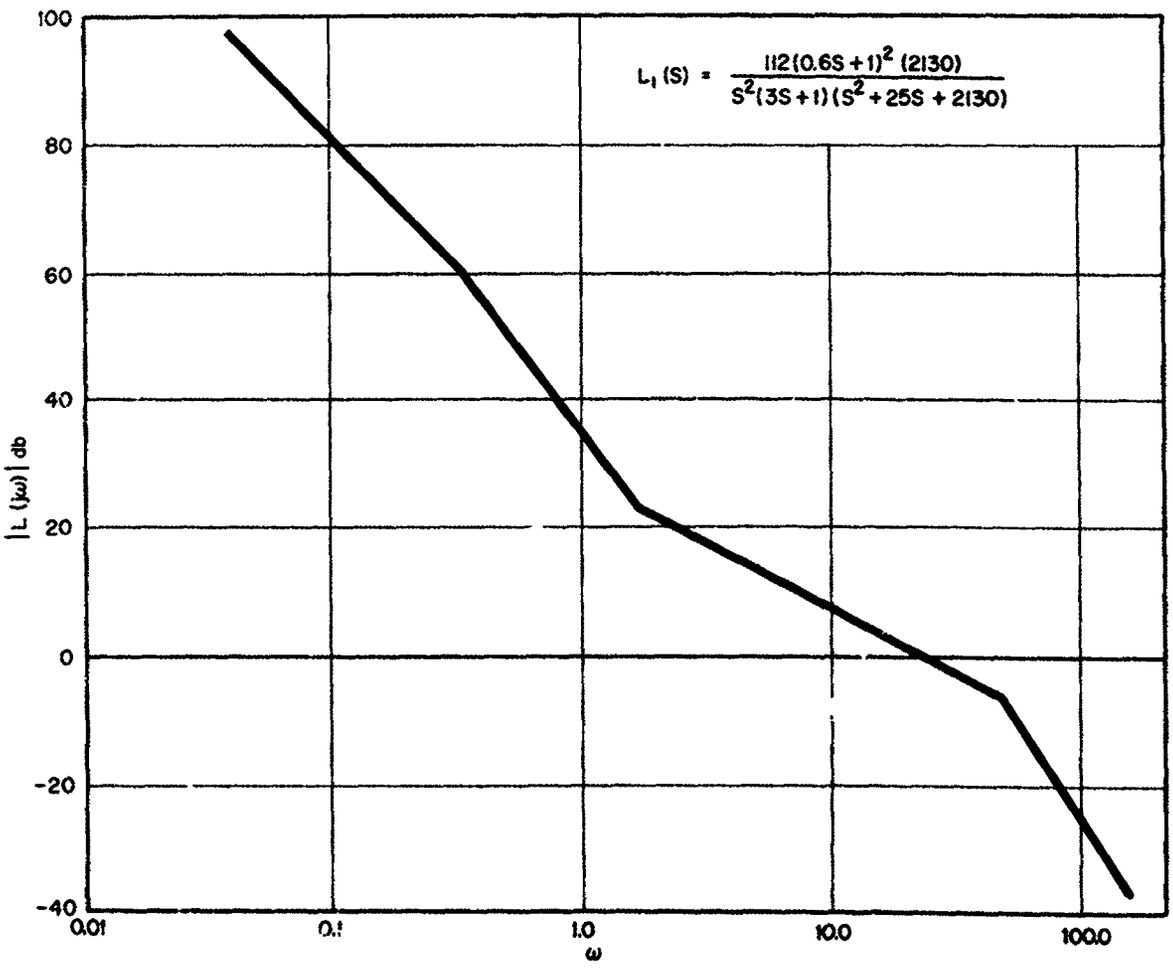

Figure 7–Bode Diagram for $L_1(s)$

The design philosophy will be considered before discussing details. This philosophy is to relieve the digital tach loop of the entire burden of meeting steady state accuracies to sinusoidal inputs for "worst case" satellite passes. This is accomplished by using a feedforward path as shown in Figure 8. With this arrangement, the accuracies mentioned above can be obtained with much lower digital tach loop bandwidth than is presently used.

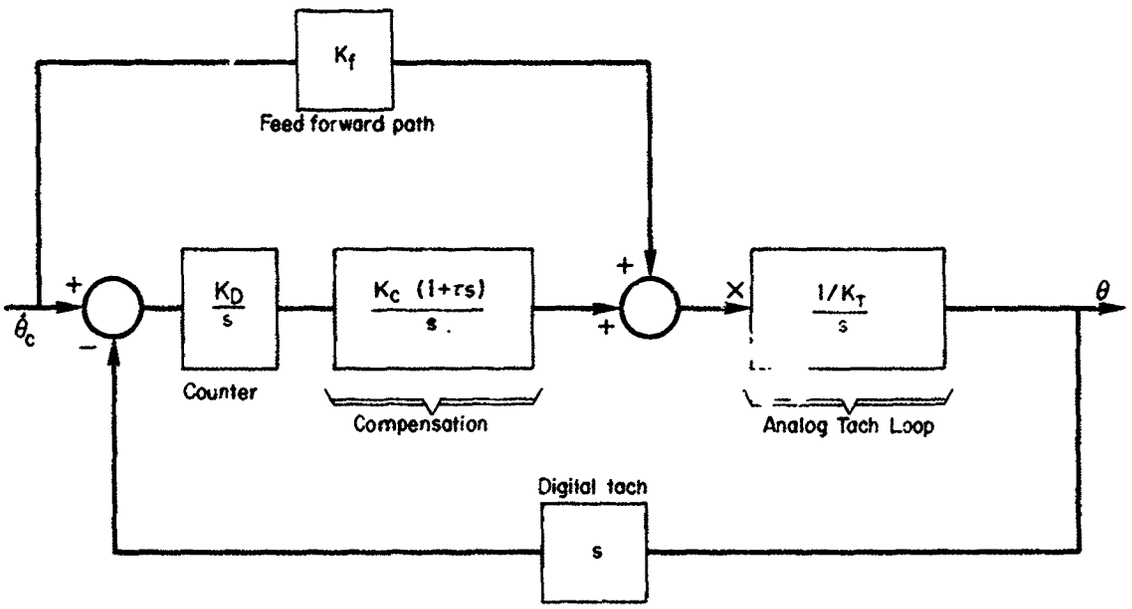

Figure 8–Feedforward Compensation

In Figure 8, $\dot{\theta}_c$ is the command rate into the digital tach loop (shown in Figure 3), and it is assumed that the closed analog tach loop has the transfer function,

$$\frac{G}{X}(s) \approx \frac{1/K_T}{S} \tag{40}$$

i.e., the analog tach loop gain is high enough so that the complex conjugate poles resulting from motor and electrical time constants are of high enough frequency to be neglected. More will be said on this point below when details of the design of the analog tach loop are discussed.

The transfer function relating $\dot{\theta}$ to $\dot{\theta}_c$ is

$$\frac{\dot{\theta}}{\dot{\theta}_c}(s) = \frac{1 + \tau s + \frac{K_f}{K_D K_C} s^2}{\frac{K_T}{K_D K_C} s^2 + \tau s + 1} \tag{41}$$

This transfer function can be made identically equal to one by choosing

$$K_f = K_T \tag{42}$$

To implement this feedforward loop, an additional D/A converter is required to convert $\dot{\theta}_c$ to an alalog signal. Note that $\dot{\theta}_c$ is available in digital form as $(y(nT))/T$ (see Figure 3) before it is converted to pulses by the rate multiplier.

An important consideration in this design is the saturation level of the power amplifier. It should be noted that if $K_T = K_f = 0.715$ volts/deg/sec., then an incremental increase $\Delta\dot{\theta}_c$ equal to .05 degrees per second, which corresponds to the largest expected value for a 100-mile orbit satellite, will produce an incremental step voltage of 35.75 millivolts into the closed analog tach loop. This must be borne in mind when designing the analog loop.

Figure 9 shows a Bode Diagram for the open loop digital tach loop transfer function. It includes the double break at $\omega_1 = 40$ which represents the natural frequency of the closed analog tach loop. This part of the transfer function was not included in Figure 8. Values which pertain to Figure 9 are:

$$K_T = 0.715$$

$$K_D = 10$$

$$K_c = 0.645$$

$$\tau = 0.477$$

If the poles at ω_1 are neglected, the characteristic equation of the closed digital tach loop is given by

$$S^2 + 4.3S + 9 \tag{43}$$

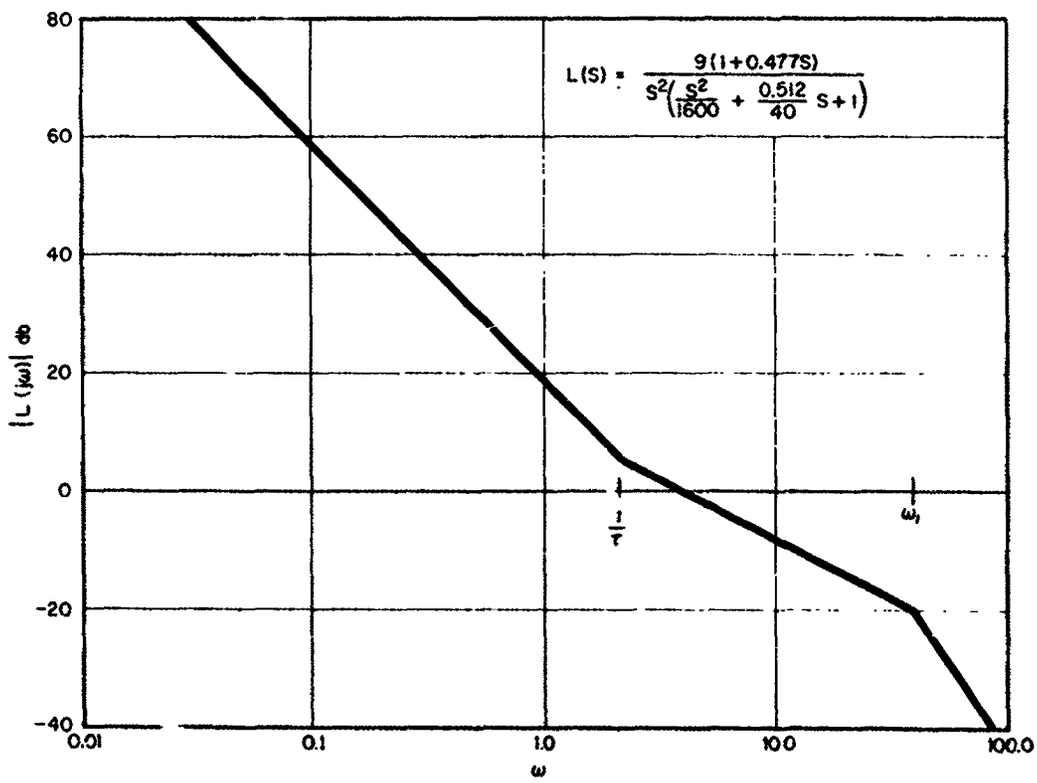

Figure 9–Bode Diagram for Digital Tach Loop

Though not underdamped, this loop has a damping ratio of 0.715, which will produce very small overshoots. This damping should be adequate to avoid limit cycles at low drive rates. In this regard, the feedforward compensation appears to have the following advantages. The command rate, $\dot{\theta}_c$, is applied, through K_f, immediately to the input of the analog tach loop. Even for low drive rates, this results in a signal which is adequate to overcome bearing friction. Thus, the mount begins to move immediately rather than having to wait for adequate signal level to develop in the counter as it must if feed forward compensation is not used.

Attention is now directed to the design of the analog tach loop. One of the difficulties associated with design of this loop is that problems may arise if the load inertia, J, varies during operation. To put these remarks on a quantitative basis, the closed analog loop transfer function is given by

$$\frac{\dot{\theta}}{V} = \frac{\dfrac{K_a K_m}{D + K_a K_m K_T}}{\left(\dfrac{D}{D + K_a K_m K_T}\right)(\tau_e \tau_m)\, s^2 + \left(\dfrac{D}{D + K_a K_m K_T}\right)(\tau_m + \tau_e)\, s + 1} \tag{44}$$

where V is applied voltage, K_a amplifier gain, K_m motor torque constant (lb-ft/volt), D axis damping (lb-ft/deg/sec), τ_m motor time constant, τ_e electrical time constant, and K_T tach constant (volts/deg/sec). For $\tau_m = 11.8$, $\tau_e = .035$, $K_m = 6.25$, $D = 8.95$, and $K_T = 0.715$, the amplifier gain required can be calculated from

$$\omega_1^2 = 1600 = \frac{D + K_a K_m K_T}{D \tau_e \tau_m} \tag{45}$$

Thus,

$$K_a = \frac{1600\,(8.95)\,(.035)\,(11.8) - 8.95}{(6.25)\,(.715)}$$

$$= 1325$$

With this value of amplifier gain, the power amplifier saturates for inputs of 56/1325 = 42.3 millivolts. Since this is greater than the incremental input of 35.75 mv occurring for "worst case" passes, the power amplifier should normally operate in the linear region without saturating.

If $\tau_m = 11.8$ is the largest value occurring during operation, and load inertia changes are not too rapid, then $\omega_1 \geqq 40$, hence the double break at ω_1 in Figure 9 should always be sufficiently far removed from the 0 db crossover frequency to be negligible.

VI. CONCLUSIONS

31156

A pulse model suitable for Z transform analysis of the system was developed. It shows that system operation is exactly as desired when secondary effects are neglected. The analysis of reference input requirements showed that in order to satisfy error requirements, inputs must be applied at least once every .232 seconds or, alternatively, rate and acceleration inputs must be used. Bearing friction was revealed as the most likely cause of the limit cycles observed while operating in the rate mode. A design was

presented which should overcome these limit cycles. It was based on increasing the digital tach loop damping, lowering its bandwidth and incorporating a feedforward path. This design requires only minimum modification of existing equipment.

Author

REFERENCES

1. D. P. Lindorff, "Theory of Sampled Data Control Systems," Wiley & Sons, Inc., N.Y., N.Y., 1965.

2. B. C. Kuo, "Analysis and Synthesis of Sampled-Data Control Systems," Prentice-Hall, Inc., Englewood Cliffs, N.J., 1963.

3. D. Graham, D. McRuer, "Analysis of Nonlinear Control Systems," Wiley & Sons, Inc., N.Y., N.Y., 1961.

4. C. N. Shen, H. Wang, "Nonlinear Compensation of a Second- and Third-Order System with Dry Friction," IEEE Applications and Industry, March 1964, pp 128-136.

N66 31157

TRACKING ACCURACY ANALYSIS OF THE 85-FOOT PARABOLIC ANTENNA AT ROSMAN, NORTH CAROLINA

by

Dr. Couros Ghaznavi
Professor, Pratt Institute

and

Dr. Teodoro Mercado-Jimenez
Assistant Professor, University of Puerto Rico
ASEE-NASA FACULTY FELLOWS
1965

ABSTRACT

Gain and noise considerations make it desirable to increase the frequency of operation of satellites. This increase in frequency places more stringent requirements on the accuracy of tracking systems.

The object of this study is to find the limitations of the 85-foot antenna tracking system at Rosman, North Carolina, and to suggest some possible modifications to the system in order to meet a specified accuracy of 0.01 degree. This accuracy which corresponds approximately to a system frequency of 8,000 Mc should also be attained for low altitude satellites.

In the absence of the exact transfer function for the system under consideration, a linear system was assumed. Although the model does not exactly represent the actual system, some insight as to the quantitative values of errors was gained from its use.

The error caused by satellite motion was calculated. It was found that this error is not negligible for low altitude (100 miles) satellites. A reduction of this error by a change in gain is not attainable without causing additional problems. This is due to the low resonant frequency of the antenna dish and the consideration of possible nonlinearities in the system.

A signal adaptive technique is proposed to reduce the tracking error. This method introduces a computer computed function at the system's input. However, this requires an accurate knowledge of satellite velocity and position.

The effects of wind torques and noise disturbances were also considered. The mean square error due to wind torques and noise were determined. It was found that in the presence of wind and present system does not satisfy the accuracy requirement it should ultimately possess. Compensation schemes were used and a way was found to improve system performance of application of proportional feedback.

As the effect of noise in the system error is dependent on the magnitude of the noise spectrum, a limit may be set in order to satisfy the required accuracy.

It is also shown that an adaptive system could reduce the error due to the noise.

BLOCK DIAGRAM AND TRANSFER FUNCTION OF SERVO DRIVE AND DISH

As the first problem encountered is the determination of tracking accuracy for the present system, its transfer function must be obtained. Unfortunately at the present time the exact system transfer function is unknown and some approximations must be made in order to describe the system. The structure of the dish, for instance, is quite complicated and the search for its transfer function presents, in itself, a sizeable task; however, it can be argued that a simplified version of the actual system function may throw much light upon the quantitative values of the errors in tracking.

Figure 1 shows the block diagram of the assumed system used for this study.

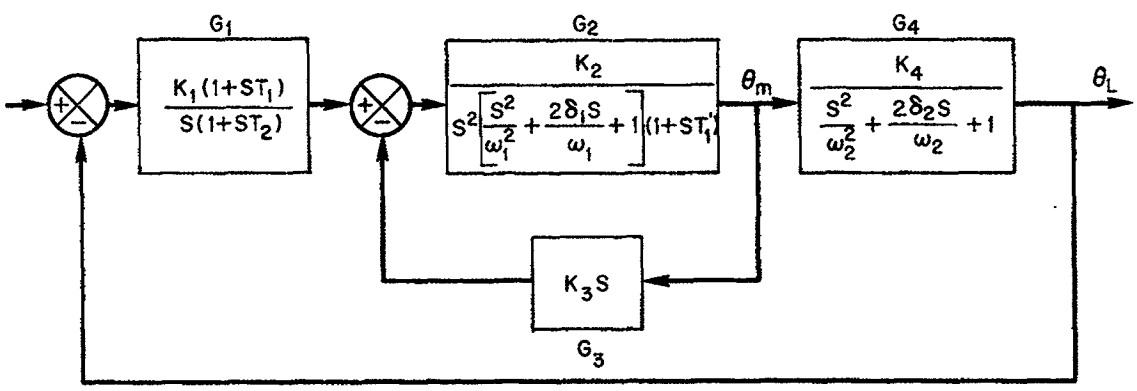

Figure 1

A more detailed block diagram of the hydraulic system is given in Figure 2. The transfer functions G_2 and G_3 may be combined yielding

$$G_5 = \frac{K_2}{K_5 S(aS^3 + bS^2 + cS + 1)}$$

Assuming the roots of the third degree polynomial in the denominator of G_5 to be away from the natural frequency W_2 of the dish, the block diagram is simplified further. Also, in order to introduce wind torque disturbances into the system, a block is added resulting in the block diagram of Figure 3.

The simplified transfer function for the system as obtained from Figure 3 is then

$$\frac{\theta_L}{E} = \frac{K(1 + ST_1)}{S^2 (1 + ST_2)(S^2/\omega_n^2 + 2\delta/\omega_n S + 1)}$$

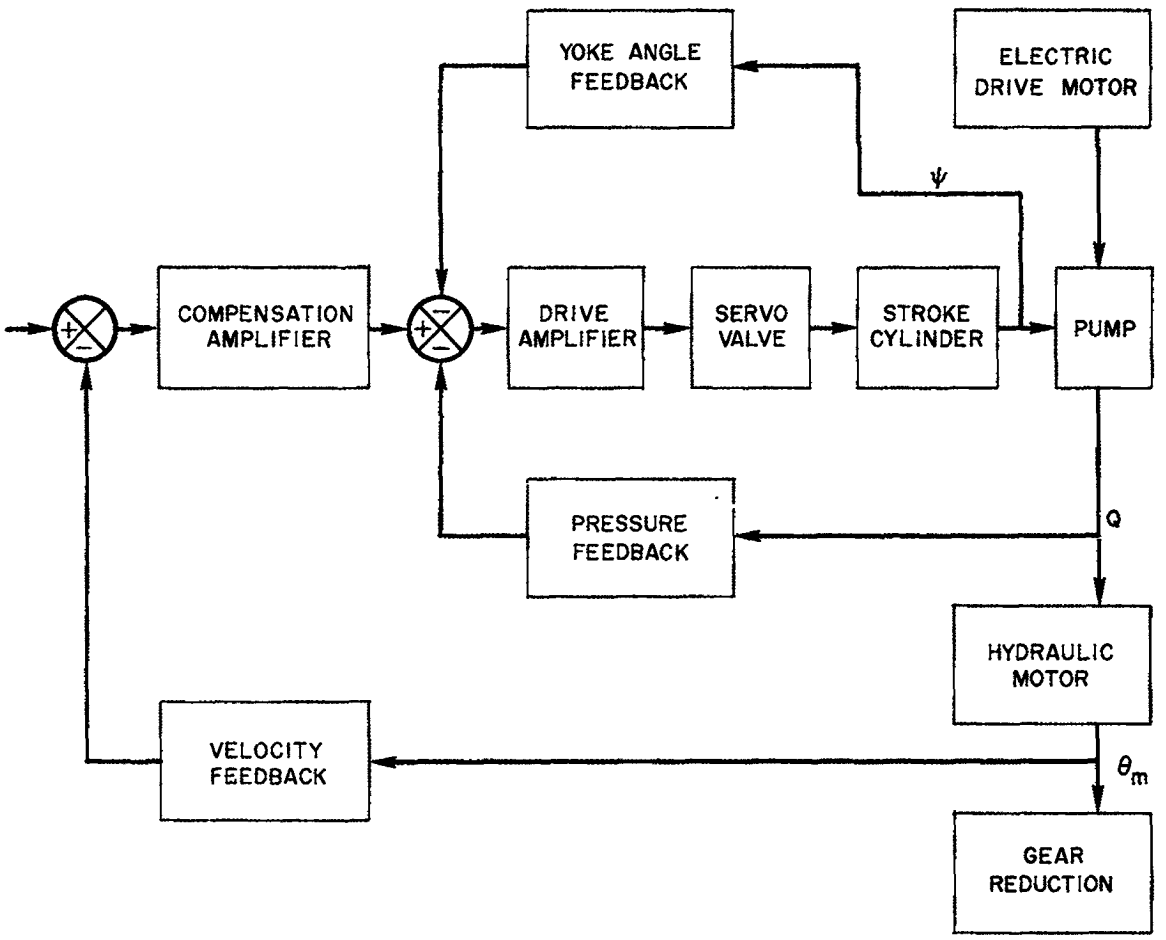

Figure 2–Hydraulic System Block Diagram

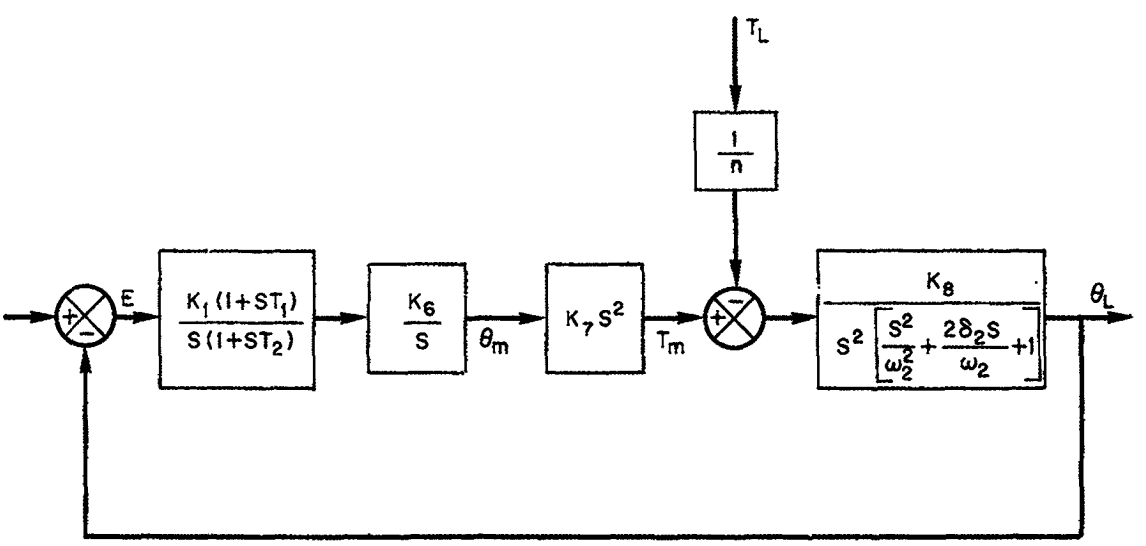

Figure 3

where, for the X-axis

$$T_1 = 0.687 \text{ sec}$$
$$T_2 = 0.167 \text{ sec}$$
$$W_n = 13.8 \text{ rad/sec}$$
$$K = 4.84$$
$$o = 0.1$$

thus

$$G(S) = \frac{4.84(1 + 0.667S)}{S^2(1 + 0.167S)\left[\frac{S^2}{(13.8)^2} + 0.0145S + 1\right]}$$

The open and closed loop magnitude plots are shown in Figure 4. From these plots, it is seen that an overshoot of forty percent is possible if the input to the system is a step function. Although this is quite a high value, it may not be of importance as the antenna in the tracking mode may not be ever subjected to such an input.

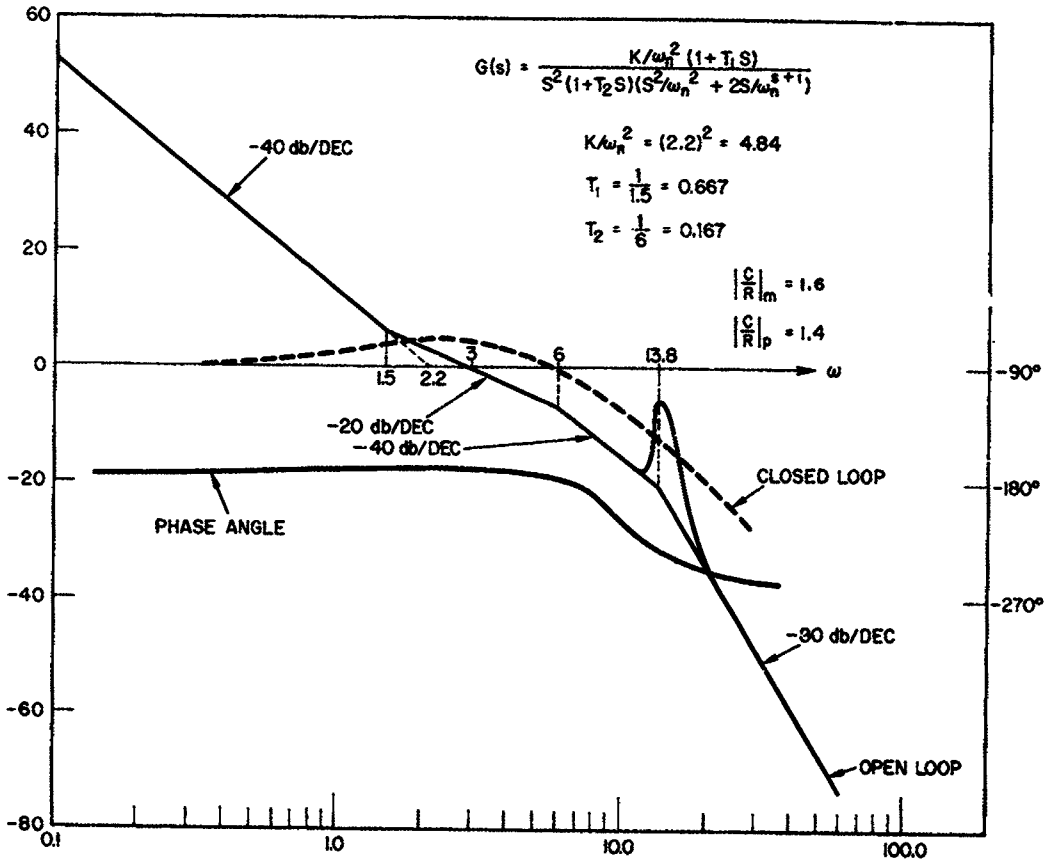

Figure 4–System Transfer Function

ERROR CAUSED BY SATELLITE MOTION

This error is a function of satellite orbit and antenna position with respect to the satellite. Larger errors are present when tracking low altitude satellites than high altitude ones. Also, if the antenna is tracking two satellites of the same orbit height, the antenna error varies depending on the position of the orbit with respect to the antenna. For an X-Y antenna, this error would be the largest on a horizontal passing rather than an overhead passing as is the case for an azimuth elevation antenna. (See also the attached computed position, velocity, and acceleration of the antenna output.)

Two methods may be used to evaluate the error and the antenna's capabilities. The sinusoidal method which is suitable for design purposes assumes the variation of position, velocity and acceleration of the antenna to be sine waves superimposed to the actual computed curves. From this sine wave the corresponding position is computed and as the acceptable error is also known, the value θ/E may be calculated. One numerically computed value corresponding to the 100-mile satellite is shown h v. Also Figure 5 shows how the sine wave is superimposed. This calculation is for an error of 0.01 degree.

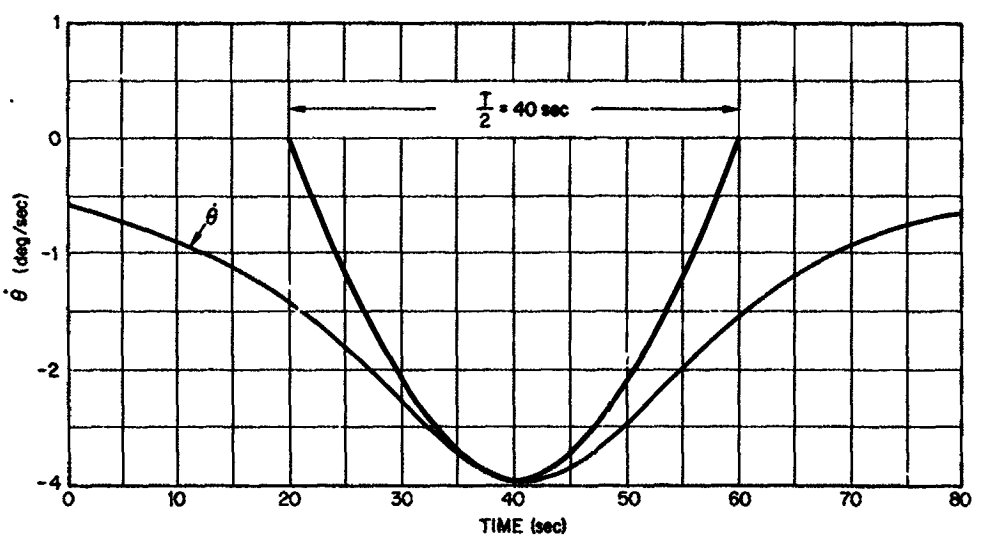

Figure 5

Position Curve

$$T = 160 \text{ sec}$$

$$W = \frac{2}{160} = 0.0392$$

$$\theta_p = \frac{64}{57.5} = 1.11 \text{ rad}$$

$$\frac{C}{E} = \frac{1.1}{1.74} \times 10^4 = 0.64 \times 10^4$$

$$\frac{C}{E} = 77.4$$

Velocity Curve

$$T = 80 \text{ sec}$$

$$W = 0.078$$

$$\theta_v = \frac{1.5}{0.078} = 19.3^\circ = 0.336 \text{ rad}$$

$$\frac{C}{E} = \frac{0.336}{1.74} \times 10^4 = 19.2 \times 10^2$$

$$\frac{C}{E} = 65.5 \text{ db}$$

Acceleration Curve

$$T = 48 \text{ sec}$$

$$W = \frac{2}{48} = 0.13$$

$$\theta_A = \frac{0.093}{(0.13)^2} \times 5.5^\circ = 0.0955 \text{ rad}$$

$$\frac{C}{E} = \frac{0.0955}{1.75} \times 10^4 = 5.45 \times 10^2$$

$$\frac{C}{E} = 54.5 \text{ db}$$

With this method we plot the open loop transfer function of the system for a given error. The actual transfer function should have a larger gain if a lower error is required. Figure 6 is the open loop plot of the control system. It shows that with the present system the error for a 100-mile satellite is larger than 0.01 degree. For a 600-mile satellite the error is less. Also, it is shown that for a 100-mile satellite the error is about two minutes.

In Figure 7 an attempt is made to reduce the error by the change of open loop characteristic. The result is not good because of the following facts. A-60 db/dec slope should not be permitted because any nonlinearity could subject the antenna to violent oscillations. Also the crossover frequency comes closer to the resonant frequency and consequently makes the settling time very long. The addition of zeros near the complex poles was tried in order to overcome this difficulty. This was not successful as the maximum gain for stable behavior was below the one obtained from Figure 6. Figure 8 is an example of this attempt for

$$\frac{C}{E} = \frac{K(S + 1.5)(1 + 385S + 200S^2)}{S(S^2 + 3S + 220)(0.07 + S)(S^2 + 20S + 400)}$$

It should be borne in mind that the assumed transfer function, from which the open loop plot was obtained, might not represent the system accurately. For this reason the actual error could well be more or less than the calculated values. It is hoped that experimental field data from the present system will result in an accurate system function description thus eliminating the uncertainty in the calculated values.

One possible method of tracking error correction would be the use of an adaptive signal according to the following: If a simple loop as shown in Figure 9a is considered, one may write

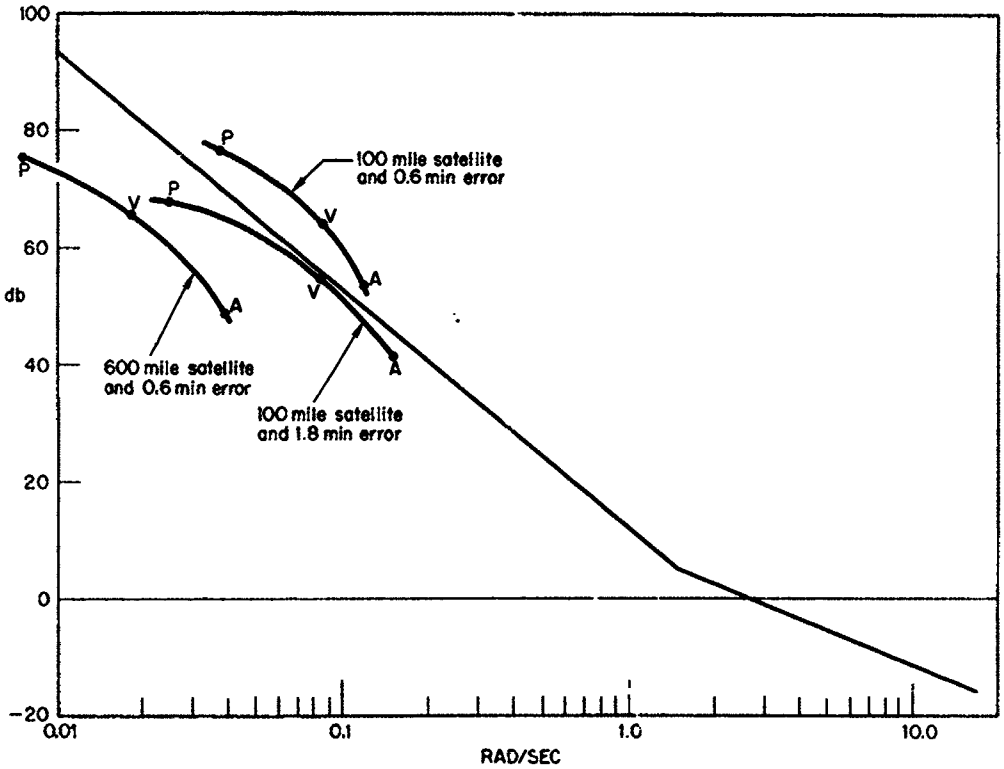

Figure 6

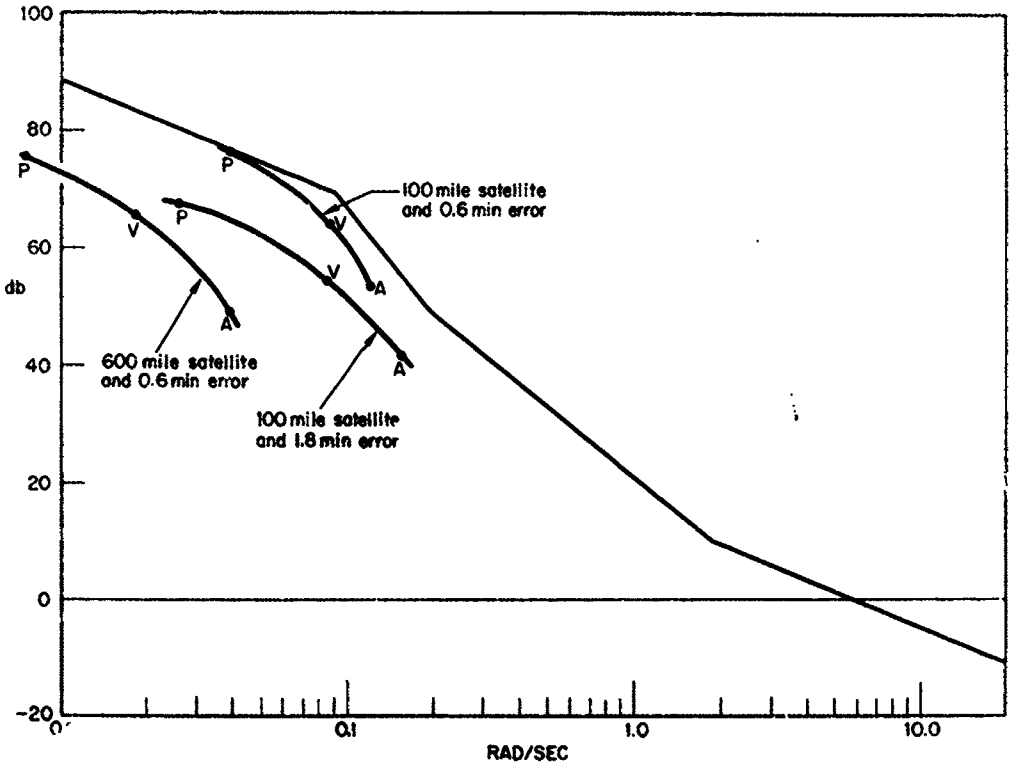

Figure 7

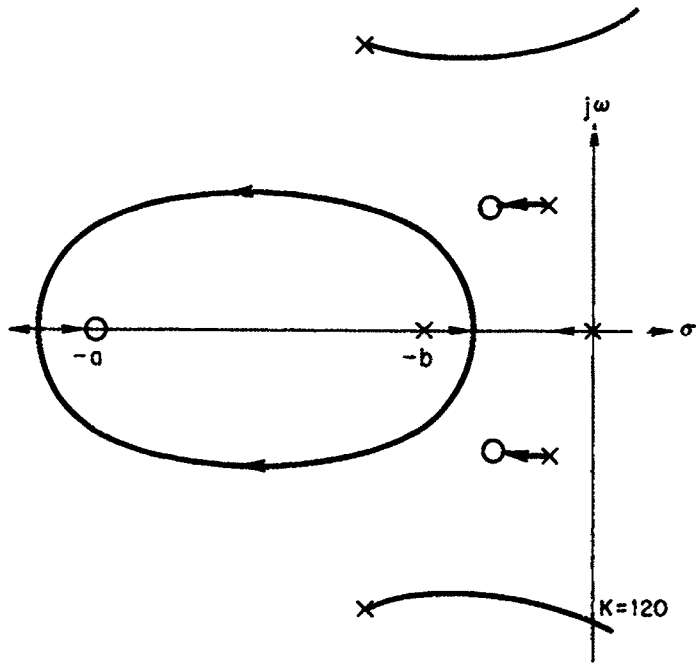

Figure 8

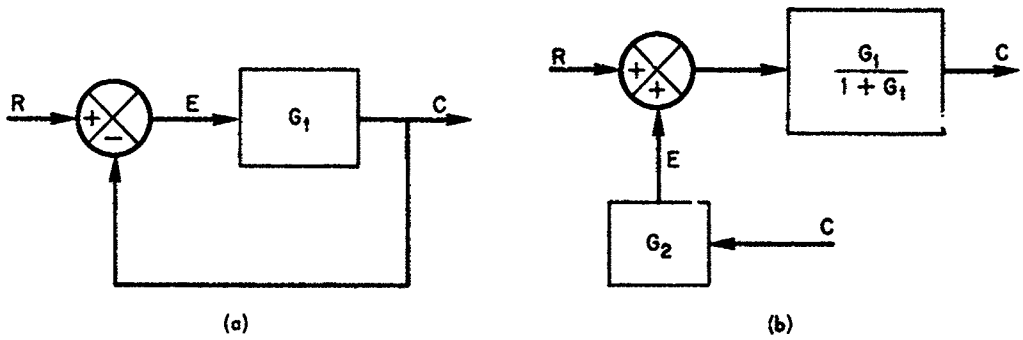

Figure 9

$$\frac{C}{R} = \frac{G_1}{1 + G_1}$$

Now considering Figure 9b,

$$C = (R + CG_2)\frac{G_1}{1 + G_1}$$

$$C\left(1 - \frac{G_1 G_2}{1 + G_1}\right) = \frac{RG_1}{1 + G_1}$$

$$\frac{C}{R} = \frac{G_1}{1 + G_1 - G_1 G_2}$$

If one wants $C/R = 1$, one should have

$$\frac{G_1}{1 + G_1 - G_1 G_2} = 1 \quad \text{or} \quad G_2 = \frac{1}{G_1}$$

This means that if one could inject the error as a function of time into the system, this basic idea may be applied to the system. However, there could be one practical drawback: the calculated error must be more accurate than the error desired. The set of curves attached to this report shows the position, velocity, and acceleration of the antenna. From these curves it is possible to calculate the error. However, in order to obtain these curves one must know not only the speed of the target but also its position. If these curves are not known accurately, even with an accurately known transfer function, the error may not be accurately calculated. If this method is to be used, then the correction should be done step by step. As at low frequency operation, a larger error can be tolerated at each run and a higher frequency and a better correction may be introduced for each satellite.

EFFECT OF WIND IN THE MSE OF THE SYSTEM

In absence of the exact transfer function for the system under consideration, the analytical model of Figure 3 was used. It was then established that the output angle and wind torque are related by the transfer function

$$G_w(S) = \frac{2.4 \times 10^{-7} (1 + 0.167S)}{0.167S^3 + S^2 + 3.22S + 4.84}$$

in the absence of an input signal.

The mean square error of the system is then determined from the relation

$$\epsilon^{-2} = \frac{1}{2\pi j} \int_{-j\infty}^{j\infty} G(s) G(-s) \Phi_{ww}(s)\, ds$$

where $\Phi_{ww}(S)$ is the power density spectrum of the wind torque.[4] For our particular study the spectrum given in page 259 of reference 1 is used, i.e.,

$$\Phi_w(S) = \frac{\beta^2}{\pi} \frac{\nu}{\nu^2 - s^2}$$

where

$$\beta = 2C_w V_0 \sqrt{\overline{V_1^2}},$$

ν = frequency in rad/sec

C_w is the constant of proportionality relating the wind torque to the square of the wind velocity.

V_0 = average wind velocity

$\overline{V_1^2}$ = RMS value of wind velocity fluctuation about the average velocity

The range of frequencies of importance here is between 0.4 and 3 rad/sec. With V_0 = 50 MPH, $\overline{V_1^2(t)}$ = 12.5 MPH and C_w = 70 LB/FT/(MPH)^2 $\beta^2/\pi = 2.44 \times 10^9$ (LB/FT)^2. Thus

$$\overline{\epsilon^2} = \frac{1}{2\pi j} \int_{-j\infty}^{j\infty} \frac{(2.4 \times 10^{-7})^2 (1 + 0.167S)(1 - 0.167S) \times 2.44 \times 10^9 \, \nu \, ds}{(0.167S^3 + S^2 + 3.23S + 4.84)(-0.167S^3 + S^2 - 3.23S + 4.84)(S + \nu)(\nu - S)}$$

or

$$\overline{\epsilon^2} = \frac{14.1 \times 10^{-5} \, \nu}{2\pi j} \int_{-j\infty}^{j\infty} \frac{(1 + 0.167S)(1 - 0.167S)}{D(s)\, D(-S)} \, ds$$

where

$$D(S) = (0.167S^3 + S^2 + 3.23S + 4.84)(S + \nu)$$

$$= 0.167S^4 + (0.167\nu + 1) S^3 + (3.23 + \nu) S^2 + (3.22\nu + 4.84) S + 4.84\nu$$

Using the tables in Appendix E of reference 1 and putting ν = 1 rad/sec,

$$I_4 = \frac{1}{2\pi j} \int_{-j\infty}^{j\infty} \frac{(1 + 0.167S)(1 - 0.167S)}{D(S)\, D(-S)} \, ds = 0.0172$$

With this value of I_4, the MSE is

$$\overline{\epsilon^2} = 14.1 \times 10^{-5} \times 0.0172 = 24.2 \times 10^{-7} \text{ rad}^2$$

and hence the mean error

$$\overline{\epsilon} = 1.55 \times 10^{-3} \text{ rad} = 0.089°$$

Evidently, if our analytical model is correct, the system does not meet the specification of a maximum error of 0.6 minutes or 0.01°.

SYSTEM COMPENSATION FOR MSE REDUCTION

The improvement of tracking accuracy for the system is dictated by the feasibility of implementation. It would appear that the use of accelerometers is the only convenient and practical addition to be made to the existing system for error reduction. With these views in mind the effect of inclusion of an accelerometer, as shown in Figure 10 with

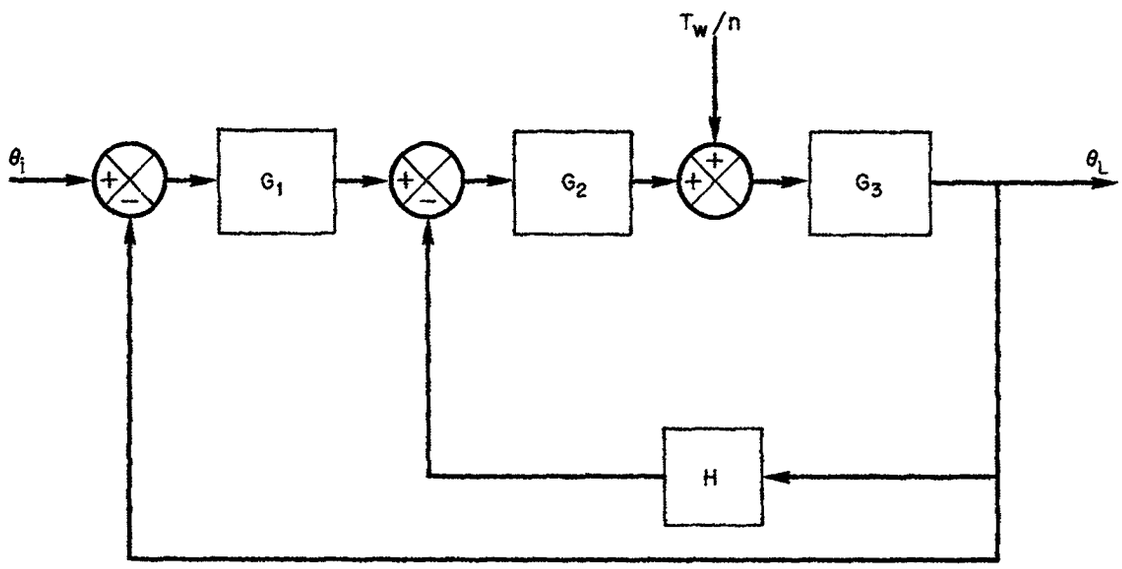

$G_1 = \dfrac{K_1(1+0.667\,S)}{S(1+0.167\,S)}$ $\qquad G_2 = KS \qquad G_3 = \dfrac{K_2}{S^2}$

$K_1 K K_2 = 4.84$ rad/volt

$K_2 = 7.33 \times 10^{-4}$ rad^3/ft-lb sec^2

$n = 3050$

Figure 10

$H = (K_A/K)\,S^2$, was investigated. The transfer function for the modified system in the absence of an input is then

$$G_A(S) = \frac{2.4 \times 10^{-7}\,(1 + 0.167S)}{12.26 \times 10^{-5}\,K_A S^4 + (7.33 \times 10^{-4}\,K_A + 0.167)\,S^3 + S^2 + 3.23S + 4.84}$$

Proceeding as before

$$\overline{\epsilon^2} = \frac{\beta^2 \nu}{2\pi^2 j} \int_{-j\infty}^{j\infty} \frac{G_A(S)\,G_A(-S)\,ds}{(S+\nu)\,(\nu - S)} \tag{1}$$

where

$$\frac{G_A(S)}{S+\nu} = \frac{2.4 \times 10^{-7}\,(1 + 0.167S)}{12.26 \times 10^{-6}\,K_A S^5 + [7.33 \times 10^{-4}\,K_A\,(1 + 0.167\nu) + 0.167]\,S^4 +}$$

$$\frac{1}{[1 + (7.33 \times 10^{-4}\,K_A + 0.167)\,\nu]\,S^3 + (3.23 + \nu)\,S^2 + 4.84\,(1 + 0.667\nu)\,S + 4.84\nu}$$

For the case of $\nu = 1$ rad/sec and $K_A = 10$, and using the tables of reference 1

$$I_S = 0.0168$$

and the error is

$$\overline{\epsilon} = 0.0897°$$

A computer program was coded to facilitate the evaluation of the mean square error for different values of K_A. The results obtained indicated that the error increased monotonically with increasing value of the accelerometer constant K_A. Thus, this approach fails to accomplish a reduction in the mean square error of the system.

The effect of rate feedback in the inner loop of the system of Figure 10 ($H = (K_R/K)\,S$) was investigated next. The transfer function was found to be

$$G_R(S) = \frac{2.4 \times 10^{-7}\,(1 + 0.167S)}{(0.167 + 12.26 \times 10^{-5}\,K_R)\,S^3 + (1 + 7.33 \times 10^{-4}\,K_R)\,S^2 + 3.23S + 4.84}$$

and

$$\frac{G_R(S)}{S + \nu} = \frac{2.4 \times 10^{-7}\,(1 + 0.167S)}{(0.167 + 12.26 \times 10^{-5}\,K_R)\,S^4 + [(0.167 + 12.26 \times 10^{-5}\,K_R)\,\nu + 1 + 7.33 \times 10^{-4}]\,S^3}$$

$$\frac{1}{+ [(1 + 7.33 \times 10^{-4})\,\nu + 3.23]\,S^2 + (3.23\nu + 4.84)\,S + 4.84\,\nu}$$

Substituting in (1) and using the aforementioned tables with $\nu = 1$ rad/sec, $K_R = 10$

$$I_4 = 0.0173$$

and

$$\overline{\epsilon} = 0.0892°$$

Results obtained from a computer program for different values of K_R showed no improvement over the previous considered case of accelerometer feedback.

Finally a signal proportional to the output signal was fed back in the inner loop ($H = K_P/K$). The transfer function for this case is

$$G_P(S) = \frac{2.4 \times 10^{-7}\,(1 + 0.167S)}{0.167S^3 + (1 + 12.26 \times 10^{-5}\,K_P)\,S^2 + (3.23 + 7.33 \times 10^{-4}\,K_P)\,S + 4.84}$$

and

$$\frac{G_p(S)}{S+\nu} = \frac{2.4 \times 10^{-7}\,(1 + 0.167S)}{0.167S^4 + (1 + 0.167\nu + 12.26 \times 10^{-5}\,K_p)\,S^3 + [(1 + 12.26 \times 10^{-5})\,\nu + 3.23 + 7.33 \times 10^{-4}]\,S^2}$$

$$\frac{1}{+\,[(3.23 + 7.33 \times 10^{-4})\,\nu + 4.84]\,S + 4.84\,\nu}$$

Thus, using equation 1 and the tables for $K_p = 10^6$ and $\nu = 1$

$$I_4 = 0.1395 \times 10^{-3}$$

and

$$\overline{\epsilon} = 0.00802^\circ = 0.49$$

minutes which meets the specifications.

It was found that for this case the error decreased monotonically with increasing K_p.

The implementation of this last scheme for improving the accuracy of the system, although not impossible, may prove difficult. The difficulty lies on the fact that an accelerometer and two integrators are required and the bias of the accelerometer would be dependent on the antenna position. However, as the existing system incorporates encoders with a resolution of one mil at the output axes, it should be possible to program the accelerometer bias based on the encoders output.

RMS TRACKING ERROR DUE TO NOISE

The effect of random noise on the servo system can be evaluated as an rms servo error. Assuming additive gaussian white noise, the rms servo error may be calculated using the same scheme utilized for wind torque effects.

The mean square error is determined from the relation

$$\overline{\epsilon_n^2} = \frac{1}{2\pi j} \int_{-j\infty}^{j\infty} G_n(S)\, G_n(-S)\, \phi_n(S)\, ds$$

where

$\overline{\epsilon_n^2}$ = mean square error

ϕ_n = noise power spectrum at the input of the servo system, equal to a constant for white noise

$G_n(S)$ = servo system closed loop function with respect to noise

The block diagram of the system with the input noise is shown in Figure 11.

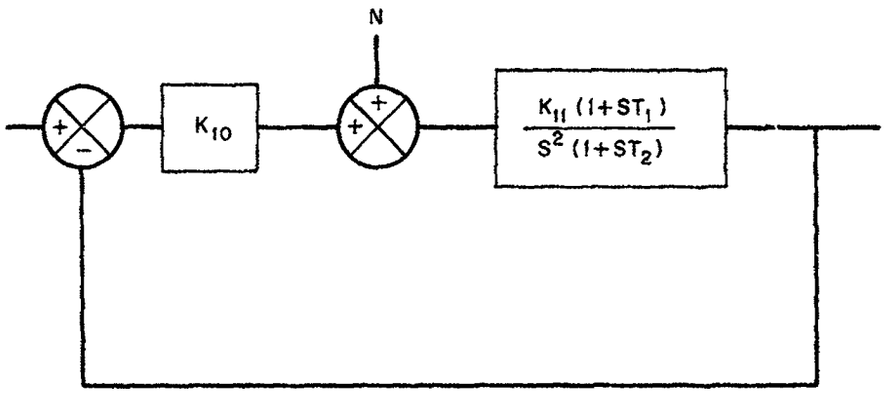

Figure 11

Then

$$\frac{\theta}{N} = \frac{\dfrac{K_{11}\ (1 + ST_1)}{K_{10}\ S^2(1 + ST_2)}}{1 + \dfrac{K_2(1 + ST_1)}{S^2(1 + ST_2)}} = \frac{K_{11}(1 + ST_1)}{K_{10}\ [S^2(1 + ST_2) + K_2(1 + ST_1)]}$$

and

$$\overline{\epsilon^2} = \frac{\phi_n}{K_{10}^2}\frac{1}{2\pi j}\int_{-j\infty}^{j\infty} \frac{K_{11}^2(1 + ST_1)(1 - ST_1)\,ds}{[S^2(1 + ST_2) + K_2(1 + ST_1)]\ [S^2(1 - ST_2) + K_2(1 - ST_1)]}$$

The total servo gain, $K_{11} = 4.84$ and K_{10} depends on the beamwidth which in turn is dependent on the frequency of operation. The expression for K_{10} is

$$K_{10} = \frac{0.7}{\alpha}$$

where

α = half beamwidth

The mean square error equation may be written as

$$\overline{\epsilon^2} = \left(\frac{K_{11}}{K_{10}}\right)^2 \phi_n \frac{1}{2\pi j}\int_{-j\infty}^{j\infty} \frac{C(S)\,C(-S)\,ds}{D(S)\,D(-S)}$$

where

$$C(S) = 1 + ST_1$$

$$D(S) = T_2S^3 + S^2 + K_{11}T_1S + K_{11}$$

For $T_1 = 0.667$, $T_2 = 0.167$, $K_{11} = 4.84$ and using Reference 1

$$I_3 = \frac{(0.667)^2 (4.84)(0.167) + 0.167}{2(4.84)(0.167)[-4.84(0.167) + 3.23]}$$

or

$$I_3 = 0.135$$

and hence

$$\overline{\epsilon_n^2} = \frac{\phi_n}{K_{10}^2} (4.84)^2 (0.135)$$

The following table shows the error due to noise for a fixed beamwidth. This is done for various radio frequencies and different values of noise spectrum as the actual values of the latter were not known for the system considered.

Table 1

Mc	Beamwidth = 2	10^{-2} rad	K_{10}	Assumed	rad^2	RMS error degree
136	6°	5.2	13.4	10^{-2}	1.76×10^{-4}	0.75
3,000	0.27°	0.23	300	10^{-2}	3.52×10^{-9}	3.4×10^{-3}
8,000	0.10°	0.087	800	10^{-1}	4.95×10^{-7}	0.04
136	6°	5.2	13.4	10^{-3}	1.76×10^{-5}	0.024
136	6°	5.2	13.4	5×10^{-3}	8.80×10^{-5}	0.54

In order to see the effect of beamwidth on the noise, we rewrite I_3 as

$$I_3 = \frac{(T_1^2 K_{11} + 1) T_2}{2K_{11} T_2 [-K_{11} T_2 + K_{11} T_1]}$$

and

$$I_3 \cong \frac{1 + K_{11} T_1^2}{2K_{11}^2 T_1}$$

Also the open loop transfer function may be approximated by

$$G(S) = \frac{0.1\,\omega_c^2}{S^2} \left(1 + \frac{S}{0.5\,\omega_c}\right)$$

From the above two relations one finds

$$\overline{\epsilon^2} = 0.071\, \phi_n\, \omega_c\, a^2$$

From the table it may be seen that for some values of noise spectrum the error would not be acceptable. For instance a noise spectrum of 10^{-2} and a frequency of operation of 136 Mc result in an unacceptable error. However, the above relation shows that if the noise spectrum occurs for a high altitude satellite, the error could be corrected by beam-width reduction. For instance, if the signal to noise ratio is such that the 10^{-2} spectrum applies for a 600-mile satellite, the gain needed is 25 db less than for a 100-mile satellite. This gain reduction reduces W_c by about a factor of four and the error by about a factor of two. From this one is led to the conclusion that an adaptive system is desirable.

ANALYSIS OF DATA

Field tests were performed in an attempt to establish an accurate transfer function for the antenna dish structure and servo drive system. The data was obtained from accelerometers placed in convenient parts of the dish, the feedbox, bull gear, tachometer, and other locations.

If the accelerometer transfer function is assumed to be KS^2, the following methods should help in the determination of the system transfer function from the experimental measurements.

A. Linear System Assumption

1. If the response of the open loop system to a step function is known, an approximate frequency response for the open loop transfer function can be found.

2. The cross correlation of system input and output for a white noise input yields the system's impulse response from which the transfer function may be determined.

3. The measurement of the impulse response itself should determine the transfer function.

4. From variable sine wave inputs the transfer function may be established.

B. Nonlinear System Assumption

The first step in this method is the funding of any nonlinearities that would hinder the operation of the antenna system. Proust's linear method may be used in detecting such nonlinearities. In a linear system of infinite bandwidth, if a square wave of frequency w is applied at the input, the Fourier series of the input and output are given respectively by:

$$\text{Input} = \frac{4M}{\pi}\left[\sin \omega t + \frac{1}{3}\sin 3\omega t + \frac{1}{5}\sin 5\omega t + \cdots\right]$$

$$\text{Output} = \frac{4M}{\pi}\left\{A(\omega)\sin\left[\omega t + \phi(\omega)\right] + \frac{1}{3}A(\omega)\sin\left[3\omega t + \phi(3\omega)\right] + \cdots\right\}$$

If the linear system has a limited bandwidth, the output would not be as shown above. However, as the amplitude of higher harmonics are small, if the frequency W is chosen in such a way that only frequencies above the cutoff are not properly represented, it is still possible to find the useful part of the frequency response. Proust suggests that W should be chosen such that the twelve db cutoff frequency of the system corresponds to the eleventh harmonic in the Fourier expansion. If the system is highly nonlinear, the amplitude and phase of the harmonics would not agree with the Fourier series.

Some types of nonlinearities may also be determined by additional tests. For instance static friction, which could be a source of instability in a system, may be detected by using a ramp input.

Field tests performed have provided open loop data for square wave, impulse function, white noise, sine wave inputs as well as some closed loop responses. A resonant frequency of two to two and a half cycles appears to be the predominant frequency of the system. A damping ratio of one tenth was also observed. However, some unexpected output variations were observed from the accelerometers' recordings. This could not be explained readily. For instance, the approximate amplitude readings on the accelerometers located at the feedbox, X-bull gear and Y-bearing for a sine wave input in the Y-direction are given in the following table:

Table 2
Amplitudes

f cps	X-Bull Gear	Y-Bearing	Feedbox
0.01	14.5	7.0	3.5
0.02	7.0	4.0	1.5
0.03	4.5	2.5	1.2
0.05	3.0	2.0	-
0.08	2.5	1.5	1.2
0.10	2.0	1.0	1.4
0.15	1.5	1.2	-
0.25	2.0	1.5	-
0.34	3.0	2.0	-
0.51	3.5	-	-
0.78	4.5	2.5	2.0
1.00	5.0	3.0	3.0

From Table II it is observed that around 0.1 to 0.15 there is a dip in amplitude in all three accelerometers. In the X-bull gear there was also a shift of 180 degrees in the phase angle at this frequency. At first it was assumed that the structure had a low resonant frequency which was the cause of this amplitude variation. Figures 12a, 12b, and 12c show the block diagram of the accelerometers and their responses. Under the above assumption, the change in phase angle should be as shown in Figure 12c. Nevertheless, the accelerometers did not exhibit this change in phase angle.

The X-bull gear showed a sudden change of 180 degrees while the Y-bearing and feedbox do not exhibit any phase variation in the range of frequencies between 0.1 and 0.15 cps. Thus the original assumption of low resonant frequency of the structure was not correct.

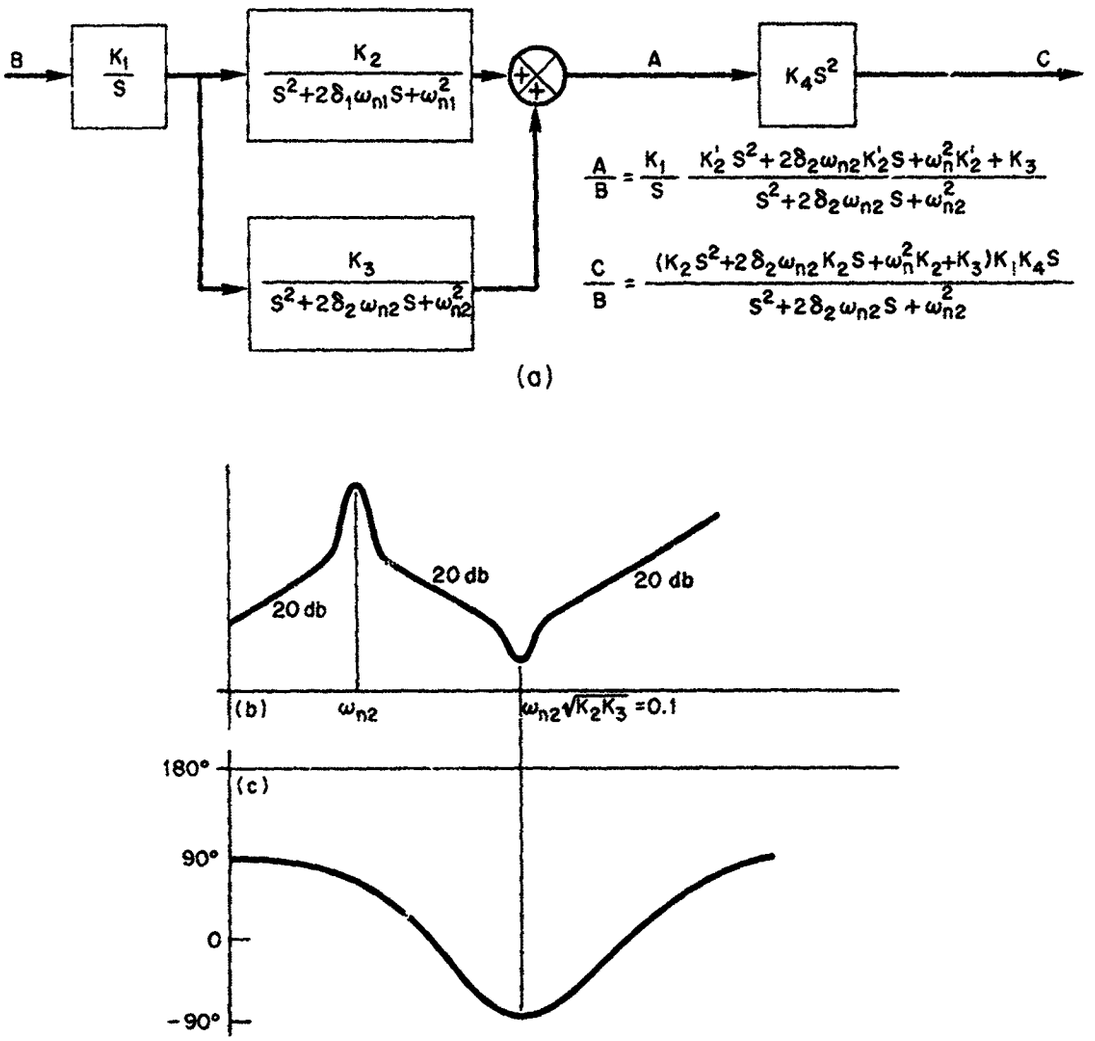

Figure 12

A second look at this situation did show that gravitational effects on the accelerometers could account for this anomaly. This may be proven mathematically. Figure 13 shows the two accelerometers located at the bull gear and the feedbox. The output voltage of an accelerometer, neglecting gravitational effects, is proportional to its acceleration. For instance, with an angular velocity $\theta' = A \cos wt$, the angular acceleration is $\theta'' = -A\omega \sin wt$ and the linear acceleration is $a = -rA\omega \sin wt$. However, in the presence of a gravitational force, and referring to Figure 12b, a force proportional to $\sin \theta$ is present. As $\theta = A/\omega \sin wt$, the force will be proportional to $\sin (A/\omega \sin wt)$. The output component of the accelerometer due to such a force obviously depends on the location of the accelerometer with respect to the rotating axis. For a sine wave input velocity the total output voltage of the accelerometers at the feedbox and bull gear could then be written as

$$e_1 = -B_F\left[\sin\left(\frac{A}{\omega}\sin\omega t\right) + \frac{rA\omega}{g}\sin\omega t\right]$$

for the feedbox accelerometer and

$$e_2 = -B_G \left[\sin\left(\frac{A}{\omega} \sin \omega t \right) - \frac{rA\omega}{g} \sin \omega t \right]$$

for the bull gear accelerometer.

The first term of the above two expressions is due to gravitational force and is a frequency modulated wave.

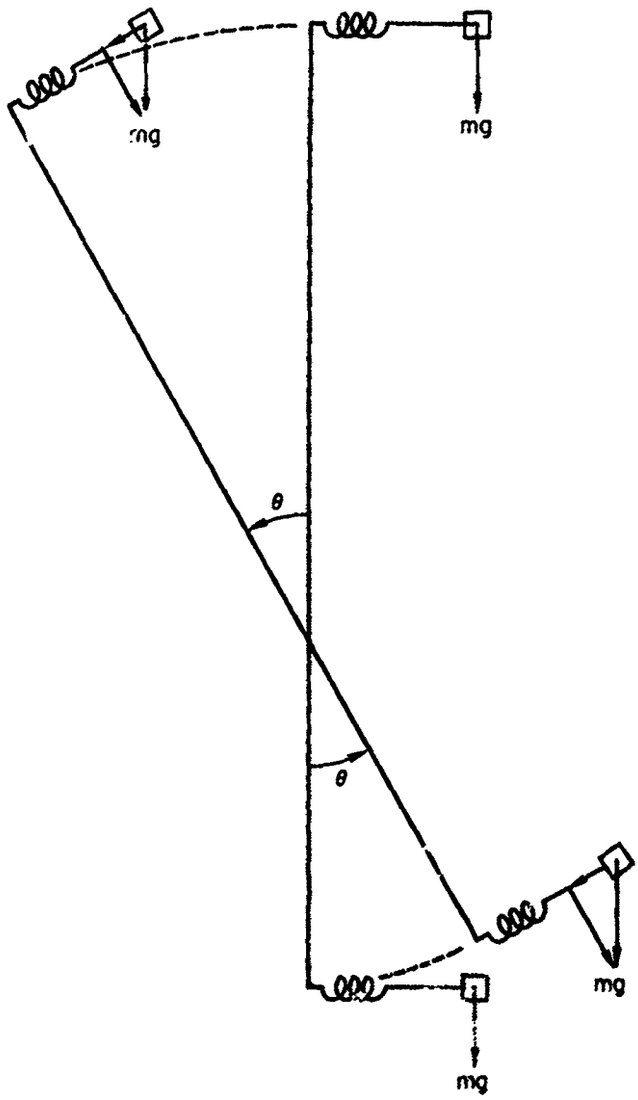

Figure 13

In order to justify the measured results, the coefficients of the corresponding Bessel series were computed with the aid of a computer and for the case of the bull gear Table 3 summarizes the results obtained.

Table 3

A, rps	$\frac{f}{CPS}$	ω, rps	$\sigma = \frac{A}{\omega}$	$J(\sigma)$	$\frac{rAW}{g}$	e_2/B_G
0.035	0.01	0.062	0.565	0.27	0.016	-0.254
0.035	0.10	0.62	0.0565	0.027	0.16	0.133
0.035	1.0	6.2	0.00565	0.0028	1.6	1.6

$$J_n(\sigma) = \sum_{k=0}^{\infty} \frac{(-1)^k}{k!\,(k+n)} \left(\frac{\sigma}{2}\right)^{n+2k}$$

This explains the reason for the change in amplitude and phase angle observed.

The noise present in most recordings of field data made impossible the determination of the exact transfer functions. In particular a 10 cps frequency was very noticeable. As this is close to the hydraulic's resonant frequency, it makes the presence of the latter.

An attempt was made to analyze the data further by means of a spectrum analyzer with very little positive results. Probably the presence of noise of considerable amplitudes plus calibration problems and nonlinearities account for this fact.

In conclusion, a 2.5 cps frequency appears to be the main resonant frequency of the system. The associated damping ratio is 0.1. It is also observed that a 12.5 cps frequency is present at some points in the feedbox and dish.

Correlation techniques were also employed as an attempt to further analyze the field data. A frequency of about 1.5 cps is apparent in some of the correlograms obtained. No explanation has been found for this and it is suggested that further work be done in both the spectrum analysis and correlation ends of the data evaluation.

REFERENCES

1. Newton, G. D., Gould, L. A., and Kaiser, J. F., "Analytical Design of Linear Feedback Controls," Ch. 9, John Wiley and Sons, 1957.
2. Truxal, J., "Automatic Feedback Control System Synthesis," Ch. 8, McGraw-Hill Book Co., Inc., 1955.
3. Titus, James W., "Wind, Induced Torques Measured on a Large Antenna," NRL Report 5549, Dec. 1960.
4. Newton, et al; op. cit.
5. Chestnut and Mayer, "Servomechanism and Regulating System Design," Volume II.
6. Gille, Pelegrin, Decaulne, "Feedback Control Systems."
7. Western Development Laboratories, "Design Criteria for a Large Multi-Purpose Tracking Antenna."

N66 31158

NOTES ON THE SPIN-HAMILTONIAN

by

H. A. Sabbagh

The spin-hamiltonian formalism, or more precisely, the effective spin-hamiltonian formalism, is a very useful one for calculating magnetic properties of paramagnetic ions imbedded in a crystal lattice. These properties are very significant in maser work. For instance, a typical calculation, which we shall later make, is that of the energy levels versus an applied d.c. magnetic field. Once these calculations are made one can then investigate such things as pumping schemes, idler and signal frequencies, etc. One can even decide if a particular material is suitable for a maser on the basis of spin-hamiltonian calculations.

The fundamental idea behind the formalism is to describe the interaction of a paramagnetic ion with its crystalline surroundings and an applied magnetic field by a function of the total spin resulting from the unpaired electrons within the ion.

The theoretical bases for prescribing the form of the spin function and the calculations resulting therefrom are, of course, quantum mechanical. The coefficients appearing in the spin function (hereafter called the spin-hamiltonian), though calculable in theory, are usually determined empirically. Indeed, this forced union of experiment and theory is what makes the formalism so powerful. We attempt to describe the theoretical behavior of a paramagnetic ion using a few emepirical constants. In this report we shall use two specific examples as a means of surveying the theory of the spin-hamiltonian. The first example is that of F^{+++} imbedded in TiO_2 (rutile); the second is Ho^{++} in a CaF_2 lattice.

I. Fe^{+++}: TiO_2 [Bleaney and Stevens, 1953; Bowers and Owen, 1955]

The 5 unpaired electrons in Fe^{3+} are each in the 3d state. This means that the ion itself is in an orbital S state, i.e., $L = 0$. To prove this we use Hund's rule together with the Pauli exclusion principle [Pake, 1962]. Hund's rules are:

1. Assign maximum S (spin) consistent with the Pauli principle.

2. Assign maximum L (orbital angular momentum) consistent with the S. L is defined to be the maximum value of the sum of the z-components of orbital angular momentum for the group of electrons.

Thus, each electron has the same energy quantum number, 3, the same orbital angular momentum quantum number, 2 (corresponding to the d state), and, if we are to assign maximum spin to the electron group, the same spin quantum number, 1/2. If there is to be no violation of the Pauli principle, therefore, each electron must have a different quantum number, m, corresponding to the z-component of orbital angular momentum. Because $l = 2$ for a d-state, we have $m = 2, 1, 0, -1, -2$. Thus electron #1 has $m = 2$, #2 has $m = 1$, etc., to #5 having $m = -2$. The total $M = m_1 + m_2 + m_3 + m_4 + m_5 = 0$. But since any arrangement of the five electrons among the five m-states always yields $M = 0$, we conclude that $L = 0$ (recall that $L = M_{max}$). Thus, Fe^{3+} is in an S-state ($L = 0$) with a spin equal to 5/2.

The spin-hamiltonian for the Fe^{3+}: TiO_2 complex is [Carter and Ckaya, 1960]:

$$H = g\beta\bar{H}\cdot\bar{S} + D(S_z^2 - 35/12) + E(S_x^2 - S_y^2)$$

$$+ (a/6)\,(S_x^4 + S_y^4 + S_z^4 - 707/16) \qquad (1\text{-}1)$$

$$+ (7/36)\,F(S_z^4 - (95/14)\,S_z^2 + 81/16).$$

The nominal values of the derived constants are:

$$g = 2.0,\ D = 20.35\ \text{gc},\ E = 2.21\ \text{gc}$$

$$a = 1.1\ \text{gc},\ F = -0.5\ \text{gc}$$

β is the Bohr magneton divided by h, Plank's constant, and is equal to $e/4\pi mc = 0.0014$ gc per gauss (e = electronic charge, m = electronic mass, and c = velocity of light). $\bar{H}$ is the applied d.c. magnetic field, measured in gauss. The spin matrices S_x, S_y and S_z are dimensionless. Thus the hamiltonian gives us frequency directly, rather than energy. Of course, energy = h x frequency.

The first term in (1-1) gives us the interaction of the total spin with the external magnetic field. The remaining terms represent the interaction of the ion with its crystalline surrounding. To understand this, consider that the crystalline field is derived from an electrostatic potential which satisfies LaPlace's equation

$$\frac{\partial^2 V}{\partial x^2} + \frac{\partial^2 V}{\partial y^2} + \frac{\partial^2 V}{\partial z^2} = 0. \qquad (1\text{-}2)$$

The solution of this equation may be expanded in a series of spherical harmonics, $Y_{lm}(\theta, \varphi)$:

$$V = \sum_{l,m} C_{lm}\, r^l\, Y_{lm} \qquad (1\text{-}3)$$

If we consider the $l = 2$ term and use the fact that $x = r \sin\theta \cos\varphi$, $y = r \sin\theta \sin\varphi$, $z = r \cos\theta$, we have for the five $l = 2$ terms (for $l = 2$ we have $m = 2, 1, 0, -1, -2$)

$$xy,\ xz,\ yz,\ 3z^2 - r^2,\ x^2 - y^2. \qquad (1\text{-}4)$$

If we replace the space coordinates x, y, z by the spin operators S_x, S_y, and S_z, respectively, we get the additional terms of the spin-hamiltonian. The justification for this substitution lies in the Wigner-Eckart theorem of quantum mechanics [Merzbacher, 1961; Slichter, 1963].

The x-, y-, and z-axes appearing in the spin-hamiltonian are referred to the crystal axes by

Hamiltonian axis	Direction in crystal
x	[1 1 0]
y	[0 0 1]
z	[1 1 0]

The Pauli spin-matrices, S_x, S_y and S_z are the 6×6 matrices

$$S_x = \frac{1}{2}\begin{bmatrix} 0 & 5^{1/2} & 0 & 0 & 0 & 0 \\ 5^{1/2} & 0 & 8^{1/2} & 0 & 0 & 0 \\ 0 & 8^{1/2} & 0 & 3 & 0 & 0 \\ 0 & 0 & 3 & 0 & 8^{1/2} & 0 \\ 0 & 0 & 0 & 8^{1/2} & 0 & 5^{1/2} \\ 0 & 0 & 0 & 0 & 5^{1/2} & 0 \end{bmatrix}$$

$$S_y = \frac{1}{2}\begin{bmatrix} 0 & -i\cdot 5^{1/2} & 0 & 0 & 0 & 0 \\ i\cdot 5^{1/2} & 0 & -i\cdot 8^{1/2} & 0 & 0 & 0 \\ 0 & i\cdot 8^{1/2} & 0 & -i\cdot 3 & 0 & 0 \\ 0 & 0 & i\cdot 3 & 0 & -i\,8^{1/2} & 0 \\ 0 & 0 & 0 & i\cdot 8^{1/2} & 0 & -i\,5^{1/2} \\ 0 & 0 & 0 & 0 & i\,5^{1/2} & 0 \end{bmatrix}$$

$$S_z = \frac{1}{2}\begin{bmatrix} 5 & 0 & 0 & 0 & 0 & 0 \\ 0 & 3 & 0 & 0 & 0 & 0 \\ 0 & 0 & 1 & 0 & 0 & 0 \\ 0 & 0 & 0 & -1 & 0 & 0 \\ 0 & 0 & 0 & 0 & -3 & 0 \\ 0 & 0 & 0 & 0 & 0 & -5 \end{bmatrix} \qquad (1\text{-}5)$$

We calculate, using ordinary matrix multiplication, the following matrices which appear in (1-1):

$$S_x^2 = \frac{1}{4}\begin{bmatrix} 5 & 0 & 40^{1/2} & 0 & 0 & 0 \\ 0 & 13 & 0 & 72^{1/2} & 0 & 0 \\ 40^{1/2} & 0 & 17 & 0 & 72^{1/2} & 0 \\ 0 & 72^{1/2} & 0 & 17 & 0 & 40^{1/2} \\ 0 & 0 & 72^{1/2} & 0 & 13 & 0 \\ 0 & 0 & 0 & 40^{1/2} & 0 & 5 \end{bmatrix}$$

$$S_y^2 = \frac{1}{4}\begin{bmatrix} 5 & 0 & -(40)^{1/2} & 0 & 0 & 0 \\ 0 & 13 & 0 & -(72)^{1/2} & 0 & 0 \\ -(40)^{1/2} & 0 & 17 & 0 & -(72)^{1/2} & 0 \\ 0 & -(72)^{1/2} & 0 & 17 & 0 & -(40)^{1/2} \\ 0 & 0 & -(72)^{1/2} & 0 & 13 & 0 \\ 0 & 0 & 0 & -(40)^{1/2} & 0 & 5 \end{bmatrix}$$

$$S_z^2 = \frac{1}{4}\begin{bmatrix} 25 & 0 & 0 & 0 & 0 & 0 \\ 0 & 9 & 0 & 0 & 0 & 0 \\ 0 & 0 & 1 & 0 & 0 & 0 \\ 0 & 0 & 0 & 1 & 0 & 0 \\ 0 & 0 & 0 & 0 & 9 & 0 \\ 0 & 0 & 0 & 0 & 0 & 25 \end{bmatrix}$$

$$S_x^4 = \frac{1}{16}\begin{bmatrix} 65 & 0 & 44\cdot 10^{1/2} & 0 & 24\cdot 5^{1/2} & 0 \\ 0 & 241 & 0 & 180\cdot 2^{1/2} & 0 & 24\cdot 5^{1/2} \\ 44\cdot 10^{1/2} & 0 & 401 & 0 & 180\cdot 2^{1/2} & 0 \\ 0 & 180\cdot 2^{1/2} & 0 & 401 & 0 & 44\cdot 10^{1/2} \\ 24\cdot 5^{1/2} & 0 & 180\cdot 2^{1/2} & 0 & 241 & 0 \\ 0 & 24\cdot 5^{1/2} & 0 & 44\cdot 10^{1/2} & 0 & 65 \end{bmatrix}$$

$$S_y^4 = \frac{1}{16}\begin{bmatrix} 65 & 0 & -44\cdot 10^{1/2} & 0 & 24\cdot 5^{1/2} & 0 \\ 0 & 241 & 0 & -180\cdot 2^{1/2} & 0 & 24\cdot 5^{1/2} \\ -44\cdot 10^{1/2} & 0 & 401 & 0 & -180\cdot 2^{1/2} & 0 \\ 0 & -180\cdot 2^{1/2} & 0 & 401 & 0 & -44\cdot 10^{1/2} \\ 24\cdot 5^{1/2} & 0 & -180\cdot 2^{1/2} & 0 & 241 & 0 \\ 0 & 24\cdot 5^{1/2} & 0 & -44\cdot 10^{1/2} & 0 & 65 \end{bmatrix}$$

and

$$S_z^4 = \frac{1}{16}\begin{bmatrix} 625 & 0 & 0 & 0 & 0 & 0 \\ 0 & 81 & 0 & 0 & 0 & 0 \\ 0 & 0 & 1 & 0 & 0 & 0 \\ 0 & 0 & 0 & 1 & 0 & 0 \\ 0 & 0 & 0 & 0 & 81 & 0 \\ 0 & 0 & 0 & 0 & 0 & 625 \end{bmatrix} \tag{1-6}$$

The constants 35/12, 707/16, and 81/16 are really the matrices (35/12) U, (707/16) U, and (81/16) U, respectively, where U is the 6 × 6 unit matrix, having 1's along the main

diagonal and zeros elsewhere. Using the results obtained so far we have for the spin-hamiltonian, H, the 6×6 matrix

$$H = \begin{bmatrix} (6.007H + 68.15) & 0 & 6.98 & 0 & 1.23 & 0 \\ 0 & (0.0042H - 14.78) & 0 & 9.37 & 0 & 1.23 \\ 6.98 & 0 & (0.0014H - 53.57) & 0 & 9.37 & 0 \\ 0 & 9.37 & 0 & (-0.0014H - 53.57) & 0 & 6.98 \\ 1.23 & 0 & 9.37 & 0 & (-0.0042H - 14.78) & 0 \\ 0 & 1.23 & 0 & 6.98 & 0 & (-0.007H + 68.15) \end{bmatrix} \tag{1-7}$$

In writing down this final form for H we have assumed that $\bar{H} = H\,\bar{a}_z$, ($\bar{a}_z$ being the unit vector in the z-direction), which means that $\bar{H}\cdot\bar{S} = HS_z$.

Derivation of Energy Levels Using the Spin-Hamiltonian

According to the general rules of quantum mechanics, the state of a system is defined in terms of the solution of Schrödinger's equation:

$$ih\frac{\partial\psi}{\partial t} = H\psi \tag{1-8}$$

If H does not depend on time then it is convenient to assume that

$$\psi = u \exp\left(-\frac{iE}{h}t\right) \tag{1-9}$$

where u is independent of time. Upon substituting (1-9) into (1-8) it follows that u must satisfy the time-independent wave equation:

$$Hu = Eu. \tag{1-10}$$

It is apparent from (1-9) that E is an energy parameter because $E/\hbar$ must be angular frequency. Thus, (1-10) is an eigen-value, or characteristic-value, equation in which u and E are the eigen-vector (or eigenstate) and energy respectively, of the system represented by the Hamiltonian H.

Because H is a 6×6 matrix, the state vector, u, must be a 6-row, 1-column vector:

$$u = \begin{bmatrix} u_1 \\ u_2 \\ u_3 \\ u_4 \\ u_5 \\ u_6 \end{bmatrix}$$

Operating on (1-11) with (1-7) gives us, for (1-10):

$$
\begin{aligned}
&(0.007H + 68.15)\, u_1 + 6.98\, u_3 + 1.23\, u_5 = E u_1 \\
&(0.0042H - 14.78)\, u_2 + 9.37\, u_4 + 1.23\, u_6 = E u_2 \\
&6.98\, u_1 + (0.0014H - 53.57)\, u_3 + 9.37\, u_5 = E u_3 \\
&9.37\, u_2 + (-0.0014H - 53.57)\, u_4 + 6.98\, u_6 = E u_4 \\
&1.23\, u_1 + 9.37\, u_3 + (-0.0042H - 14.78)\, u_5 = E u_5 \\
&1.23\, u_2 + 6.98\, u_4 + (-0.007H + 68.15)\, u_6 = E u_6
\end{aligned}
\tag{1-12}
$$

or, after transposing the right-hand side:

$$
\begin{aligned}
&(0.007H + 68.15 - E)\, u_1 + 6.98\, u_3 + 1.23\, u_5 = 0 \\
&(0.0042H - 14.78 - E)\, u_2 + 9.37\, u_4 + 1.23\, u_6 = 0 \\
&6.98\, u_1 + (0.0014H - 53.57 - E)\, u_3 + 9.37\, u_5 = 0 \\
&9.37\, u_2 + (-0.0014H - 53.57 - E)\, u_4 + 6.98\, u_6 = 0 \\
&1.23\, u_1 + 9.37\, u_3 + (-0.0042H - 14.78 - E)\, u_5 = 0 \\
&1.23\, u_2 + 6.98\, u_4 + (-0.007H + 68.15 - E)\, u_6 = 0
\end{aligned}
\tag{1-13}
$$

This is a homogeneous system of linear equations to be solved for u_1, u_2, u_3, u_4, u_5, u_6. In order for at least one of these u's to be non-zero, it is necessary that the determinant of the coefficient matrix vanish. We require, therefore, that:

$$
\det \begin{bmatrix}
(0.007H+68.15-E) & 0 & 6.98 & 0 & 1.23 & 0 \\
0 & (0.0042H-14.78-E) & 0 & 9.37 & 0 & 1.23 \\
6.98 & 0 & (0.0014H-53.57-E) & 0 & 9.37 & 0 \\
0 & 9.37 & 0 & (-0.0014H-53.57-E) & 0 & 6.98 \\
1.23 & 0 & 9.37 & 0 & (-0.0042H-14.78-E) & 0 \\
0 & 1.23 & 0 & 6.98 & 0 & (-0.007H+68.15-E)
\end{bmatrix} = 0 \tag{1-14}
$$

For each value of the magnetic field, H, there correspond six values of E satisfying (1-14). A program for computing these eigen-values was written by Mr. Henry Miller for the IBM-7094. This program gives not only the eigen-values, E, but also the corresponding eigen-vectors, u. The numerical results are shown in Fig. 1.

It is noted that the zero-field energies occur in pairs. Each pair is called a Kramers' doublet to signify that it may be interpreted by Kramers' theorem which states that in a system containing an odd number of electrons, an electric field (in this case the crystalline electric field) cannot completely remove all degeneracies (when two or more energy states coincide, the corresponding energy level is said to be degenerate).

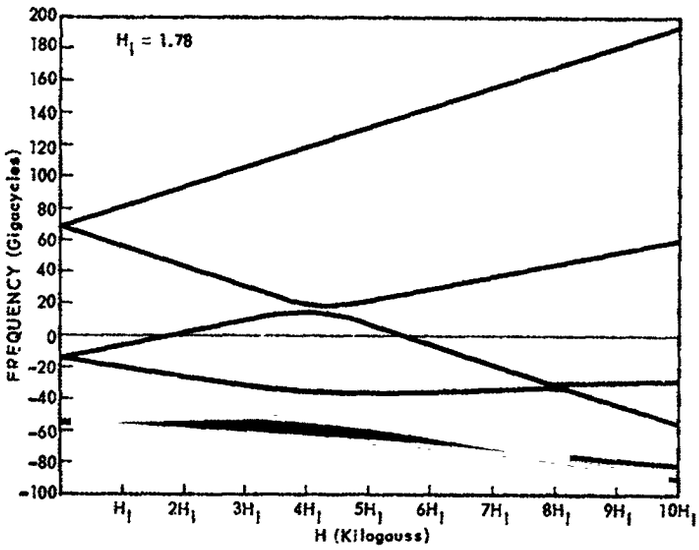

←Figure 1

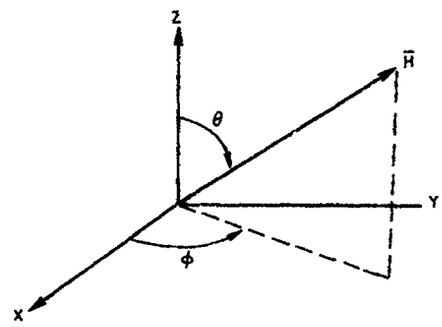

Figure 2

We may calculate the energy levels for different orientations of $\bar{H}$ by modifying the $\bar{H}\cdot\bar{S}$ term appearing in (1-1). Figure 2 illustrates the spherical coordinates to be used.

In terms of the spherical coordinates we have:

$$\bar{H} = H \sin\theta \cos\varphi\, \bar{a}_x + H \sin\theta \sin\varphi\, \bar{a}_y + H \cos\theta\, \bar{a}_z, \tag{1-15}$$

where

$$H = |\bar{H}|.$$

Thus

$$\bar{H}\cdot\bar{S} = (H \sin\theta \cos\varphi)\, S_x + (H \sin\theta \sin\varphi)\, S_y + H \cos\theta\, S_z, \tag{1-16}$$

where S_x, S_y, and S_z are the spin matrices of (1-5). The effect of (1-16) is to introduce new terms in the spin-hamiltonian matrix, H. This modifies (1-7) and (1-14) showing that the energy levels vary with θ and φ and, hence, with the orientation of $\bar{H}$.

II. Ho^{++}: CaF_2 [Sabisky and Lewis, 1963].

Holmium is a type 4f rare earth, which means that the divalent Holmium ion has its unpaired electrons in the 4f shell where they are effectively screened from their crystalline surroundings by electrons in the outer shells. Therefore, as a reasonable approximation to the effective spin-hamiltonian we may discard any terms that represent the crystalline field. We must, however, include the spin-spin interaction between the unpaired electrons and the nucleus because these electrons are relatively close to the nucleus. Thus, we use the following spin-hamiltonian

$$H = g\beta\bar{H}\cdot\bar{S} + A\bar{I}\cdot\bar{S}, \tag{2-1}$$

where $g = 5.91$, $\beta = 0.0014$ gc/gauss, $A = 3.924$ gc, $\bar{S}$ is the electron spin operator, with effective spin 1/2, and $\bar{I}$ is the nuclear spin operator with spin 7/2.

Because we are dealing with a system of two particles (electron plus nucleus) we cannot simply form matrix products in order to evaluate H. In (2-1) the term $\bar{I} \cdot \bar{S}$ must be interpreted as the direct-product of the operators $\bar{I}$ and $\bar{S}$. This concept will be explained in more detail.

The effective electron spin of 1/2 means that there are $2 \times 1/2 + 1 = 2$ possible projections of the electronic spin vector upon (say) the Z-axis: spin "up" and spin "down". The nuclear spin of 7/2 implies that there are $2 \times 7/2 + 1 = 8$ possible orientations of the nuclear spin moment. Hence, there are 16 possible states jointly involving the nucleus and electron, eight corresponding to electronic spin up and eight more for spin down.

If

$$\begin{aligned} \alpha_1 &= [1\ 0] \\ \alpha_2 &= [0\ 1], \end{aligned} \tag{2-2}$$

stand for electronic spin up and spin down, respectively, and

$$\begin{aligned} \beta_1 &= [1\,0\,0\,0\,0\,0\,0\,0], & \beta_5 &= [0\,0\,0\,0\,1\,0\,0\,0] \\ \beta_2 &= [0\,1\,0\,0\,0\,0\,0\,0], & \beta_6 &= [0\,0\,0\,0\,0\,1\,0\,0] \\ \beta_3 &= [0\,0\,1\,0\,0\,0\,0\,0], & \beta_7 &= [0\,0\,0\,0\,0\,0\,1\,0] \\ \beta_4 &= [0\,0\,0\,1\,0\,0\,0\,0], & \beta_8 &= [0\,0\,0\,0\,0\,0\,0\,1] \end{aligned} \tag{2-3}$$

stand for the eight nuclear spin states, then the direct-products of the electronic and nuclear spin states are represented by the 1×16 matrices (or row-rectors):

$$\begin{aligned} |1\rangle &= [1\ 0 \cdots\cdots\cdots 0] \\ |2\rangle &= [0\ 1\ 0 \cdots\cdots\cdots 0] \\ |3\rangle &= [0\ 0\ 1\ 0 \cdots\cdots 0] \\ |4\rangle &= [0\ 0\ 0\ 1\ 0 \cdots\cdots 0] \\ &\vdots \\ &\text{etc.} \\ &\vdots \\ |15\rangle &= [0\ 0\ 0 \cdots\cdots 0\ 1\ 0] \\ |16\rangle &= [0\ 0 \cdots\cdots 0\ 0\ 1]. \end{aligned} \tag{2-4}$$

The first eight direct-product states correspond to electronic spin up and the last eight to spin down.

If we arbitrarily take the magnetic field, $\bar{H}$, to lie along the z-axis, then $g\beta\bar{H}\cdot\bar{S} = g\beta HS_z$, where H is the magnitude of $\bar{H}$. We must treat this operator as the direct product of S_z and U, where

$$S_z = \frac{i}{2}\begin{bmatrix} 1 & 0 \\ 0 & -1 \end{bmatrix}, \tag{2-5}$$

and

$$U = \begin{bmatrix} 1 & 0 & 0 & 0 & 0 & 0 & 0 & 0 \\ 0 & 1 & 0 & 0 & 0 & 0 & 0 & 0 \\ 0 & 0 & 1 & 0 & 0 & 0 & 0 & 0 \\ 0 & 0 & 0 & 1 & 0 & 0 & 0 & 0 \\ 0 & 0 & 0 & 0 & 1 & 0 & 0 & 0 \\ 0 & 0 & 0 & 0 & 0 & 1 & 0 & 0 \\ 0 & 0 & 0 & 0 & 0 & 0 & 1 & 0 \\ 0 & 0 & 0 & 0 & 0 & 0 & 0 & 0 \end{bmatrix} \tag{2-6}$$

is the 8×8 unit (or identity) matrix.

The direct product of these two matrices is given by the 16×16 matrix

$$S_z \times U = \frac{1}{2}\left[\begin{array}{cccccccc:cccccccc} 1 & 0 & 0 & 0 & 0 & 0 & 0 & 0 & & & & & & & & \\ 0 & 1 & 0 & 0 & 0 & 0 & 0 & 0 & & & & & & & & \\ 0 & 0 & 1 & 0 & 0 & 0 & 0 & 0 & & & & & & & & \\ 0 & 0 & 0 & 1 & 0 & 0 & 0 & 0 & & & & & & & & \\ 0 & 0 & 0 & 0 & 1 & 0 & 0 & 0 & & & & 0 & & & & \\ 0 & 0 & 0 & 0 & 0 & 1 & 0 & 0 & & & & & & & & \\ 0 & 0 & 0 & 0 & 0 & 0 & 1 & 0 & & & & & & & & \\ 0 & 0 & 0 & 0 & 0 & 0 & 0 & 1 & & & & & & & & \\ \hdashline & & & & & & & & -1 & 0 & 0 & 0 & 0 & 0 & 0 & 0 \\ & & & & & & & & 0 & -1 & 0 & 0 & 0 & 0 & 0 & 0 \\ & & & & & & & & 0 & 0 & -1 & 0 & 0 & 0 & 0 & 0 \\ & & & & & & & & 0 & 0 & 0 & -1 & 0 & 0 & 0 & 0 \\ & & & & 0 & & & & 0 & 0 & 0 & 0 & -1 & 0 & 0 & 0 \\ & & & & & & & & 0 & 0 & 0 & 0 & 0 & -1 & 0 & 0 \\ & & & & & & & & 0 & 0 & 0 & 0 & 0 & 0 & -1 & 0 \\ & & & & & & & & 0 & 0 & 0 & 0 & 0 & 0 & 0 & -1 \end{array}\right] \tag{2-7}$$

Next, we must calculate the direct-product, $\bar{I} \times \bar{S}$, of $\bar{I}$ and $\bar{S}$. By definition $\bar{I} \times \bar{S} = \bar{I}_x \times S_x + I_y \times S_y + I_z \times S_z$, where, for the system being studied:

$$S_x = \frac{1}{2}\begin{bmatrix} 0 & 1 \\ 1 & 0 \end{bmatrix} \quad S_y = \frac{1}{2}\begin{bmatrix} 0 & -i \\ i & 0 \end{bmatrix} \quad S_z = \frac{1}{2}\begin{bmatrix} 1 & 0 \\ 0 & -1 \end{bmatrix} \tag{2-8}$$

$$I_x = \frac{1}{2}\begin{bmatrix} 0 & 7^{1/2} & 0 & 0 & 0 & 0 & 0 & 0 \\ 7^{1/2} & 0 & 12^{1/2} & 0 & 0 & 0 & 0 & 0 \\ 0 & 12^{1/2} & 0 & 15^{1/2} & 0 & 0 & 0 & 0 \\ 0 & 0 & 15^{1/2} & 0 & 4 & 0 & 0 & 0 \\ 0 & 0 & 0 & 4 & 0 & 15^{1/2} & 0 & 0 \\ 0 & 0 & 0 & 0 & 15^{1/2} & 0 & 12^{1/2} & 0 \\ 0 & 0 & 0 & 0 & 0 & 12^{1/2} & 0 & 7^{1/2} \\ 0 & 0 & 0 & 0 & 0 & 0 & 7^{1/2} & 0 \end{bmatrix}$$

$$I_y = \frac{1}{2}\begin{bmatrix} 0 & -i7^{1/2} & 0 & 0 & 0 & 0 & 0 & 0 \\ i7^{1/2} & 0 & -i12^{1/2} & 0 & 0 & 0 & 0 & 0 \\ 0 & i12^{1/2} & 0 & -i15^{1/2} & 0 & 0 & 0 & 0 \\ 0 & 0 & i15^{1/2} & 0 & -i4 & 0 & 0 & 0 \\ 0 & 0 & 0 & i4 & 0 & -i15^{1/2} & 0 & 0 \\ 0 & 0 & 0 & 0 & i15^{1/2} & 0 & -i12^{1/2} & 0 \\ 0 & 0 & 0 & 0 & 0 & i12^{1/2} & 0 & -i7^{1/2} \\ 0 & 0 & 0 & 0 & 0 & 0 & i7^{1/2} & 0 \end{bmatrix}$$

$$I_z = \frac{1}{2}\begin{bmatrix} 7 & 0 & 0 & 0 & 0 & 0 & 0 & 0 \\ 0 & 5 & 0 & 0 & 0 & 0 & 0 & 0 \\ 0 & 0 & 3 & 0 & 0 & 0 & 0 & 0 \\ 0 & 0 & 0 & 1 & 0 & 0 & 0 & 0 \\ 0 & 0 & 0 & 0 & -1 & 0 & 0 & 0 \\ 0 & 0 & 0 & 0 & 0 & -3 & 0 & 0 \\ 0 & 0 & 0 & 0 & 0 & 0 & -5 & 0 \\ 0 & 0 & 0 & 0 & 0 & 0 & 0 & -7 \end{bmatrix}$$

The required direct-products are given by the 16 × 16 matrices:

$$S_x \times I_x = \frac{1}{4}\left[\begin{array}{cccccccc:cccccccc}
 & & & & & & & & 0 & 7^{1/2} & 0 & 0 & 0 & 0 & 0 & 0 \\
 & & & & & & & & 7^{1/2} & 0 & 12^{1/2} & 0 & 0 & 0 & 0 & 0 \\
 & & & & & & & & 0 & 12^{1/2} & 0 & 15^{1/2} & 0 & 0 & 0 & 0 \\
 & & & & & & & & 0 & 0 & 15^{1/2} & 0 & 4 & 0 & 0 & 0 \\
 & & & & & & & & 0 & 0 & 0 & 4 & 0 & 15^{1/2} & 0 & 0 \\
 & & & & & & & & 0 & 0 & 0 & 0 & 15^{1/2} & 0 & 12^{1/2} & 0 \\
 & & & & & & & & 0 & 0 & 0 & 0 & 0 & 12^{1/2} & 0 & 7^{1/2} \\
 & & & & & & & & 0 & 0 & 0 & 0 & 0 & 0 & 7^{1/2} & 0 \\
\hdashline
0 & 7^{1/2} & 0 & 0 & 0 & 0 & 0 & 0 & & & & & & & & \\
7^{1/2} & 0 & 12^{1/2} & 0 & 0 & 0 & 0 & 0 & & & & & & & & \\
0 & 12^{1/2} & 0 & 15^{1/2} & 0 & 0 & 0 & 0 & & & & & & & & \\
0 & 0 & 15^{1/2} & 0 & 4 & 0 & 0 & 0 & & & & & & & & \\
0 & 0 & 0 & 4 & 0 & 15^{1/2} & 0 & 0 & & & & & 0 & & & \\
0 & 0 & 0 & 0 & 15^{1/2} & 0 & 12^{1/2} & 0 & & & & & & & & \\
0 & 0 & 0 & 0 & 0 & 12^{1/2} & 0 & 7^{1/2} & & & & & & & & \\
0 & 0 & 0 & 0 & 0 & 0 & 7^{1/2} & 0 & & & & & & & &
\end{array}\right]$$

$$S_y \times I_y = \frac{1}{4}\left[\begin{array}{cccccccc:cccccccc}
 & & & & & & & & 0 & -7^{1/2} & 0 & 0 & 0 & 0 & 0 & 0 \\
 & & & & & & & & 7^{1/2} & 0 & -12^{1/2} & 0 & 0 & 0 & 0 & 0 \\
 & & & & & & & & 0 & 12^{1/2} & 0 & -15^{1/2} & 0 & 0 & 0 & 0 \\
 & & & & & & & & 0 & 0 & 15^{1/2} & 0 & -4 & 0 & 0 & 0 \\
 & & & & & & & & 0 & 0 & 0 & 4 & 0 & -15^{1/2} & 0 & 0 \\
 & & & & & & & & 0 & 0 & 0 & 0 & 15^{1/2} & 0 & -12^{1/2} & 0 \\
 & & & & & & & & 0 & 0 & 0 & 0 & 0 & 12^{1/2} & 0 & -7^{1/2} \\
 & & & & & & & & 0 & 0 & 0 & 0 & 0 & 0 & 7^{1/2} & 0 \\
\hdashline
0 & 7^{1/2} & 0 & 0 & 0 & 0 & 0 & 0 & & & & & & & & \\
-7^{1/2} & 0 & 12^{1/2} & 0 & 0 & 0 & 0 & 0 & & & & & & & & \\
0 & -12^{1/2} & 0 & 15^{1/2} & 0 & 0 & 0 & 0 & & & & & & & & \\
0 & 0 & -15^{1/2} & 0 & 4 & 0 & 0 & 0 & & & & & & & & \\
0 & 0 & 0 & -4 & 0 & 15^{1/2} & 0 & 0 & & & & & 0 & & & \\
0 & 0 & 0 & 0 & -15^{1/2} & 0 & 12^{1/2} & 0 & & & & & & & & \\
0 & 0 & 0 & 0 & 0 & -12^{1/2} & 0 & 7^{1/2} & & & & & & & & \\
0 & 0 & 0 & 0 & 0 & 0 & -7^{1/2} & 0 & & & & & & & &
\end{array}\right]$$

$$
S_z \times I_z = \frac{1}{4}
\left[\begin{array}{cccccccc:cccccccc}
7 & 0 & 0 & 0 & 0 & 0 & 0 & 0 & & & & & & & & \\
0 & 5 & 0 & 0 & 0 & 0 & 0 & 0 & & & & & & & & \\
0 & 0 & 3 & 0 & 0 & 0 & 0 & 0 & & & & & & & & \\
0 & 0 & 0 & 1 & 0 & 0 & 0 & 0 & & & & 0 & & & & \\
0 & 0 & 0 & 0 & -1 & 0 & 0 & 0 & & & & & & & & \\
0 & 0 & 0 & 0 & 0 & -3 & 0 & 0 & & & & & & & & \\
0 & 0 & 0 & 0 & 0 & 0 & -5 & 0 & & & & & & & & \\
0 & 0 & 0 & 0 & 0 & 0 & 0 & -7 & & & & & & & & \\
\hdashline
 & & & & & & & & -7 & 0 & 0 & 0 & 0 & 0 & 0 & 0 \\
 & & & & & & & & 0 & -5 & 0 & 0 & 0 & 0 & 0 & 0 \\
 & & & & & & & & 0 & 0 & -3 & 0 & 0 & 0 & 0 & 0 \\
 & & & & & & & & 0 & 0 & 0 & -1 & 0 & 0 & 0 & 0 \\
 & & & & 0 & & & & 0 & 0 & 0 & 0 & 1 & 0 & 0 & 0 \\
 & & & & & & & & 0 & 0 & 0 & 0 & 0 & 3 & 0 & 0 \\
 & & & & & & & & 0 & 0 & 0 & 0 & 0 & 0 & 5 & 0 \\
 & & & & & & & & 0 & 0 & 0 & 0 & 0 & 0 & 0 & 7
\end{array}\right]
\qquad (2\text{-}9)
$$

Upon substituting (2-7) and (2-9) into (2-1), we get (2-10) as the final form of the spin-hamiltonian matrix. All entries not shown are zero, and H is measured in kilogauss.

From this point on the analysis proceeds as in the treatment of iron-doped rutile. We must calculate the eigen-values of (2-10) as a function of H. The results of the IBM-7094 computations are shown in Figure 3.

A comparison of Figures 1 and 3 shows that Ho^{++} has a much more uniform variation of energy (and hence resonant frequency) with H than does Fe^{++}. This follows, as has been mentioned before, because the unpaired electrons in Ho^{++} are screened from the crystalline field, whereas those of Fe^{3+} are not. Hence, Ho^{2+} behaves, for H greater than 3 kilogauss, as a free spin in an external magnetic field. We would expect this same qualitative behavior for many of the 4f rare earths, no matter what the crystal lattice is.

$$
H = \begin{bmatrix}
4.12H+6.87 & & &

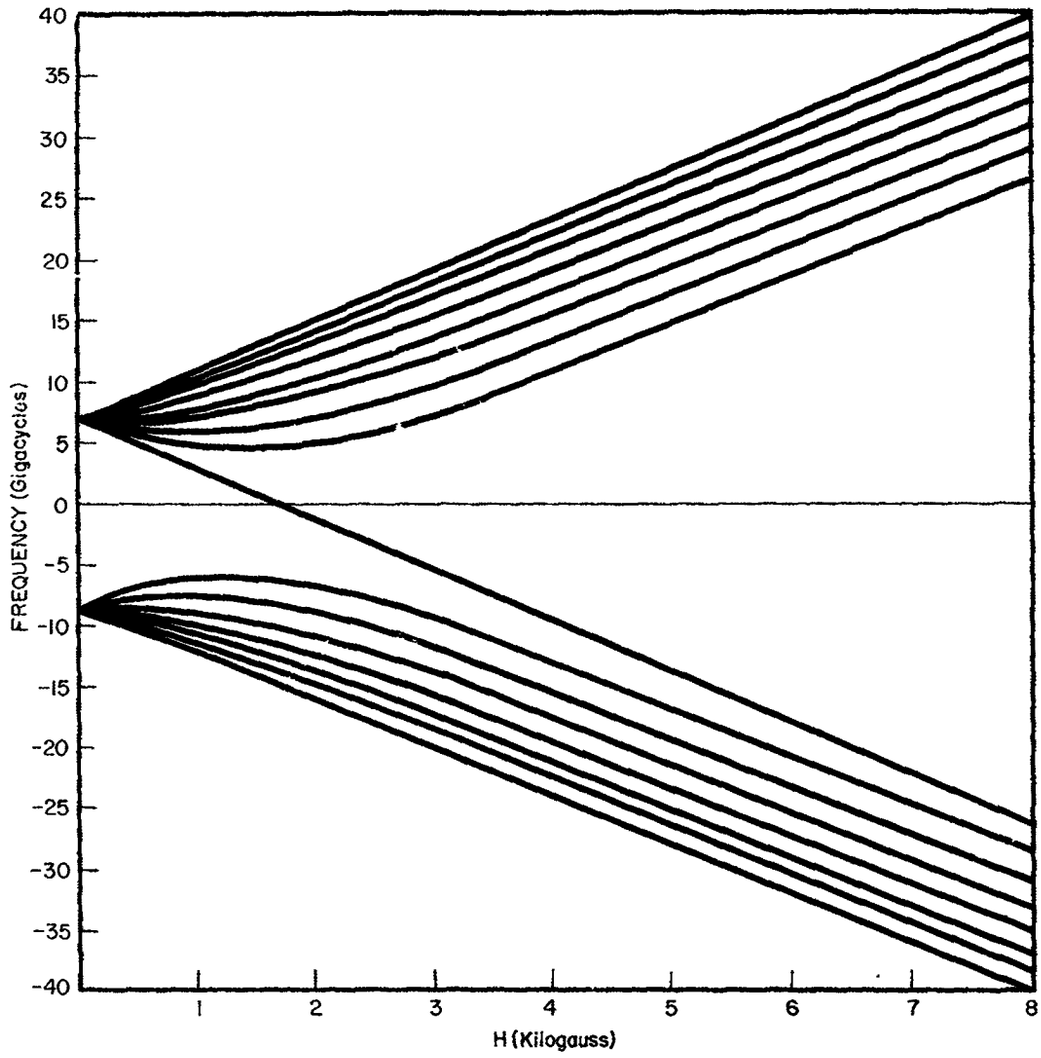

Figure 3

REFERENCES

B. Bleaney and K. W. H. Stevens, Repts. Progr. in Phys., 16, 108 (1953)

K. D. Bowers and J. Owen, Repts. Progr. in Phys., 18, 304 (1955)

D. L. Carter and A. Okaya, Phys. Rev., 118, No. 6, 1485 (1960)

E. Merzbacher, Quantum Mechanics, John Wiley & Sons, Inc., New York, 1961.

G. E. Pake, Paramagnetic Resonance, W. A. Benjamin, Inc., New York, 1962.

E. S. Sabisky and H. R. Lewis, Proc. IEEE, 51, No. 1, 53 (1963).

C. P. Slichter, Principles of Magnetic Resonance, Harper & Row, New York, 1963.

N66 31159

A PRELIMINARY STUDY OF HOLOGRAPHY

by

L. G. McCracken, Jr., Associate Professor
Electrical Engineering, Lehigh University
Bethlehem, Pennsylvania

31159

I. SUMMARY

This is a preliminary study of holograms for information processing, attention being directed toward their formation, reconstruction of their images, and the images resolution. The formation of holograms is studied with respect to information preservation for two- and three-dimensional objects and resolution of the interference patterns controlled by frequency dispersion, beam collimation, and relative motions of the laser light source and objects to be imaged. Here, the emphasis has been placed on contrast and energy ratios; so that a suitable quantization measure can be determined. For reconstruction of the images from holograms, the problem of "twinning" and its removal, multiple images spatially and/or frequency separated, and aperture limiting phenomena are explored. Finally, the image resolution upon reconstruction, manifesting the completeness of the hologram process, is found to depend on the previously discussed factors in such a way that additional study is required to obtain a meaningful measure.

Author

II. FORMATION AND RECONSTRUCTION OF HOLOGRAMS

Information Preservation with Holograms

A two-dimensional screen with (N_x, N_y) elements per unit length is interposed along a collimated path of monochromatic radiation of wavelength λ from a source Q_1 to a recording medium Σ of elements $p \in P$, the observation point. Simultaneous with radiation from a source Q_1 is a similar monochromatic, unobscured source Q_2 radiating along a path oriented at an angle θ with respect to the normal to the medium's plane, Σ. The information content[1] for the interposed screen Σ_1, $\mathcal{H} = \log_2 N_x + \log_2 N_y$, is preserved in the original mapping via Q_1, and the interference pattern induced by the addition of the second source Q_2 suffers no loss of information content as evidenced by the equivalent field[2] generated by the "complementary"[3] screen, whose current distribution complements the original screen distribution. Thus, one sees the typical interference pattern for two

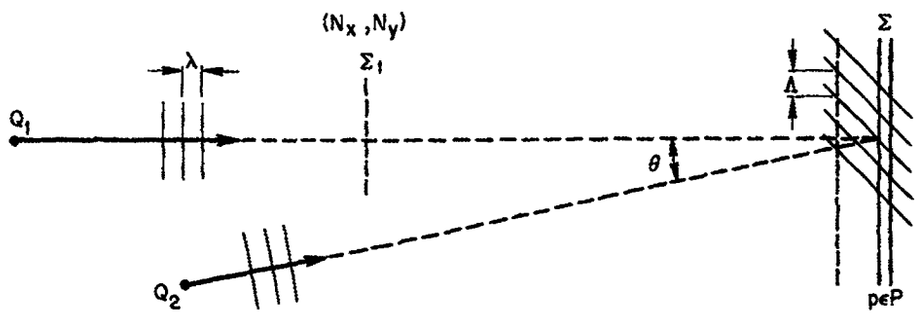

Figure 1--Formation of hologram

sources from which is subtracted the complementary field, and for black-white screens one easily notes there is no information loss.

Collapsing Loss in Imaging with Holograms

Allow a three-dimensional configuration of objects to be illuminated by a collimated monochromat of wavelength λ.

$$\psi(P) = \psi_2(P) + \psi_S(P)$$

$$\psi(P) = \psi_2(P) + \sum_{k=1}^{n} \frac{1}{4\pi} \int_{\Sigma_k} I(\sigma_k) \frac{e^{ikRpq_k}}{Rpq_k} d\sigma_k$$

$$\psi(P) = \psi_2(P) + \psi_1(P) = \overline{\psi_S(P)}$$

$$\psi(P) = 2 \cos\left(\frac{2\pi y}{\Lambda}\right) - \overline{\psi_S(P)}. \tag{1}$$

The radiation from the configuration has an equivalent distribution of current sources on the screen Σ_1, hence the information content for the screen is preserved in its imaging on the recording medium. Because the distribution on the screen has a collapse of dimension, a loss of information necessarily does occur in the formation of a hologram.

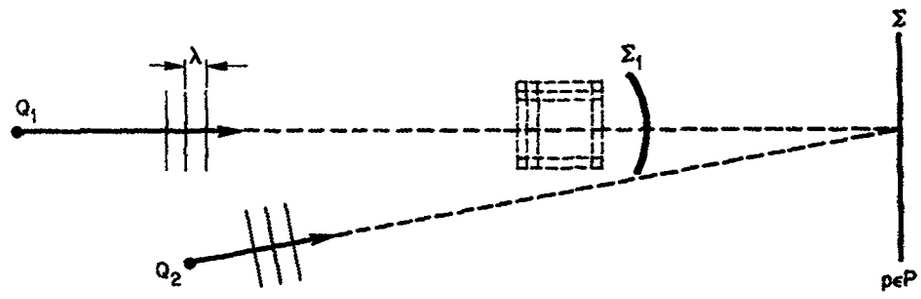

Figure 2–Equivalent screen

Supposing one could vary the observation point upon readout from the hologram, one could alter the "screen's" location, modify the shadowing or silouhetting that one sees and thus recover the information lost via collapse.

Twinning and Loss of Information for Holograms

In the formation of a hologram, one cannot avoid a difference of intensities for ψ_1 (P) and ψ_2 (P), though they be coherent sources. For reference, ψ_1 (P) and ψ_2 (P) have been chosen conveniently to be of unit magnitude, hence we can refer to them as $\psi_{1,0}$ (P) and $\psi_{2,0}$ (P), respectively; again, for convenience, we can choose ψ_2 (P) = $\Gamma\, \psi_{2,0}$ (P), Γ a complex constant, in order that we can refer back to the simplest case when $\Gamma = 1$.

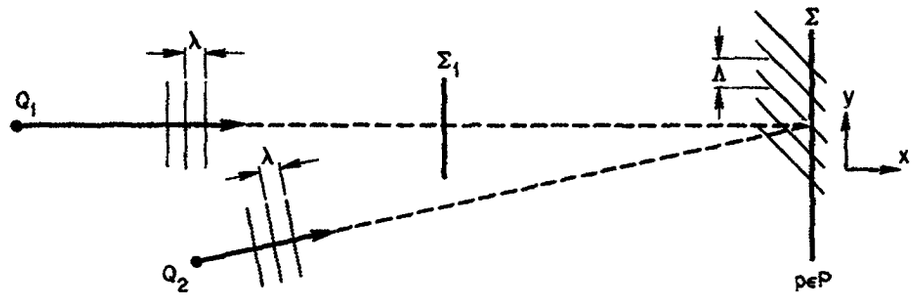

Figure 3–The hologram scene

The image formed on the surface Σ, for $p \in P$, is of wave potential $\psi(P)$,

$$\psi(P) = \psi_2(P) + \frac{1}{4\pi}\int_{\Sigma_1} I(\sigma_1)\,\frac{e^{j\vec{k}\cdot\vec{R}_{p\sigma_1}}}{R_{p\sigma_1}}\,d\sigma_1 \tag{2}$$

where $I(\sigma_1)$ is the equivalent current distribution for the screen Σ_1 containing the projected information from the geometrical array of objects placed between the source Q_1 and the screen, and the appropriate kernel function is for free-space. Were the objects removed, the screen's distribution becoming uniform because of the collimated light source Q_1, the interference pattern at Σ would show the difference of Q_1 and Q_2; upon replacement, the information on the screen would be preserved in the new interference pattern. One would find the wave potential $\psi(P)$ to be

$$\psi(P) = \psi_2(P) + \psi_1(P) - \int_{\Sigma_1} \overline{I(\sigma_1)}\,G(p;\sigma_1)\,d\sigma_1$$

where $\overline{I(\sigma_1)}$ is now the "complementary current distribution, and in terms of the reference solution $\psi(P)$ is

$$\psi(P) = 2\cos\left(\frac{2\pi y}{\Lambda}\right) - (1-\Gamma)\,\psi_{2,0}(P) - \int_{\Sigma_1} \overline{I(\sigma_1)}\,G(p;\sigma_1)\,d\sigma_1 \tag{3}$$

The new term $(1-\Gamma)\,\psi_{2,0}(P)$ prevents perfect cancellation in the interference pattern, decreases the contrast ratio, and thus serves to destroy information stored in the hologram. This is a significant effect and accounts for "binary erasures" in the readout process.

Subject to the formation of a perfect hologram, in the sense that $\Gamma = 1$, one is able to reconstruct the image O and its conjugate O" by illumination of the screen Σ with a coherent source Q_1. The conjugate image O', the twin, is out-of-focus with respect to O, unwanted,[4] and can be eliminated by various methods, two of which are illustrated here. The first, due to Bragg and Rogers,[5] relies on the utilization of a complementary hologram H_2 placed at twice the focal distance d from the hologram H_1. It can be seen that the image O' is cancelled by its opposite O" in the focal plane where the arrow appears. The second, due to Lohmann,[6] makes use of a perfectly conducting half-plane placed between the hologram H_1 and the focal plane at O. The screen Σ with its interference pattern is

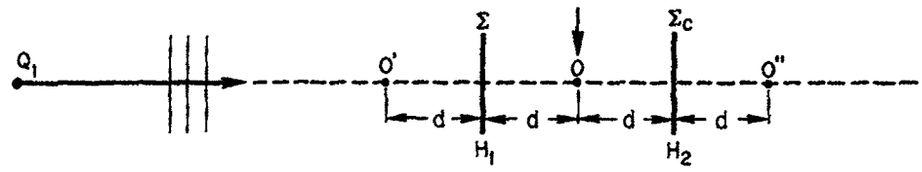

Figure 4–Bragg-Rogers cancellation method

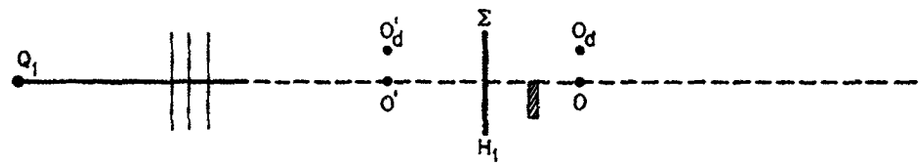

Figure 5–Lohmann cancellation method

like an antenna whose current distribution has been reduced to zero over half the aperture. The effect is to displace the radiation pattern toward the illuminated region, so that the Fraunhofer region contains no radiation from the dark space. The rays in both cases should contain no "twin" information, hence the resolution would be significantly improved.

Multiple Image Reconstruction from Holograms

Several images of objects irradiated by the same or different collimated light sources can be stored on a hologram for a multiplex communication system[7,8] or a navigation reference.[9] In the former application, several diffraction gratings are individually angularly modulated proportional to the intelligence to be transmitted or appropriately digitally coded, and the hologram formed contains the several channels of information; in the latter application, a Fresnel zone plate is optically spatially correlated, with x-ray emanations from stars in outer space, and the hologram contains their angular informations. Upon reconstruction, one expects to recover the object information.

When the objects are angular disjoint with respect to one another and when there is no loss of resolution in the process, the image reconstruction can retain the angular disjointness subject only to the confusion offered by the reading beam and twin,[10,11] or conjugate, images. That this is the case is easily seen below.

The reconstructed wavefronts from the hologram are "plane," the spreading over an angular sector Φ for a typical wavefront arising from errors in the current distribution on the hologram H. The intensity of scattered radiation in the forward direction $J(P)$ is described as

$$J(P) = \frac{1}{(4\pi)^2} \sum_{i=1}^{N} \iint_{\Sigma_H} I^i(\sigma_1) I^{*i}(\sigma_2) \frac{e^{ikRp\sigma_1}}{Rp\sigma_1} \cdot \frac{e^{-ikRp\sigma_2}}{Rp\sigma_2} d\sigma_1 \, d\sigma_2 +$$

$$+ \frac{1}{(4\pi)^2} \sum_{i \neq j}^{N} \sum_{j \neq i}^{N} \iint_{\Sigma_H} I^i(\sigma_1) I^{*j}(\sigma_2) \frac{e^{ikRp\sigma_1}}{Rp\sigma_1} \cdot \frac{e^{-ikRp\sigma_2}}{Rp\sigma_2} d\sigma_1 \, d\sigma_2 , \qquad (4)$$

where the first-term is the angularly-disjoint intensity for the real image and the second term, normally zero, is the correlation of the currents and their fields mutually exclusively. The out-of-focus ensemble, or set of twins, is not included in this description, and, in addition, to remove them entails some loss as to the number of objects and their sectors that can be stored. This is a consequence of the half-plane technique of twin removal.

Image Reconstruction from Finite Holograms

To determine the minimum size of a hologram for information storage purposes, one intuitively thinks[12, 13] of an aperture-controlled grating, the grating establishing orders of diffracted waves and the aperture their individual resolutions. The ruled lines on the hologram constitute the grating, and they are interferometrically formed by the original and side illuminations. Desirably, one wants a many wave length regular grating for image formation with irregularities less than a quarter-of-a-wavelength[14] to avoid ghost intensities.[15]

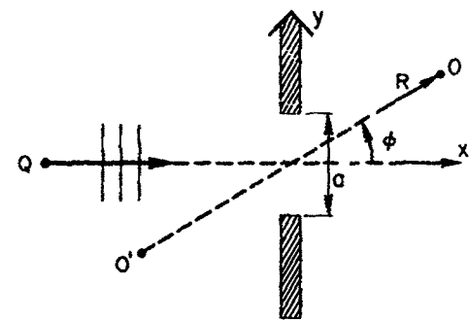

Figure 6—Finite Pupil

The ghost phenomena of Rowland[16] has been reported by Z. H. Heller[17] for a He-Ne laser, 6943A, and an aperture-controlled grating of 15,000 lines/inch and width 2.5×10^{-2} cms. Comparing the resolution and ghosts for this situation against a similar one of a sodium source, where the slit width was 2.5×10^{-3} cms., he found decided advantage for laser source; the corresponding situation for linear antennas is one of a few hundred linear elements contrasted to one of twenty elements. On this basis, one is led to the intuitively and satisfactory condition $a >> \lambda$ with an upper bound determined by the extent to which coherent phase addition applies to the emerging wavefronts on reconstruction.

The situation of a limited aperture is easily expressed by[18]

$$\psi(P) = \psi_H(P) * A(P),$$

where the convolution of the hologram and aperture fields give rise to the diffracted field. Even in reconstruction a twin-image will appear due to the conjugate one at O'. The angular distribution of intensity is well-known for the uniformly-illuminated screen, and it is

$$J(\phi) = \frac{k}{R^{1/2}} \int_{-a/2}^{a/2} e^{ikR - iky\sin\phi}\, dy, \quad k = \text{constant}$$

i.e.,

$$J(\phi) = \frac{ka\, e^{ikR}}{R^{1/2}} \; \frac{\sin\left(\frac{ka\sin\phi}{2}\right)}{\left(\frac{ka\sin\phi}{2}\right)} \tag{5}$$

showing a typical Fresnel behavior of a $(\sin a/\lambda)$ distribution. The angular spread between the two nulls symmetrically displaced with respect to the real image's ray is $\Phi = 2\sin^{-1}(\lambda/a)$, corresponding to twice the "space-sampling angle," and an excellent

reconstruction of the image occurs only if this angle ϕ be very small. For hundreds of wavelengths of extent for the hologram, the reconstruction of the real image tends to reach a limit of resolution controlled by hologram irregularities and the sources frequency dispersion.

III. RESOLUTION FOR HOLOGRAM IMAGES

Interference Pattern Shift Induced by Frequency Dispersion

What effect does the spectrum of the emitted, radiation from a laser have on the resolution property of a hologram? With simplifications in mind, one can start with a periodic one formed by two plane waves impinging on the screen at some now-zero relative angle. Allowing one to be normal, the other inclined at an angle θ, the undulations of the intensity of illumination follow a cosinusoidal law with well-known regularly-spaced maxima and minima. As the locations of peaks and valleys are sensitive to the wave-number of emission, its probability distribution affects the average peak and removes the null of the pattern. Although the spectrum is typically a quadratic functional, little error will be introduced if the nose of the spectrum, parabolic in shape, be fitted to a Gaussian error function and this be used to determine the ratio of average maximum to average minimum intensities.

On the hologram itself the maxima shift in accordance with the relation

$$\left|\frac{dy}{d\lambda}\right| = \left|\frac{m}{\sin\theta}\right| ,$$

where m is the number of the maxima, $m = 0$ implying the origin $y = 0$, consequently the distribution $p(y)$ is

$$p(y) = \frac{1}{\sqrt{2\pi\sigma_y^2}} \exp\left\{-\frac{(y - y_0)^2}{2\sigma y^2}\right\},$$

with

$$\sigma_y = \left|\frac{m\sigma_\lambda}{\sin\theta}\right| .$$

As the same applies to the minima, m permitted to assume half-integer values ($\pm$ 1/2, $\pm$ 3/2, ..., $\pm$ N/2), the expectations of the minimum and maximum intensities are

$$\left\langle J_{min}\right\rangle \cong \int_{\Delta y} \frac{4\left(\frac{u}{\Lambda}\right)^2}{\sqrt{2\pi\sigma_y^2}} \exp\left\{-\frac{u^2}{2\sigma_y^2}\right\} du$$

$$\cong \frac{4\sigma_y^2}{\Lambda^2} , \ \sigma_y = \text{value for } m = \left(\pm\frac{1}{2}, \pm\frac{3}{2}, \pm \cdots\cdots, \pm N\right).$$

and

$$\left\langle J_{max} \right\rangle \cong 4.$$

The ratio of these intensities is then seen to be

$$P = \frac{\left\langle J_{max} \right\rangle}{\left\langle J_{min} \right\rangle} = \frac{\Lambda^2}{\sigma_y^2}. \tag{6}$$

Inspection of the intensity ratio shows a dependence on the "noise" in the hologram, and one appreciates the significance of this ratio where one is asked for a measure suitable spatial resolution comparisons. The amount of information stored in the hologram also depends on this quantity. A related quantity is the Michelson contrast ratio

$$C = \frac{I_{max} - I_{min}}{I_{max} + I_{min}},$$

and as in the case of Diederich and Lohmann,[19] who studied roughness of lens surfaces on image formations, one finds

$$C = \frac{\Lambda^2 - \sigma_y^2}{\Lambda^2 + \sigma_y^2}. \tag{7}$$

Amplitude Quantization Induced by Dispersive Radiation

Let α and β be randomly distributed variables taking into account the divergence of an otherwise collimated, monochromatic beam radiating from Q_1 and sympathetically from Q_2. The wave potential $\psi(P)$ for $p \in P$ induces currents with random distributions on the screen Σ. In terms of the random angles θ_1 and θ_2, where $\theta_1 = \vec{k}_1 \cdot (\vec{r} - \vec{r}_1)$ and $\theta_2 = \vec{k}_2 \cdot (\vec{r} - \vec{r}_2)$, one has

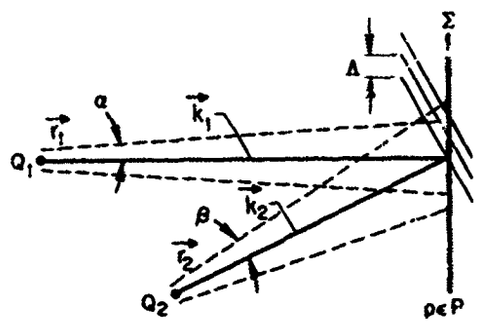

Figure 7—Beam Spreading

$$\psi(P) = e^{i\theta_1} + e^{i\theta_2},$$

so that

$$J(P) = |\psi(P)|^2 = 4\cos^2\left(\frac{\theta_1 - \theta_2}{2}\right).$$

Near the maxima, specifically when $\theta_1 - \theta_2 = m(2\pi)$, $m = 0, \pm 1, \pm 2, \pm \cdots\cdots, \pm N$, the intensity $J(P)$ is

$$J(P) \cong 4\left[1 - \frac{(\theta_1 - \theta_2)^2}{4}\right].$$

and for $\theta_2 = k\theta_1$,

$$J(P) \cong 4\left[1 - \frac{\sigma_1^2}{4}(1-k)^2\right]$$

with a statistical average

$$\left\langle J(P)\right\rangle \cong 4\left[1 - \frac{\sigma_{\theta_1}^2}{4}(1-k)^2\right].$$

This result allows us to see a deterioration of the brightness of the hologram Σ, when the radiation from O_1 is shadowed by interposed objects. Though the deterioration is not rapid, the effect cannot be neglected. In sharp contrast, the minima are seriously affected, and they follow first

$$J(P) \cong 4\left(\frac{\theta_1 - \theta_2}{2} - \frac{(2m+1)\pi}{2}\right)^2, \quad m = 0, \pm 1, \pm 2, \pm \cdots, \pm N$$

$$J(P) \cong [\theta_1(1-k) - (2m+1)\pi]^2,$$

second

$$\left\langle J(P)\right\rangle \cong \left\langle \theta_1^2\right\rangle (1-k)^2 - \left\langle \theta_1\right\rangle 2(1-k)(2m+1)\pi + (2m+1)^2\pi^2$$

$$\left\langle J(P)\right\rangle \cong \sigma_{\theta_1}^2 (1-k)^2,$$

and one finally sees imperfect cancellation with a ratio of maxima-to-minima statistically becoming

$$P = \frac{\left\langle J_{max}\right\rangle}{\left\langle J_{min}\right\rangle}$$

$$P = \frac{4\left[1 - \frac{\sigma_{\theta_1}^2}{4}(1-k)^2\right]}{\sigma_{\theta_1}^2 (1-k)^2}. \tag{8}$$

The comparison of this result with the frequency dispersive relation reveals the quantal sensitivity of the respective phenomena, frequency and angular dispersions. The ratio k of beam angles is dependent only on the first-order relations corresponding to the geometry of the sources and hologram screen Σ. Thus, the control of resolution for the hologram is centered on the required quantal sensitivities and the extent to which they are important in the face of fundamental resolution for the hologram itself.

Vibration and Contrast Ratio for Holograms

The hologram screen Σ can move randomly relative to the (x, y) reference frame and thereby contribute to a loss of resolution. As unidirectional movement only can occur,

the displacement of maxima and minima occur. The greater sensitivity occurs for the minima of intensity, and its expectation is proportional to the variance of motion. One looks for σ_y^2 and finds it to be

$$\sigma_y^2 = \tan^2 \theta \, \sigma_x^2$$

Earlier, we saw the effect of frequency dispersion and the induced shift of the hologram, so now we can easily see the minima's expectation to be

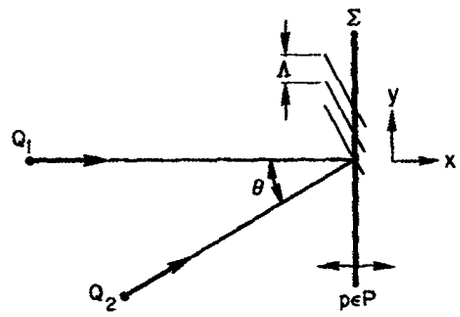

Figure 8–Relative Motion for Hologram

$$\langle J_{min} \rangle = \frac{4 \tan^2 \theta \, \sigma_x^2}{\Lambda^2}$$

and the contrast ratio to be

$$\frac{\langle J_{max} \rangle - \langle J_{min} \rangle}{\langle J_{max} \rangle + \langle J_{min} \rangle} = \frac{1 - \dfrac{\tan^2 \theta \, \sigma_x^2}{\Lambda^2}}{1 + \dfrac{\tan^2 \theta \, \sigma_x^2}{\Lambda^2}}$$

$$C = \frac{\Lambda^2 - \tan^2 \theta \, \sigma_x^2}{\Lambda^2 + \tan^2 \theta \, \sigma_x^2} \tag{9}$$

Energy Ratio, its Dependence on the Emulsion's Properties

For the emulsion, the transfer characteristic has been taken, for convenience and good approximation, to be[20] linear with respect to intensity between two limits J_{max} and J_{min}, the transmittance, or opacity, lying on the scale from zero to one but also limited to t_1 and t_0, respectively. The second-order effect of graininess, accounting for spread of the images, has been included in P. Clark Jones' analysis of information content of emulsions. It is now the object of the present analysis to use these desiderata in realizing the energy ratio and resolution for holograms.

We consider, fundamentally that the transmittance will be probabilistically controlled over the screen $\Sigma(s, y)$ in response to the wave-potential $\psi(y, z)$, and the density function will be a continuous function thereof, that is

$$dP\,[t(y, z)] = p[\psi(|\psi\{y, z\}|^2]\; dy\,dz \quad \text{for} \quad y \in Y,\; z \in Z.$$

What we shall look for is an increased variance σ_y^2 on the hologram arising from the random response of the screen Σ, and the simplest case to examine is the interference pattern for two plane waves. Here, the variance $\sigma\psi^2$ is known to be normally dependent on frequency dispersion, beam spreading, and vibration phenomena for the laser source. These being independent phenomena, for instance, one would find

$$\sigma_y^2 = \left|\frac{m\sigma_\lambda}{\sin\theta}\right|^2 \left| + \right| \cdots\cdots\cdots\cdots \Big|^2 + \left|\sigma_x \tan\theta\right|^2, \quad m = 0, \pm 1, \pm\cdots, \pm N$$

the terms arising in the order given above and the variances determined at the minima of the interference pattern. No term exists for the "variance" of the dispersed beam situation, the null losing its sharpness and becoming diffusively blurred. However, one can still deal with the term "variance" as it does influence the qunatization for the hologram, the energy ratio being

$$\rho \equiv \frac{J_{max}}{J_{min}^{(1)} + J_{min}^{(2)} + \cdots\cdots\cdots\cdots + J_{min}^{(n)}},$$

the minima determined by the variances. From foregoing analyses, we find

$$\rho_m = \frac{4}{4\left|\frac{m\sigma_\lambda}{\Lambda \sin\theta}\right|^2 + \left|(1-k)\sigma_{\theta_1}\right|^2 + 4\left|\frac{\tan\theta\,\sigma_x}{\Lambda}\right|^2} \tag{10}$$

$$m = 0, \pm 1, \pm 2, \pm\cdots\cdots, \pm N$$

and note an equivalent variance.

Now, to account for the variation in transmittance. First, under the linear conditions of P. Clark Jones, we note ρ is one for those wave potentials outside the limits of the emulsion, is (t_1/t_0) for extreme potentials still outside the limits, and is the above number for those on the linear portion. Second, to reduce the energy ratio because of $t \neq 1$, we observe that

$$\langle t^2 \rangle = \int_0^1 t^2\, dP\,[t(y, z)] \quad \text{for} \quad y \in Y,\ z \in Z,$$

$$\langle t^2 \rangle = \int_0^1 t^2\, p\,[t(|\psi(y, z)|^2)]\, dt.$$

But $p(t) = P(t_0)\,\delta(t - t_0) + p(t_0 < t < t_1) + P(t_1)\,\delta(t - t_1)$, so in the vicinity of a minimum, $J_{min} \approx 0$,

$$\sigma_t^2 = \int_0^{t_0^+} t^2\, p\,[t\,(T_{min})]\, dt$$

$$\sigma_t^2 = t_0^2,$$

while for a maximum, $J_{max} \approx 4$,

$$\sigma_t^2 = (1 - t_1)^2.$$

Note these are fluctuations with respect to the nulls and peaks, respectively. Clearly, the variance is intensity sensitive and the same energy ratio t_1/t_0 is still realized under extreme conditions. However, in the linear portion, we find

$$\left\langle t^2 \right\rangle = \int_{t_0}^{t_1} t^2 \, p\,[t(T)]\, dt$$

and

$$\sigma_t^2 = \int_{\bar{t}-\frac{\Delta t}{2}}^{\bar{t}+\frac{\Delta t}{2}} (t-\bar{t})^2 \left[\frac{1 - P(t_0) - P(t_1)}{\Delta t} \right] dt$$

$$\sigma_t^2 = \int_{-\frac{\Delta t}{2}}^{+\frac{\Delta t}{2}} u^2 \left[\frac{1 - P(t_0) - P(t_1)}{\Delta t} \right] dt$$

$$\sigma_t^2 = \left[\frac{1 - P(t_0) - P(t_1)}{\Delta t} \right] \frac{(\Delta t)^3}{12},$$

when a uniform distribution is assumed. This variance implies that the energy ratio is

$$\rho_m = \frac{4}{4\left|\frac{m\sigma_\lambda}{\Lambda \sin\theta}\right|^2 + \left|(1-k)\sigma_{\theta_1}\right|^2 + 4\left|\frac{\tan\theta\,\sigma_x}{\Lambda}\right|^2 + 4\left[\frac{1 - P(t_0) - P(t_1)}{12}\,\Delta t^2\right]} \qquad (11)$$

$$m = 0, \pm 1, \pm 2, \pm, \cdots\cdots\cdots, \pm N$$

when $T_{min} > t_0 > 0$. Usually $\Delta t << \bar{t}$, the graininess, hence the simpler relation for the energy ratio is the one previously derived.

As a result of the study presented above, we see that the resolution was not obtained, the variance σ_y^2 not being determined readily, although the energy ratio fell on it quite naturally. Additional study should reveal the resolution for the hologram.

IV. ACKNOWLEDGMENTS

Whisked away to Aberdeen Proving Ground, Aberdeen, Md., the author was shown an optical bench for making holograms and reconstructing images therefrom. The interest of Mr. R. Rowe of BPL, coupled with observations by Messr. A. Shulman and W. Olden of Goddard Space Flight Center, served to stimulate the author toward making this preliminary study. This study was a portion of the Summer NASA/ASEE Faculty Fellowship Program.

V. BIBLIOGRAPHY

1. C. E. Shannon, "The Mathematical Theory of Communication," Univ. of Illinois Press, Urbana, Ill., 1949, Chp. 1.
2. S. A. Schelkur ›ff, "Kinchhoff's Formula, its Vector Analogue, and Other Field Equivalence Theorems," Symp. on Electromagnetic Theory, N.Y.U., June 1950, Interscience Publ., pp. 107-123.
3. B. B. Baker and E. T. Copson, "The Mathematical Theory of Huyghen's Principle."
4. W. L. Bragg and G. L. Rogers, "Elimination of the Unwanted Image in Diffraction Microscopy," Nature, Vol. 167, Feb. 3, 1951, pp. 190-191.
5. Ibid.
6. A. Lohmann, "Optische Einseitenbandübertragung angewandt auf des Gabor Mikroscop," Optica Acta (Paris), Vol. 3, 1956, pp. 97-99.
7. A. Lohmann, "Theta Modulation in Optics," Jour. Opt. Soc. of Amer., Vol. 53, 1963, pp. 1351-1351.
8. R. E. Williams, "The Panchromatic Principle in Optical Filtering," I.E.E.E. Trans. on Information Theory, Vol. IT-10, 1964, pp. 227-234.
9. L. Mertz and N. O. Young, "Fresnel Transformation of Images," Proc. Conf. on Optical Instruments and Technology, London, 1961, Chapman and Hall, pp. 305-312.
10. W. L. Bragg and G. L. Rogers, op. cit.
11. A. Lohmann, 1956, op. cit.
12. A. Lohmann, "Contrast Transfer in the Grating Spectrograph," Optica Acta, Vol. 6, 1959, pp. 175-185.
13. J. A. Armstrong, "Fresnel Holograms: Their Imaging Properties and Aberrations," IBM Jour. of Res. and Dev., Vol. 9, No. 3, May 1965, pp. 171-178, espec. 174-175.
14. A. Lohmann, 1959, op. cit., p. 179 and 181.
15. J. Guild, "The Interference Systems of Crossed Diffraction Gratings," Oxford Univ. Press, 1956, pp. 125-126.
16. H. A. Rowland, "Physical Papers," Johns Hopkins Univ., 1902, p. 536.
17. Z. H. Heller, "Rowland Ghosts Observed with Laser Illumination," Jour. Opt. Soc. of Amer., Vol. 53, 1963, pp. 395-397.
18. E. Leith and J. Upatrieks, "Reconstructed Wavefronts and Communication Theory," Jour. Opt. Soc. of Amer., Vol. 52, 1962, pp. 1123-1130.
19. E. Diederichs and A. Lohmann, "Der Einfluss der Rauhigkeit von Linsenoberflöchen auf den Ubertragungsfaktor," Optik, Vol. 15, 1958, pp. 751-757.
20. P. C. Jones, "Information Capacity of Photographic Films," Jour. Opt. Soc. of Amer., Vol. 51, 1961, pp. 1159-1171.

N66 31160

CORRELATION BETWEEN JITTER AND INFORMATION RECOVERY IN PCM TELEMETERED DATA

by

Dr. Paul Goodman
Assistant Professor,
Newark College of Engineering,
New Jersey

PROBLEM STATEMENT

The project objective was to create a method and equipment which would take as input a PCM signal containing data, and produce as output a single number (called K in the following) which would reliably predict the relative ease or difficulty of recovering error-free data from the tape.

Such a method would allow greater care to be used when processing a tape predicted (by K) to be difficult. Conversely, poor data recovery from a tape predicted to be excellent would indicate malfunctioning processing (data recovery) equipment.

Procedures and Methods

A perfect, noiseless, split phase PCM signal has the following useful property: the time interval between successive negative to positive (or positive to negative) transitions is restricted to three values fixed by the bit transmission rate. For example, when one thousand bits per second are transmitted, theory predicts measured transition times of 1, 1.5, and 2 milliseconds. Let us define three narrow intervals centered around these three times, and let K be the fraction of all measurements falling within all three intervals. Then it seems clear that K = 1.0 for a perfect signal, and K should decrease as signal distortion increases, or equivalently as signal to noise ratio decreases. It also seems clear that increasing signal distortion causes more errors in reading data. Therefore a reasonable hypothesis is that a correlation exists between K and error rate, which will allow K to be used as indicated in the introduction.

The work performed at GSFC this summer consisted of defining the problem, planning an experiment to test the hypothesis just mentioned, setting up equipment and carrying out the experiment, and interpreting the results. In more detail, the following was done.

1. Eleven tapes containing data as telemetered from the OGO S-49 satellite were chosen for the experiment. The tapes spanned a range from very poor to excellent data recovery.

2. Equipment was set up and transition times were measured automatically and recorded. Each tape was sampled randomly, and approximately one thousand samples per tape were recorded.

3. The measurements were transferred to punched cards, and a computer was then used to find K for each tape, using intervals of ±5% around each of the three noise-free transition times.

4. The values of K were compared with a prior knowledge of data errors in order to establish the degree of correlation.

RESULTS AND CONCLUSIONS

Out of eleven tapes, one could not be used because of experimental errors. Of the remainer, six showed good correlation, two were border line, and two were poor.

In some cases a tape was run twice, and K was computed separately for each run. Differences in K indicated that larger samples were called for, not a surprising conclusion when one takes into account that one tape may contain forty million bits. Sample size restricted to one thousand per tape because each measurement had to be transferred by hand to a punched card, the resulting bottleneck making more samples impractical.

The correlation seems as good as possible, considering the small sample size. Another unknown factor is errors caused by a malfunctioning process line. One tape in particular was run twice, K was the same both times and was high enough to indicate very few errors, yet relatively many errors had been noted when the tape was processed.

The final conclusion is that the results are promising and justify further experiments. Equipment must be devised to automate the sampling procedure, especially the process of getting the samples into final form suitable for computer input. This will allow larger samples to be used and many more tapes to be analyzed.

A report now being written by the author contains more complete discussions, data, conclusions, and recommendations for future investigations. This report forms the introduction to the more complete report.

Data Selection

The following tapes were selected by M. Pasternack as a representative cross-section of signal characteristics, based on a prior knowledge of slippage rate (SR) and bit error rate (BER).

Table 1
Tape Ratings

Station #	16	16	19	19	19	20	20	20	20	20	20	20
Tape #	14	213	425	450	491	14	633	878	915	1418	1621	1667
SR	P	-	H	P	E	-	E	E	H	H	F	H
BER	H	-	P	H	P	E	E	E	P	H	F	F

Each tape was rated for SR and BER as H (horrible), P (poor), F (fair), E (excellent). If possible, future investigations should replace these with numerical values for SR and BER, in order to permit an actual computation of correlation. Tape #425 was never delivered, and tape #14, Station 20 was not used for technical reasons.

Equipment

Tapes were played on a Consolidated Electro-dynamics Tape Recorder, Model VR-2600. The signal was taken in all cases from channel 2 containing the so called "raw data." It was then, in most cases, passed through a low-pass filter in order to eliminate tape deck noise, whenever noise and signal were sufficiently separated in frequency. Tape deck noise was always above forty thousand cps, and signal frequency could be lowered by changing tape speed. The filter output drove a Hewlett Packard 52436 Electronic Counter whose reading was printed by a Hewlett Packard 560A Digital Recorder.

The counter had a 10 megacycle clock, permitting resolution to 0.1 microsecond, which was more than adequate.

The numbers thus obtained were punched on cards and then sorted to give the number of times each measurement occured. This was to be plotted as a distribution function by the 4020 plotter, but the programs were never successful. However, the distributions were printed as output, and this permitted K to be computed by hand. Of course this could be done much more easily by the computer, but it was not clear exactly what was necessary when the program was written.

Results and Conclusions

Table 2 gives a summary of measurements, from which our conclusions are drawn. Let us make a very simple rule and see how well SR is predicted. We assume that H corresponds to $0 \leq K < 0.25$, P to $0.25 \leq K < 0.5$, F to $.50 \leq K < .75$, and E to $0.75 \leq K < 1.0$. In cases where two runs correspond to one tape, the average value of K is taken.

Table 2
Computed values of K

Tape	SR	BER	K	f	f	Run #
19-450	P	H	.21	40	8	1
19-14	P	H	.39	60	16	2
19-425	H	P	.27	40	8	3
20-633	E	E	.81	40	1	4
20-1667	H	F	.61	40	1	5
20-878	E	E	.86	40	8	6
20-915	H	P	.85	40	8	7
20-915	H	P	.85	∞	8	8
20-1621	F	F	.30	∞	1	9
20-1621	F	F	.50	30	1	10
19-491	E	P	.74	40	8	11
19-991	E	P	.34	40	8	12
20-1418	H	H	.69	40	8	13

Table 3 shows the results for this and for predicting SR by the same rule.

Table 3
Predicted and Actual BER, SR

Tape	K	BER (Predicted)	BER (Actual)	SR (Predicted)	SR (Actual)
19-450	.21	H	H	H	P
16-14	.39	P	H	P	P
19-425	.27	P	P	P	H
20-633	.81	E	E	E	E
20-1667	.61	F	F	F	H
20-878	.86	E	E	E	E
20-915	.85	E	P	E	H
20-1621	.40	P	F	P	F
19-491	.54	F	P	F	E
20-1418	.69	F	H	F	H

BER is predicted correctly for 5 tapes, in three cases the prediction must be shifted up or down by one category (i.e., from P to H for tape 16-14) and in two cases a shift of two categories is necessary. Corresponding numbers for SR are three correct, four must be shifted by one category two need a shift of two, and one prediction is as far as possible from being correct. Clearly there is a greater correlation between K and BER than K and SR. In the former case results seem quite promising, leading to a tentative conclusion that K can be used to predict BER.

Returning to Table 2, we see that three tapes were run twice (runs 7-12). If K is to have any meaning it must be constant for any one tape. Therefore, the changes in K between runs 9 and 10, and between 11 and 12 must be eliminated. The cause of such changes is very likely the very limited sample size, and the fact that each set of samples were taken from, at most, about 25% of the tape. The number of bits per tapes may be of the order of ten million, thus, one thousand samples is not very much in comparison. Therefore, future experiments must use many more samples, and the samples should be spread uniformly over the entire part of the tape which contains data.

Visual Inspection of Waveforms

A visual inspection of signals on all eleven tapes was made. The object was to explore the possibility of direct prediction of SR or BER by some easily recognized pattern or signal distortion. The tapes were divided into four categories on the basis of observed signal to noise ratio, and the results are shown in Table 4.

Comparing this with Table 3 we see that BER was predicted correctly five times by K vs. four times visually, SR was correct three times in either case. Apparently K still is more indicative of BER than SR, and is a better predictor than visual recognition. Other reasons for preferring K are: it does not depend on human interpretation, it may lead to more sophisticated ways to treat the samples in a statistical sense.

Table 4
Visual Rating of Signals

Tape	Rating (Visual)	BER	SR
19-450	H	H	H
16-14	P	P	H
19-25	F	P	P
20-633	E	E	E
20-1667	E	F	F
20-878	P	E	E
20-915	P	E	P
20-1621	E	P	F
19-491	F	F	P
20-1418	P	F	H

The waveforms were reduced to strip charts showing amplitude vs. time, using two tape recorders, a Consolidated Electrodynamics VR-2600, and an Ampex FR-600. Each tape was played on the VR 2600 at 3.75 i.p.s. and recorded on the FR 600 at 60 i.p.s., then the recording was played back at 1-7/8 i.p.s. and recorded on a Honeywell 1508 Visicorder. It was necessary to use FM modules on the tape recorders for good low-frequency response.

Future Work

Before this work is continued on an experimental basis, it is necessary to set up equipment capable of automatically transferring readings from the HP electronic counter to either punched cards or tape, the latter being preferable because of the rapidity with which it can be entered into a computer. A larger number of tapes should be chosen, and numerical values of BER should be known for them. Then if K and numerical BER are related, it will be apparent from experimental results. A range of ±5% for computing K is not necessarily best, and a range of such values should be used to see the effect of change.

Theoretical investigations should be made for comparison with experimental results. Two questions of a statistical nature seem appropriate:

1. What is the expected distribution of transition times as a function of signal to noise ratio, for various well known types of noise such as white noise, shot noise, etc?

2. What is an appropriate number of samples to ensure K being statistically reliable?

These are questions the author hopes to investigate during the coming school year.

Acknowledgments

The author is happy to express his thanks to the personnel of GSFC, whose cooperation made this project possible. In particular the help and interest of B. Harrow, T. Terashi, and F. Wulff were invaluable.

N66 31161

DEVELOPMENT OF THE 10.6-MICRON LASER

by

Dr. Zbigniew D. Jastrzebski, Professor
Lafayette College, Easton, Pa.

STATEMENT OF THE PROBLEM

The use of 10.6-micron laser for optical communication systems may offer certain advantages as compared with the pulsed ruby laser used presently for tracking experiments. These advantages are higher degree of beam coherence, less energy required for an information bit at the receiver, and less atmospheric loss per unit distance.

The GSFC Optical Systems Branch has initiated the program aiming at the development of an effective optical tracking system for communication between the Goddard Optical Research Facility and the Echo II satellite. As a part of this program, I was assigned to study and develop the 10.6-micron nitrogen-carbon dioxide laser.

PRESENT STATE OF KNOWLEDGE

A strong C. W. lasing action in a nitrogen-carbon dioxide mixture under low pressures (~1mm Hg) has been reported in literature. Lasing in infrared takes place when vibrationally excite N_2 molecules (V = 1) excite through inelastic collisions the CO_2 molecules (00°0) to the upper laser level (00°1). Nitrogen molecules fall back to their vibrational ground-level (V = 1), leaving behind a large population of the excited CO_2 molecules. The main output lines occur at 10.5915 microns and at 10.5716 microns on two rotational transitions of the 00°1 - 10°0 vibrational band with a C.W. power output which may be as high as 11.9 watts.

EXPERIMENTAL

Two experimental setups have been designed which differ mainly in the arrangement of flat reflective mirrors in respect to the Vycor discharge tube of 24mm I.D. and 122 cm length. In one setup the goldplated mirrors form an integral part of the laser assembly, being vacuum-tight connected to the ends of the discharge tube through metallic bellows. In the second setup the gold-plated mirrors are located externally to the discharge tube which is terminated by vacuum-tight Brewster angle windows. These windows and one of the two gold-coated mirrors are made of Barium Fluoride. This mirror has one-millimeter diameter hole in the gold coating for coupling out the radiation; the other mirror is 100% opaque.

The discharge tube is connected through an outlet with the manifold of the vacuum system so that it is possible to control precisely low partial pressures of the gaseous ingredients. The necessary pumping power is obtained using a Viking Invader Transmitter (C.W. 1000 watts) providing rf discharge of 28 Mc/sec. Only qualitative measures for the detection of the infrared laser beam are now available.

CONCLUSIONS

The experimental setups have been found to function satisfactorily. At the moment of this writing, no appreciable lasing action has yet been noticed, but concrete results are expected very shortly.

This project has been carried out under the guidance of Mr. Nelson McAvoy and with assistance of the other staff members of the Quantum Optics Section.